WIRELESS RESOURCE MANAGEMENT IN INDUSTRIAL INTERNET OF THINGS

Zhanwei Hou

A thesis submitted in fulfillment
of the requirements of the degree of
Doctor of Philosophy

THE UNIVERSITY OF
SYDNEY

CENTRE OF EXCELLENCE IN TELECOMMUNICATIONS
SCHOOL OF ELECTRICAL AND INFORMATION ENGINEERING
THE UNIVERSITY OF SYDNEY

March 2019

To my loving wife Haiqin Li

and

my beloved parents Xilong Hou and Zhimei Li

Acknowledgements

First, I would like to acknowledge the help and supports from my supervisors: Prof. Branka Vucetic and Prof. Yonghui Li. I am grateful to have the privilege of being their student. To Prof. Vucetic, thank you for inviting and taking me as a PhD student, and maintaining such a research driven lab environment. Her visions in terms of research trends and industrial demands are so insightful, which lead us to focus on the most important problems. To Prof. Li, thank you for having been so supportive, knowledgeable and very kind during the past three years. He not only guided me to learn how to do research, but also taught me how to be a good person, which will be the lifetime treasure for me.

I would also like to acknowledge the suggestions and help from Dr. Changyang She and Dr. He Chen. Thank you for your insightful discussions and working so closely with me during the last few years. Thank you for your supportive encouragement and valuable suggestions in incredible details when I was encountering hurdles during the research, without which I could not learn how to ask the right questions, how to tackle a problem, and how to make into a research paper. Moreover, I would like to thank Dr. Peng Cheng for his discussions and suggestions about both of my research and career.

Many thanks to current and past members of the center of excellence in IoT and telecommunications in the University of Sydney, including but not limited to Zheng Dong, Phil, Mahyar, Xiaoli, Wanchun, Dawei, Yuehua, Youjia, Rana, Matt, Yi Zhou, Allen, Ray, Wenhao, Chuan Ma, Di Zhai, Zhouyou, Deyou, Yizhen, Zun Yan, Qian Wang, Dora, Yifan, Yuhong, Sina, for your companying and creating a pleasant research environment during the last few years.

I would like to thank for the financial support from the International Postgraduate Research Scholarship (IPRS) and Australian Postgraduate Awards (APA), and the Norman I Prize scholarship. Moreover, I would like to thank Prof. Branka Vucetic

and the University of Sydney's PRSS scheme for their financial support, which enables me to attend several international conferences.

At last, I am indebted to my wife and parents for their unconditional love, generous support, and encouragement through the ups and downs of the last few years. My family always provides the greatest support to allow me dedicated to my research. I would like to devote the achievements of my research to my family.

Zhanwei Hou
Sydney, Australia
December 2018

Statement of Originality

The work presented in this thesis is the result of original research carried out by myself, in collaboration with my supervisors, while enrolled in the School of Electrical and Information Engineering at the University of Sydney as a candidate for the Doctor of Philosophy.

These studies were conducted under the supervision of Prof. Branka Vucetic and Prof. Yonghui Li. It has not been submitted for any other degree or award in any other university or educational institution.

Zhanwei Hou
School of Electrical and Information Engineering
The University of Sydney
December 2018

Abstract

Industrial Internet of Things (IIoT) provides a promising opportunity to revolutionize the industrial sectors. By enabling the sense of tactile, Tactile Internet will support the skill-set delivery network for IIoT. The traditional industrial sectors mainly depend on cables for communications or supplying energy. To realize the vision of future flexible, scalable and customized manufacturing in IIoT, wireless capability is highly demanded to enable mobility, or deploy in harsh environments, such as high temperature, high pressure, toxic or radioactive scenarios. Unfortunately, the current industrial wireless communication protocols are mainly modified from IEEE 802.11 standard family and working in unlicensed spectrum, which cannot support the real-time and reliability requirements in IIoT.

To meet the stringent requirements from industrial wireless communications, the fifth generation (5G) communications will support machine type communications (MTC): ultra-reliable low-latency communications (URLLC) for mission critical communications and massive machine type communications (mMTC). Despite the academia research and on-going standardization efforts, there are still many challenges, including the ultra-high reliability and low latency requirements, spectral shortage, and limited energy supply. According to the vision of 5G, 1 ms end-to-end (E2E) delay and the reliability of 99.999% (i.e., 10^{-5} packet loss probability) should be guaranteed, which is challenging to be met at the same time. Moreover, to improve reliability in the low latency domain, different diversities need to be applied and thus redundant resources are utilized. Together with the exponentially increase of IIoT devices, the spectrum will be far from enough. To reap the full benefits of wireless, cables for energy supply should be replaced by batteries. As it is well known, limited battery capability is always a long standing bottleneck for IIoT. To tackle the above challenges, we will focus on wireless resource management in IIoT in this thesis by designing novel framework, analyzing performance and optimizing wireless resources.

First, we consider local area network of IIoT. Local area network, within the range

of several kilometers, refers to the scenario with one BS or several BS connected by high speed backhauls in IIoT. We focus on the application of Tactile Internet, the traffic of which is very bursty. Using this feature, we propose to classify the packet arrival process of each user into high or low traffic state. For users in high traffic state, dedicated bandwidth is reserved to avoid resource scheduling delay. For users in low traffic state, a unified resource pool is shared to save spectral resources, i.e., bandwidth. The most challenging part is that the classification is not error-free. To tackle this issue, we minimize the reserved bandwidth taking into account the classification errors while ensuring the latency and reliability requirements. Simulation and results show that with around 10^{-2} classification error probability, our method can achieve 10^{-5} packet loss probability. Meanwhile, 40% to 70% bandwidth can be saved compared with the baseline method. Our results are further validated by the practical packet arrival processes acquired from experiments using a real tactile hardware device.

Next, we extend to the more challenging long distance communications for IIoT, which can support the global skill-set delivery network. It is challenging because the propagation delay and routing delay resulting from the backhauls and the core network are in the order of tens of milliseconds in long distance communications. In this scenario, it seems impossible to achieve 1 ms delay by using traditional methods, which only designs and optimizes the communications system. For example, when the distance is larger than 300 km, the propagation delay of the electromagnetic wave in core network would be 1 ms. To this end, we propose to predict the future system state and send to the receiver in advance, and thus the delay experienced by the user is reduced. We first analyze the closed-form relationship between the prediction time and prediction error probability, and then characterize the relationship between communication E2E delay and packet loss probability. Based on the analyses, we minimize the bandwidth usage to ensure delay and reliability requirements. The proposed method can achieve zero delay experience for users in both local and long distance communications in IIoT. Numerical results verify the effectiveness of the proposed method. The tradeoff between reliability and bandwidth in the zero experienced delay is also revealed by simulations, which shows that the tradeoff is fundamentally changed by predictions. The results are further evaluated by practical motion data acquired from experiments by a real hardware device.

Finally, we address the issue of energy supply in IIoT. To reap the full benefits of wireless, cables for energy supply should also be removed and replaced with batteries.

However, due to the limitations of battery technology, the current battery capability is not enough for the increasing demands from the exponentially increasing IIoT devices. Radio frequency energy harvesting (RFEH) is a promising technology to charge unattended IIoT low-power devices remotely and continuously. In future energy market, some third-party operators specialized in energy harvesting may provide the charging services for the IIoT devices. The telecommunication operator should provide incentives to motive the surrounding third-party operator to charge its IIoT devices. Different from existing incentive schemes, we consider a practical scenario with asymmetric information, where the telecommunication operator does not know the channel conditions and energy costs of the third-party operators. To deal with asymmetric information more efficiently, we develop a contract theory-based framework, where the optimal contract is derived to maximize the social welfare. Numerical simulation results show that information asymmetry can lead to severe performance degradation for the Stackelberg game-based framework, while the proposed contract theory-based scheme using asymmetric information outperforms the Stackleberg game-based approach with complete information. This implies that the performance of the considered system depends largely on the market structure (i.e., whether the third-party operators are allowed to optimize their received power at the IIoT devices with full freedom or not) than on the information availability (i.e., the complete or asymmetric information).

Contents

List of Figures

List of Acronyms

5G	the fifth generation
ACK	acknowledgement
AWGN	addictive white Gaussian noise
CAN	controller area network
CCDF	complementary cumulative distribution function
CDF	cumulative distribution function
CPS	cyberphysical system
CSI	channel state information
DAP	data access point
DIC	downward incentive compatibility
DL	downlink
D2D	device-to-device
E2E	end-to-end
EAP	energy access point
GE	General Electric
HARQ	Hybrid Automatic Repeat reQuest
IC	incentive capability
i.i.d.	independent and identically distributed
IIoT	Industrial Internet of Things
IoT	Internet of Things
IR	individual rationality
JND	just noticeable differences

KKT	Karush-Kuhn-Tucker
LAN	local area network
LDIC	local downward incentive compatibility
LUIC	local upward incentive compatibility
MAC	media access control
MTC	machine type communications
mMTC	massive machine type communications
N-P	Neymman Person
NR	New Radio
QoS	quality of service
RFEH	Radio frequency energy harvesting
RTE	real-time Ethernet
SBS	small-cell base station
SCV	squared coefficient of variation
SE	Stackelberg equilibrium
SNR	signal-to-noise ratio
SPP	switched Poisson process
SWIPT	simultaneous wireless information and power transfer
UL	uplink
UIC	upward incentive compatibility
URLLC	ultra-reliable low-latency communications
WLAN	wireless local area network
WPAN	wireless personal area network

List of Publications

The following is a list of publications in refereed journals and conference proceedings produced during my Ph.D. candidature. In some cases, the journal papers contain material overlapping with the conference publications.

Journal Papers

[J1] Zhanwei Hou, Changyang She, Yonghui Li, Tony Quek, and Branka Vucetic, "Burstiness aware bandwidth reservation for ultra-reliable and low-latency communications (URLLC) in Tactile Internet," *IEEE Journal on Selected Areas in Communications*, vol. 36, no. 11, pp. 2401-2410, Nov., 2018.

[J2] Zhanwei Hou, He Chen, Yonghui Li and Branka Vucetic, "Incentive mechanism design for wireless energy harvesting-based Internet of Things," *IEEE Internet of Things Journal*, vol. 5, no. 4, pp. 2620-2632, Dec., 2017.

[J3] Zhanwei Hou, Yiqing Zhou, Lin Tian, Jinglin Shi, Yonghui Li, and Branka Vucetic, "Radio environment map aided Doppler shift estimation in LTE-Railway," *IEEE Transactions on Vehicular Technology*, vol. 66, no. 5, pp. 4462-4467, Aug., 2016.

[J4] Zhanwei Hou, Changyang She, Yonghui Li, and Branka Vucetic, "Prediction and communication co-design for ultra-reliable low-latency communications," in preparation.

[J5] Changyang She, Zhanwei Hou, Yonghui Li, and Branka Vucetic, "A tutorial

on ultra-reliable and low-latency communications: methodologies, solutions, and open Issues,", in preparation.

[J6] Daquan Feng, Changyang She, Kai Ying, Lifeng Lai, Zhanwei Hou, Quek Tony, Yonghui Li, and Branka Vucetic, "Towards ultra-reliable low-latency communications: typical scenarios, possible solutions, and open issues," submitted to *IEEE Vehicular Technology Magazine* and under major revisions, 2018.

Conference Papers

[C1] Zhanwei Hou, Changyang She, Yonghui Li, and Branka Vucetic, "Ultra-Reliable and Low-Latency Communication: Prediction and Communication Co-design," submitted to 2019 IEEE International Conference on Communications (ICC), Shanghai, China, June, 2019.

[C2] Zhanwei Hou, Changyang She, Yonghui Li, Tony Quek, and Branka Vucetic, "Burstiness aware bandwidth reservation for uplink transmission in tactile internet," in Proc. of 2018 IEEE International Conference on Communications Workshop (ICCW), Kansas City, USA, June, 2018.

[C3] Zhanwei Hou, He Chen, Yonghui Li, Zhu Han, and Branka Vucetic, "Contract-based incentive mechanism for energy harvesting-based Internet of Things." in Proc. of 2017 IEEE International Conference on Communications (ICC), Paris, France, June, 2017.

[C4] Jiangnan Lin, Zhanwei Hou, Yiqing Zhou, Lin Tian, and Jinglin Shi, "MAP estimation based on Doppler characterization in broadband mobile LEO satellite communications," in Proc. of 2016 IEEE Vehicular Technology Conference (VTC Spring), Nanjing, China, July, 2016.

Chapter 1

Introduction

1.1 Industrial Internet of Things

The current industrial sectors are undergoing a tremendous change with the introduction of the Internet of Things (IoT), cyberphysical system (CPS) and Tactile Internet [1]. The previous three industrial revolutions are characterized by steam power, the use of mass production and electricity, automation and computing technology, respectively [2]. The latest trends influencing the traditional industrial sectors are IoT, CPS and the emerging Tactile Internet, which leads to a fourth industrial revolution, also referred to as "Industry 4.0" or "Industrial Internet of Things (IIoT)" or "Industrial Internet" [3]. Specifically, the term of "Industry 4.0" was originally developed in Germany and more focused on the aspects of the industrial revolution [4]. The terms of "Industrial Internet of Things" or "Industrial Internet" were coined much earlier in the United States, which addresses more on the enabling technology of the fourth industrial revolution [5]. In our work, we will not differentiate the subtle differences among these terms, but use the term "Industrial Internet of Things" instead.

Unlike the concept of IoT, the definition of IIoT is still an on-going process. There is no single widely-accepted definition of IIoT in academia and industry communities. According to the definition of General Electric (GE), the leading company in industrial automation, IIoT is *" the network of a multitude of industrial devices connected by communications technologies that results in systems that can monitor, collect, exchange, analyze, and deliver valuable new insights like never before,"* [6]. After reviewing a wide range of academic literature, authors in [7] provide a comprehensive definition of IIoT as follows.

"Industrial Internet of Things: A system comprising networked smart objects, cyber-physical assets, associated generic information technologies and optional cloud or edge computing platforms, which enable real-time, intelligent, and autonomous access, collection, analysis, communications, and exchange of process, product and/or service information, within the industrial environment, so as to optimise overall production value. This value may include; improving product or service delivery, boosting productivity, reducing labour costs, reducing energy consumption, and reducing the build to- order cycle,"[7].

Although there are various definitions of IIoT [6–9], which may be confusing sometimes, they all addresses the importance of communications in IIoT. Next, we will briefly review some major applications of IIoT [4, 10].

- *Manufacturing:* Sensors are used to monitor all kinds of activities during the manufacturing. This data are sent to an analytic center which can predict the possible failure of the system or other problems. Actions can be taken before the problem occurs. The concept can be extended to the cloud-control or edge-control. All data collected by the sensors can be sent to the edge or cloud,

and the corresponding actions can be executed automatically. By continuously monitoring the process values and environmental conditions, together with an intelligent data analytic tool, it will be continuously optimizing the production processes and products.

- *Power utility:* In the electric gird applications, operation parameters such as electrical voltage, current and phase are monitored. Together with other data such as the temperature of transformers, weather and power consumption, it will optimize the usage of the current gird system, which provides better stability and matches the production of consumption of electricity.

- *Transportation:* Intelligent traffic control systems can be used to monitor and control the traffic flow. The internet of vehicles can supports the information exchange among vehicles, so that the vehicles can cooperate with each other. Together with the self-driving system, the transportation can become more efficient and safer.

- *Healthcare service:* In healthcare service industry, all medical equipment, medicine and even humans can be monitored and tracked continuously. Due to the global connectivity capability, tele-diagnosis, tele-therapy, tele-surgery will be possible in combination with the haptic sense introduced by Tactile Internet. By collecting the personal data of health by mobile phones or wearable devices, the healthcare can be mobilized and personalized.

1.2 Communications for IIoT

In this section, we will introduce the history, the state-of-art and the role of 5G communications in IIoT.

1.2.1 Wired Industrial Communications

In the early stage of industrial communications, dedicated wired networks named "fieldbus" were used to replace the parallel cables between sensors, actuators, and controllers [11]. Various kinds of fieldbus are defined, most of which are very simple[12]. A typical fieldbus is a controller area network (CAN), which still exists in many applications of industrial communications. The big problem of a fieldbus system is the incompatibility with the Ethernet or IP based local area network (LAN), which becomes a great hurdle of the integration between the industrial network with external Internet.

When IP based Internet becomes popular and widely employed, a new wave of Ethernet-based networks emerges [13]. However, the standard Ethernet traditionally provides services in a best-effort way. The lack of real-time capability prevents the deployment of one singe Ethernet solution. Some modifications are made to improve the real-time capability of the standard Ethernet. Among these efforts, real-time Ethernet (RTE) is still a very active research area [14, 15].

Currently, RTE has become the standardization for wired communications for industrial automation, which are composed of some mutually incompatible implementations [3]. According to the real-time level and the efforts of modifications of the standard Ethernet protocol, there are three classes of RTE solutions [16]. The class A is realized on top of the transport layer and provides a cycle time in the order

of 100 ms. The class B is realized directly over the media access control (MAC) layer by using prioritization, which can provide a cycle time in the order of 10 ms. The class C modifies the MAC layer of Ethernet, which can provide a cycle time in the order of 1 ms.

1.2.2 Wireless Industrial Communications

The advantages of wireless connections for industrial communications are obvious, which get rid of the cables and provide greater flexibility. In many scenarios with mobility, or deployment in remote areas, toxic environment, underwater and so on, the wired communication is either costly or even impossible at all.

The current wireless industrial communication protocols are mainly modified from the existing IEEE 802 family [11]. Most of the wireless industrial communications protocols used now are based on IEEE 802.11, i.e., wireless local area network (WLAN) [17], or IEEE 802.15.4, i.e., wireless personal area network (WPAN) [18], or IEEE 802.15.1, i.e., Bluetooth [19]. The upper layers are modified to be compatible with the wired networks.

The main problem of these protocols is that the low latency and high reliability cannot be guaranteed due to the limitations of the best-effort nature of the IEEE 802 family working on competitive unlicensed spectrum.

1.2.3 The Role of 5G in IIoT

With low latency and high reliability integrated into the requirements of 5G, it will provide an unprecedented opportunity for revolutionizing the wireless industrial communications.

According to the vision of IIoT, the future industry will be organized in a distributed way by wirelessly connected factories, equipments, and products, and enhanced by collaborative robotics [4]. With the novel distributed organization, the production capability can be flexible and scalable, and the resources and infrastructure can be shared and reused; as a result, the capability of order fulfilments will be significantly improved. By providing mission critical connections and massive access capability, 5G will play a critical role in realizing the above vision.

Some possible solutions for ensuring the low latency and high reliability in 5G have been proposed in the existing literature [20–25]. The studies in [20] optimized packet scheduling scheme to maximize energy efficiency under the delay constraint, where the decoding error in short blocklength regime was considered. The throughput of a decode-and-forward relay system with limited blocklength was studied in [21], where effective capacity was applied in characterizing queueing delay. A framework for cross-layer optimization was proposed in [22], where the required maximal transmit power to ensure the latency and reliability requirements was minimized. To improve reliability, multi-path diversity was applied in [23]. The authors of [24] proposed a tactile data quantization scheme, and discussed how to reduce quantization errors. A grant-free uplink transmission scheme was proposed in [25] to avoid scheduling delay.

1.3 Research Problems and Contributions

There are two types of MTC supported by 5G [26–29]: one is ultra-reliable low-latency communications (URLLC) [30, 31]; the other is massive MTC (mMTC)[32]. In this work, we will focus on the designs, analyses and optimizations of wireless resources to achieve the stringent performance requirements of MTC in terms of

latency, reliability, spectrum usage and energy supply.

There are many challenges for MTC, such as ensuring ultra-reliable low-latency, spectrum scarcity, scalability of the network, energy and security issues. In this work, we mainly focus on some communication related challenges, which are summarized as follows.

- *Low Latency requirement:* The E2E delay is composed of uplink/downlink transmission delay, queuing delay, access delay, propagation delay and processing delay in local area communications within the range of several kilometers. The aim of 1 ms E2E delay in 5G is challenging to be met due to the complicated composition of delay [26]. In long distance communications, as suggested by the visions of cloud-controlling or global Tactile Internet, the E2E delay may also include the routing delay in backhauls and the core network, and the propagation delay in the communication range of hundreds or thousands of kilometers will be dominant. For example, the propagation delay alone in a distance of 300 km is 1 ms with the speed of light in vacuum of 3×10^8 m/s. As such, the requirement of 1 ms E2E delay seems even impossible to meet in long distance communications. As a result, it is challenging to achieve the ultra-low latency of 1 ms E2E delay requirement imposed by 5G.

- *High Reliability requirement:* The reliability is characterized by the packet loss probability, the components of which are closed related to the E2E delay. During the transmissions, packets may be lost due to dynamic channel conditions, which is named transmission error. Another component of packet loss results from the queueing delay violation [31]. When serving the randomly arriving packets with a highly dynamic wireless channel, the queueing delay violation probability is

challenging to be guaranteed to some certain threshold. The third component of packet loss may come from the collisions during the random access when the spectrum is shared by multiple users. In 5G, the ultra-high reliability of 99.999%, i.e., the packet loss probability of 10^{-5}, should be guaranteed [26]. As such, the above mentioned components of the packet loss should be in a smaller order, e.g., in the order of 10^{-6} or even lower. As a result, it is challenging to achieve high reliability in the low latency domain.

- *Spectrum shortage:* It is not an easy task to ensure ultra-reliable low-latency requirements for an E2E communication link, while it becomes more challenging considering that limited spectral resources shared by multiple devices need to be used to achieve the above goal. To ensure the ultra-high reliability requirement, different forms of diversities should be introduced. By introducing diversities, the reliability is improved at the cost of reduced resource utilization efficiency and thus more spectrums are required. Together with the exponentially increase of IIoT devices, the limited spectrum will be a great hurdle for wide applications of IIoT.

- *Energy supply limitations:* With the capability of wireless communications in IIoT, the cables for communications can be removed and thus high flexibility can be achieved. However, to reap the benefits from wireless connections, the cables for energy supply should also be removed, and thus batteries will become the state-of-art solutions for energy supply of devices in IIoT instead. Along with the rapid growth of IIoT applications, the energy consumption of IIoT devices has also increased exponentially [33]. As such, the limited capability of IIoT device batteries is always a long-standing problem in IIoT, and continues

to be a critical bottleneck of the future IIoT.

The above mentioned challenges cannot be addressed independently, because these factors are affected by each other. To satisfy the ultra-low E2E delay requirement, some techniques have been applied to reduce latency in the existing literature, such as using "mini-slot" in 5G New Radio (NR) to reduce the transmission delay [34] and grant-free access to reduce the access delay [35]. However, these approaches greatly degrade the reliability performance of the system when reducing the latency. To improve the reliability in the short delay regime, different kinds of diversities are introduced, such as time and frequency diversities (e.g., K-repetition with frequency hopping [31, 36]), spatial diversity (e.g., massive MIMO [37]), and multi-connectivity [38, 39]. By introducing diversities, the reliability is improved at the cost of reduced resource utilization efficiency. Since the spectral resources shared by multiple devices for communications are quite limited, *achieving the E2E delay and reliability requirements with affordable spectral resources and limited energy supplies is very challenging, especially in the long distance communications.*

To tackle these challenges, we will investigate three research problems, which are briefly summarized as follows.

- The first research problem (Chapter 3) is how to minimize the bandwidth reservation to ensure the stringent latency (i.e., 1 ms E2E delay) and reliability (i.e., 10^{-5} packet loss probability) requirements in a local area network, which addresses the delay and packet loss during the packet transmission, queueing, and random access in the radio access network.

- The second research problem (Chapter 4) extendes to the long distance communications, which further includes the propagation delay and routing delay

resulting from the backhauls and the core network, i.e., in the order of tens of milliseconds. In this scenario, we will study whether we can still achieve the ultra-low latency (i.e., 1 ms E2E delay) and ultra-high reliability requirements, and how we can achieve the requirements by using predictions.

- The third research problem (Chapter 5) addresses the issue of limited battery capabilities. Third-party chargers are introduced to charge the IIoT devices wirelessly by using radio frequency energy harvesting. We will study how to design effective incentive mechanisms to ensure the cooperation of the third party chargers, as well as to maximize the social welfare.

Along with the research problems, the corresponding contributions are listed as below.

1.3.1 Burstiness Aware Bandwidth Reservation for URLLC of Local Area Network in IIoT

As we mentioned above, ensuring URLLC with limited bandwidth is crucial for local area network in IIoT. In this work, we focus on the Tactile Internet, which enables the transmission of tactile sense in IIoT [40]. There are many potential applications of Tactile Internet in IIoT, such as intelligent robotic grasping, precision remote control and human-machine collaborations, which will enable the skill-set delivery network in IIoT [41]. Recent studies found that the packet arrival processes in Tactile Internet are very bursty [42]. This observation enables us to design a spectrally efficient resource management protocol to meet the stringent delay and reliability requirements while minimizing the bandwidth usage. In this work, both

model-based and data-driven unsupervised learning methods are applied in classifying the packet arrival process of each user into high or low traffic states, so that we can design efficient bandwidth reservation schemes accordingly. However, when the traffic state classification is inaccurate, it is very challenging to satisfy the ultra-high reliability requirement. To tackle this problem, we formulate an optimization problem to minimize the reserved bandwidth subject to the delay and reliability requirements by taking into account the classification errors.

To the best knowledge of the authors, this is the first work for exploiting burstiness to optimize bandwidth reservation for URLLC in Tactile Internet for IIoT. The main contributions of this research problem include:

- We establish a cross-layer framework for designing burstiness-aware bandwidth reservation for UL transmission of URLLC in Tactile Internet of IIoT, where multiple delay components and packet loss factors resulting from queueing, short packet transmissions, and random access, are taken into account. The bandwidth reservations are optimized for users classified into high and low traffic states subject to the UL delay and reliability requirements.

- Two types of classification methods are applied in traffic state classification: a model-based Neymman Person (N-P) method [43] and a data-driven unsupervised learning method, i.e., k-means method [44]. Experiment results show that if the traffic model is inaccurate, the data-driven method outperforms the model-based method.

- The traffic state classification errors are taken into account when we design transmission schemes and optimize bandwidth reservations. Simulation results

show that with around 10^{-2} classification error probability, our method can achieve 10^{-5} packet loss probability. Meanwhile, 40% to 70% bandwidth can be saved compared with the baseline method.

1.3.2 Prediction based Bandwidth Optimization for URLLC of Long Distance Communications in IIoT

Next, we extend the scenario from local area network to long distance communications in IIoT. The long distance communications will allow the skill-set delivery globally. For example, the technical support teams located in different continents can work synchronously and seamlessly for a factory located in another continent. As we mentioned before, it is very challenging to satisfy the ultra-low E2E delay requirements in long distance communication scenarios since the delay in backhauls and core networks could be tens of milliseconds. In this work, we aim to reduce the latency experienced by users by prediction and communication co-design, where the transmitter predicts its future states and sends them to the receiver in advance. Considering that the prediction is not error free, we take prediction errors and the packet loss in communications into account when analyzing the reliability of the system. Then, we formulate an optimization problem that minimizes the required bandwidth to satisfy the E2E delay and reliability requirements of URLLC. With our method, it is possible to achieve zero latency when the prediction time equals to the communication delay. Although there are some research using prediction in URLLC [40, 45–51], they did not quantitatively co-design communication and predictions taking account of the prediction errors. To our best knowledge, this is the first work to quantitatively co-design communication and predictions for URLLC. The main contributions of this

research problem include:

- We establish a co-design framework of communication and prediction, where the future system states, such as locations and forces, are predicted and sent to the receiver in advance. In this way, the experienced delay can be reduced.
- We first derive the relationship between prediction error and prediction time in closed-form. Then, we analyze the relationship between packet loss probability, bandwidth usage and end-to-end communication delay. Based on these results, we formulate an optimization problem to minimize the required bandwidth for ensuring the delay and reliability requirements. By using the proposed algorithm, we can achieve zero user experienced delay for both local and long distance communication scenarios.
- Simulation results verify the effectiveness of the proposed method, and show that the tradeoffs among bandwidth, reliability, and latency can be fundamentally improved with prediction and communication co-design. The results are further evaluated by practical motion data acquired from experiments by a real hardware device.

1.3.3 Incentive Mechanism Design for Wireless Energy Harvesting-Based IIoT

In our third work, we address the issue of limited battery capabilities, the long standing bottleneck for IIoT. Radio frequency energy harvesting (RFEH) is a promising technology to charge unattended IIoT low-power devices remotely. To enable this, in future IIoT system, besides the traditional data access points (DAPs) for collecting

data, energy access points (EAPs) should be deployed to charge IIoT devices to maintain their sustainable operations. Practically, the DAPs and EAPs may be operated by different operators [1], and the DAPs thus need to provide effective incentives to motivate the surrounding EAPs to charge their associated IoT devices. Different from existing incentive schemes, we consider a practical scenario with asymmetric information, where the DAP is not aware of the channel conditions and energy costs of the EAPs. We first extend the existing Stackelberg game-based approach with complete information to the asymmetric information scenario, where the expected utility of the DAP is defined and maximized. To deal with asymmetric information more efficiently, we then develop a contract theory-based framework, where the optimal contract is derived to maximize the DAP's expected utility as well as the social welfare. To the best knowledge, this is the first work that systematically studies the RFEH-based IoT system under asymmetric information. The main contributions along with this research problem are summarized as follows.

- We develop the framework of RF energy trading in the RFEH-based IIoT system and systematically design the incentive mechanisms for a practical scenario with asymmetric information.

- To explore the performance degradation due to lack of full information, we first extend the existing Stackelberg game-based approach to the considered case

[1]Since the RFEH is still in its infant stage, it is highly likely that some specialized energy harvesting service operators will emerge in the future market during the process of commercialization. These operators are specialized in the wireless energy harvesting technology and own the necessary licensed spectrum for wireless energy transfer. They could originate from the traditional telecom companies as well as from incumbent energy corporations. These operators can provide wireless energy charging services for the existing telecom operators and act as third-party operators like EAPs competing with each other in the radio frequency energy trading market considered in the work.

without instantaneous channel condition and energy costs of the EAPs by optimizing the expected utility function of the DAP. As the contract theory [52] is a powerful economic theory for designing incentive mechanism with asymmetric information, we then reformulate the problem by using the contract theory. In our contract design, we characterize the necessary and sufficient conditions for the contract feasibility, i.e, individual rationality (IR) conditions and incentive capability (IC) conditions [52]. Subject to the IR and IC constraints, the optimal contract under information asymmetry is achieved by maximizing the DAP's expected utility as well as the social welfare.

- To compare the performance of the proposed contract theory-based approach using asymmetric information with that of the existing Stackelberg game-based method with complete information, we generalize the existing Stackelberg game formation with unified pricing to the case with discriminative pricing and derive the new Stackelberg equilibrium in closed-form. Here discriminative pricing means that we set different energy prices for different EAPs to fully exploit their potentials for the enery charging service. Numerical simulation results show that information asymmetry can lead to severe performance degradation for the Stackelberg game-based framework, while the proposed contract theory-based scheme using asymmetric information outperforms the Stackleberg game-based approach with complete information. This implies that *the performance of the considered system depends largely on the market structure (i.e., whether the EAPs are allowed to optimize their received power at the IoT devices with full freedom or not) than on the information availability (i.e., the complete or asymmetric information).*

Chapter 2

Preliminaries

In this chapter, we will provide some preliminary information on the mathematical tools used in the analyses and optimizations in the thesis.

2.1 Short Packet Communications

In this thesis, short packet transmissions are considered in the physical layer. This is because the packets produced by sensors or controllers are generally small (e.g., 32byte or even smaller [26]), which is the typical traffic type exchanged in the wireless communications of IIoT. It is fundamentally different from the long packet communications in a traditional LTE system. As such, new tools from the information theory society need to be introduced to accurately characterize the relationship among rate, reliability and packet length.

In communications, the channel coding process is to map information (bits) into continuous-time signal, which is usually expressed in complex signal with real and imagine parts. The continuous-time signal can be characterized by the multiplications of the approximate bandwidth B and transmission duration D, which is the number of degrees of freedom (i.e., channel uses) to convey certain coding block. So $BD \approx$

N_{BL} is also referred to as packet length, or blocklength. We thus define the short packet more accurately by using the terminology "channel uses", which is from the societies of information theory and coding theory [53]. By using this, short packet communications refer to the communications with small blocklength.

2.1.1 Shannon Capacity

Before touching the details of short packet communications, we first start from the Shannon capacity. Shannon capacity is an asymptotic result in infinite blocklength, which is accurate in the long packet length range. To better understand this, we first define Shannon capacity from information theory and then relate it with the form used in wireless engineering.

In information theory, the rate R_1 (bits per block) is usually defined as b/N_{BL}, which is the fraction of information bits b to the blocklength N_{BL}. The aim of a communication system is to achieve a larger rate R_1 with a small packet error probability ε_{BL}, and thus $R_1^*(N_{BL}, \varepsilon_{BL})$ is defined as the largest rate at blocklength N_{BL} with a packet error probability equal to or less than ε_{BL}, and the corresponding largest information bits is b^*.

The Shannon capacity is defined as the largest rate R_1 so that there is some coding scheme whose packet error probability can be arbitrarily small by using large enough blocklength [54]. In information theory, the Shannon capacity of an addictive white Gaussian noise (AWGN) channel with a certain signal-to-noise ratio (SNR) γ can be defined as

$$C_1 = \lim_{\varepsilon_{BL}\to 0, N_{BL}\to\infty} R_1^*(N_{BL}, \varepsilon_{BL}), \tag{2.1.1}$$

which is given by

$$C_1 = \frac{b^*}{N_{BL}} = \frac{b^*}{BD} = \log(1+\gamma) \quad (bits/block). \tag{2.1.2}$$

Equally, (2.1.3) can be transformed into another form, which is widely used in wireless engineering as follows,

$$C_2 = \frac{b^*}{D} = B\log(1+\gamma) \quad (bits/second). \tag{2.1.3}$$

2.1.2 Achievable Rate of Short Packet

In the short blocklength range, the Shannon capacity is no longer accurate. This can be explained intuitively [53]. As we mentioned before, a channel code is the mapping from information bits to the signal over N_{BL} channel uses. During transmission in the wireless channel, the received signal suffers from noises and distortions. The receiver is to recover the transmitted information bits from the received signal. The Shannon capacity suggests that when the packet length N_{BL} is large, b^* information bits can be recovered with an arbitrarily small error probability. When packet length is large, the distortions and noisy effects can be averaged out according to the law of large numbers. However, in short packet length, the averaging is no longer effective.

To achieve the accurate capacity for short packet, the expression of $R_1^*(N_{BL}, \varepsilon_{BL})$ should be derived. However, it is an N-P hard problem with complexity increasing with N_{BL} doubly exponentially [55]. Alternatively, [56] provides an approximation of the largest achievable rate for short packet as follows,

$$R_1^*(N_{BL}, \varepsilon_{BL}) = \frac{b^*}{BD} \approx C_1 - \sqrt{\frac{V}{N_{BL}}} f_{\mathrm{Q}}^{-1}(\varepsilon_{BL}) \quad (bits/block), \tag{2.1.4}$$

where $V = 1 - (1+\gamma)^{-2}$ is channel dispersion (see Def. 1 in [56]), $f_{\mathrm{Q}}^{-1}(\cdot)$ is the inverse function of the Q-function $f_{\mathrm{Q}}(x) = \int_x^\infty \frac{1}{\sqrt{2\pi}} e^{-t^2/2} dt$. $\gamma = \frac{\alpha g P_{\mathrm{t}}}{\phi N_0 B}$ is the SNR,

where α denotes the large-scale channel gain, g is the small-scale channel gain with the probability density function $f_g(x) = \frac{1}{(N_\mathrm{r}-1)!}x^{N_\mathrm{r}-1}e^{-x}$, i.e., Rayleigh fading, P_t is the transmission power, N_r is the number of received antenna, $\phi > 1$ presents the signal-to-noise ratio loss due to inaccurate channel estimation at the BS, and N_0 is the noise power spectral density.

The approximation in (2.1.4) suggests that to ensure a certain packet loss probability ε_{BL} with a finite packet length N_{BL}, there is an extra penalty on the Shannon capacity. From (2.1.4), we can derive the relationship between the average packet loss probability $\bar{\varepsilon}_{BL}$ and transmission duration D in closed-form as follows,

$$\bar{\varepsilon}_{BL} \approx \int_0^\infty f_\mathrm{Q}\left\{\sqrt{\frac{DB}{V}}\left[\ln\left(1+\frac{\alpha g P_\mathrm{t}}{\phi N_0 B}\right) - \frac{b^* \ln 2}{DB}\right]\right\} f_g(x)dx. \tag{2.1.5}$$

2.2 Traffic State Classifications

We will first define the problem of traffic state classification and then introduce the model based method and data driven method to solve it.

Definition 2.2.1 (**Traffic State Classification**)**.** We have a sample ℓ, which is the number of arriving packets for a total time duration of T_w continuous time slots. It is assumed that within the T_w continuous time slots, the traffic state is not changed. The problem of traffic state classification is to determine whether the current sample ℓ is taken from the high arrival rate state or the low state.

Based on the definition of the traffic state classification, there are two kinds of errors: classifying a user with the low traffic state as high, and classifying a user with the high traffic state as low. In URLLC, the former kind of error leads to conservative bandwidth reservation, while the latter kind of error leads to packet loss or long delay,

i.e., the quality of service (QoS) requirements will be violated due to this kind of error. These two types of errors are unavoidable but can be traded off against each other by designing proper algorithms.

To address this issue, we will introduce the model based method from signal detection and the data driven method from machine learning.

2.2.1 Signal Detection - Model based Method

Signal detection theory is fundamental to design an electronic information system [43], such as radar, communications, control, etc. In a radar system, we are interested in detecting the presence of an approaching plane. In a communication system, signal detection theory is used to detect the received waveform representing information bit of "1" or "0", which is usually distorted by the noise and dynamic wireless channel. In a control system, it is used to detect the occurrence of an abrupt change in the system state to be controlled.

To tackle the problem of traffic state classifications, we utilized N-P method [43] to classify the traffic, where the probability of classifying a user with high traffic state as low is bounded by a threshold. Following the N-P method, we can assume:

H_0: the sample is taken from high traffic state,

H_1: the sample is taken from low traffic state,

where H_0 is the null hypothesis and H_1 is the alternate hypothesis.

A detector is to decide either H_0 or H_1 based on observed samples. This can be regarded as a mapping from each sample ℓ to a decision. In particular, let D_0 be the set of samples that map into the decision H_0, defined as

$$D_0 = \{\ell : decide\ H_0\}. \tag{2.2.1}$$

Similarly, let D_1 be the set of samples that map into the decision H_1, defined as

$$D_1 = \{\ell : decide\ H_1\}, \tag{2.2.2}$$

and D_1 is the complement set of D_0. We have $D_0 \cap D_1 = \varnothing$ and $D_0 \cup D_1 = \mathcal{N}$ since D_0 and D_1 partition the set of all natural numbers $\mathcal{N}$.

The likelihood ratio is defined as

$$\Gamma(\ell) = \frac{P(\ell|H_1)}{P(\ell|H_0)}. \tag{2.2.3}$$

In N-P detection, the relationship between the likelihood ratio and a threshold γ_t is used as the criterion to the division of D_0 and D_1. The design of a N-P detector is mainly to design the optimal threshold γ_t of the likelihood ratio.

Using the above definitions, the probability of false alarm is defined as $P_{\mathrm{f}} = P(D_1|H_0)$, the probability of missing detection rate is defined as $P_{\mathrm{s}} = P(D_0|H_1)$, and the probability of detection rate is defined as $P_{\mathrm{d}} = P(D_1|H_1)$.

According to N-P method [43], the probability of successful detection is maximized with the constraint of certain probability of false alarm. Therefore, we have the optimization problem as follows:

$$\begin{aligned} (\mathbf{P1}): \quad & \max_{\gamma_t} P_{\mathrm{d}} \\ s.t. \quad & P_{\mathrm{f}} \leq \varepsilon^{\mathrm{f}} \end{aligned} \tag{2.2.4}$$

where γ_t is the threshold of the likelihood ratio, and ε^{f} is the threshold of false alarm probability.

Instead of solving Problem P1 directly, we first solve the following Problem P2.

$$\begin{aligned} (\mathbf{P2}): \quad & \max_{\gamma_t} P_{\mathrm{d}} \\ s.t. \quad & P_{\mathrm{f}} = \varepsilon^{0} \end{aligned} \tag{2.2.5}$$

where $\varepsilon^0 \leq \varepsilon^{\mathrm{f}}$, and we will explain later how to choose ε^0.

According to [43], the threshold of the likelihood ratio of N-P method for Poisson

distributions with parameters λ_H and λ_L is given by

$$\begin{aligned}\Gamma_\ell &= \frac{P(\ell|H_1)}{P(\ell|H_0)} \\ &= e^{(\lambda_H-\lambda_L)}\left(\frac{\lambda_L}{\lambda_H}\right)^\ell\end{aligned} \tag{2.2.6}$$

or equally

$$\ell \leq \frac{\ln(\gamma_t)-(\lambda_H-\lambda_L)}{\ln(\lambda_L)-\ln(\lambda_H)} \triangleq \hat{\ell}. \tag{2.2.7}$$

When $\Gamma(\ell) \geq \Gamma_\ell$, it is classified as D_1, i.e., low traffic state. When $\Gamma(\ell) < \Gamma_\ell$, it is classified as D_0, i.e., high traffic state.

So we can rewrite the probability of false alarm as

$$\begin{aligned}P_{\mathrm{f}} &= \sum_{R_1} P(\ell|H_0) \\ &= P\left(\Gamma(\ell) \geq \gamma_t|H_0\right) \\ &= P\left(\ell \leq \hat{\gamma}_t|H_0\right).\end{aligned} \tag{2.2.8}$$

Note that under the condition of H_0, it is assumed that ℓ follows Poisson distribution with average arrival rate of λ_H. P_{f} in (2.2.8) is the Poisson cumulative distribution function (CDF) with λ_H. To solve $P_{\mathrm{f}} = \varepsilon^{\mathrm{f}}$, we actually solve the inverse function of the above CDF function. We will find the largest $\hat{\ell}$ to make sure that CDF $\varepsilon^0 \leq \varepsilon^{\mathrm{f}}$. Accordingly, the successful detection rate can be calculated as

$$\begin{aligned}P_{\mathrm{s}} &= \sum_{R_0} P(\ell|H_1) \\ &= P\left(\varepsilon^{\mathrm{f}} > \hat{\ell}|H_1\right) d\gamma_t.\end{aligned} \tag{2.2.9}$$

It should be noted that in Poisson distribution, we only need to take one sample in the sample window, instead of multiple samples. This is because the sum of multiple samples from independent Poisson distribution is also a Poisson distribution. The average arrival rate of new Poisson distribution is the sum of those of independent Poisson distributions.

2.2.2 Machine Learning - Data Driven Method

When the traffic model is unavailable, data-driven machine learning methods can be used [44]. Machine learning originated from pattern recognition, which enables machines to improve automatically with experience [57]. There are generally four types of learning approaches: supervised learning, unsupervised learning, semi-supervised learning, and reinforcement learning.

In machine learning, training is to construct the potential relationship between input and output [58]. Supervised learning algorithms are trained with labeled data, where the inputs and desired outputs are known to the algorithms. Supervised learning is used in the scenario when labels are available. In computer vision, the labeling is a time consuming process with great costs. Unsupervised learning algorithms are trained with unlabeled data, the purpose of which is to explore some data structure directly from the unlabeled data, e.g., clustering. Semi-supervised learning is used when both labeled and unlabeled data are available. Reinforcement learning is not trained from previous data, instead, it is trained by the data when using it. The aim of reinforcement learning algorithms is to learn an environment and find the best strategies.

Considering that the labels of training data are not available at the BS, supervised learning methods cannot be applied. In contrast, the k-means method is an effective unsupervised learning method that can be applied without the labels of training data. In this part, we will show how to apply the k-means method in traffic state classification.

First, the k-means method is trained by historical arrival processes, i.e., $\mathcal{K} = \{\ell_1, \ell_2, \cdots, \ell_{K_\mathrm{s}}\}$, which denotes the number of packets arriving in each of K_s sample

windows. The target of the k-means method is to partition the input data into a certain number of clusters. According to the real packet arrival processes in [42], we assume that there are two clusters, which means that there are two traffic states.

With k-means clustering method, we need to find a centroid of each cluster. We assume that that $k = 2$ clusters exist, and denote the centroids as $\nu_j, j = \{1, 2\}$, which are randomly selected initially. Then, the algorithm proceeds by iteratively running the following two steps until each of the centroid is convergent and does not change.

Classifying step: In this step, we classify training data according to their distances to each of the centroid. Let $c_i \in \{1, 2\}$ be the cluster index of ℓ_i. If the c_ith centroid is the nearest one to ℓ_i, then k_i is classified in the c_ith cluster, i.e.,

$$c_i = \arg\min_j ||\ell_i - \nu_j||^2. \tag{2.2.10}$$

for all $i = 1, ...K_\mathrm{s}$, and $j = 1, 2$.

Updating centroid step: In this step, we update the location of each cluster centroid according to the following expression,

$$\nu_j = \frac{\sum_{i=1}^{K_\mathrm{s}} \mathbf{1}\{c_i = j\}\, \ell_i}{\sum_{i=1}^{K_\mathrm{s}} \mathbf{1}\{c_i = j\}}, \tag{2.2.11}$$

where $\mathbf{1}\{c_i = j\}$ is an indicator function. If ℓ_i is classified in cluster j, then $\mathbf{1}\{c_i = j\} = 1$. Otherwise, $\mathbf{1}\{c_i = j\} = 0$. So (2.2.11) is the mean of the data classified into the jth cluster.

After the training process, we obtain two centroids ν_1^* and ν_2^* that will be used to classify traffic state according to (2.2.10).

It is possible to further reduce classification error probability by applying more advanced machine learning algorithms, which deserves further study [44]. However,

the performance limit of the classification accuracy is determined by the data. If the data in the two clusters are partly overlapped, classification errors are unavoidable.

2.3 Contract Theory

Contract theory is some mathematical tools developed in the economic society, which is within the scope of the theory of incentive and the economics of information [52]. Many key contributors to this theory have been awarded with the Nobel prize in economics, including Oliver Hart and Bengt Holmstrom in 2016, Jean Tirole in 2014, James A. Mirrlees in 1995, which is still an active research field in economics [59, 60]. There are two kinds of problems studied in contract theory: one is hidden-information problem, and the other is hidden-action problem [52]. The former problem is also referred to as adverse selection problem, where the employee has some private information in terms of their capability or willingness to do certain task. However, this information is hidden from the employer. The latter problem is also referred to as moral hazard problem, where the employer cannot observe the actions of the employees. For example, the employer cannot know exactly in practice how hard an employee worked. In this case, the employee's action is hidden from the employer. In this thesis, we are mainly interested in the adverse selection problem, i.e., hidden information.

Contract theory can be used to study the interactions between employer and employee. In a typical scenario, the employer is in a monopoly status. There is some private information for the employees, such as their capabilities or preferences for work, which is called information asymmetric. This information is generally unknown to the employer. To maximize the employer's utility and the social welfare as well, the

employer will provide a group of contract items for the employee to choose from. For the employee, it will choose the contract item maximizing its utility, which suggests that the employee will only accept the contract item when the benefits it gets should be larger than the efforts it pays. This is called individual rationality. The key idea of contract theory is to impose the incentive compatibility constraints in the designed contract items, which will maximize the employee's utility only when it chooses the contract item design for its type of private information.

Due to its effectiveness in design incentives under information asymmetry, contract theory has been employed to address incentive design problems in wireless communication areas, such as mobile edge computing [61], device-to-device (D2D) communications [62] and cooperative spectrum sharing [63]. In [61], contract theory is used to design incentive mechanism in a distributed caching system relying on small-cell base stations (SBSs). The network service provider is the monopolist in charge of the SBSs. The content providers would like to rent these SBSs from the network service provider. The network service provider is not aware of the exact popularity status of each content provider, i.e., information asymmetry. As such, a contract is designed to overcome the information asymmetry and thus maximize the utility of the network service provider. In [62], contract theory is used to motive the cooperation of D2D communication users, where the user's preference to D2D communications is unknown to the BS, i.e., information asymmetry. In [63], cooperative spectrum sharing is considered, where the secondary user's wireless channel condition is its private information, which is not aware of the primary user. To overcome the information asymmetry, contract theory is used to design a group of contract items, which are combinations of spectrum accessing time (reward) and relaying power (efforts).

Chapter 3

Burstiness Aware Bandwidth Reservation for URLLC of Local Area Network in IIoT

3.1 Chapter Introduction

With ultra-reliable and low-latency connectivity, Tactile Internet enables delivering real-time control and tactile feedback in both human-to-human and human-to-machine communications for IIoT [40]. Typical applications include intelligent robotic grasping, precision remote control and human-machine collaborations [41]. To provide satisfactory user experience, the latency of tactile feedback should be around 1 ms [64]. For some remote control applications, achieving ultra-high reliability is crucial [40]. As a result, one of the key challenges of Tactile Internet in IIoT is how to achieve URLLC, e.g., 1 ms E2E delay and 10^{-5} packet loss probability [40]. In this chapter, we mainly focus on a local area network, i.e., the communication between multiple IIoT devices with a local base station.

The traditional uplink (UL) multiple access protocols are based on request-and-grant mechanism. The users first need to transmit a scheduling request and then

wait for the scheduling grant from the base station. This process introduces significant delay and cannot meet the stringent latency requirement of Tactile Internet. An effective solution to reduce latency is to pre-reserve a certain amount of bandwidth for delay-sensitive users, so that they can transmit their data immediately on the bandwidth reserved for them whenever they have the data to send without going through the time-consuming scheduling request and grant process [65]. The bandwidth reservation was originally designed for VoIP services, where the transmission rate is generally fixed and known in advance. However, the packet arrival process of Tactile Internet is completely different and very bursty, i.e., the high traffic state with the peak packet arrival rate occurs aperiodically [42]. This uncertain traffic arrival rate makes the bandwidth reservation very challenging. This is because reserving dedicated bandwidth for all users regardless of their real packet arrival rate will result in low resource usage efficiency.

Motivated by the above issues, we classify a packet arrival process of Tactile Internet into high and low traffic states, and investigate their statistic properties, based on which we then design the corresponding bandwidth reservation and transmission. By sharing the reserved bandwidth among users in a low traffic state, instead of reserving dedicate bandwidth for all users regardless of their traffic states, we can achieve efficient bandwidth utilization. The major challenge is that we cannot sacrifice latency and reliability to achieve high bandwidth utilization. Specifically, we will answer the following questions in this chapter: 1) Is it possible to ensure ultra-high reliability (i.e., 10^{-5} packet loss probability) when the traffic state classification is inaccurate (e.g., 10^{-2} classification error probability)? 2) If yes, how to design transmission

schemes and optimize bandwidth reservations when taking into account the burstiness properties of traffic and the classification errors? 3) How much bandwidth can be saved by exploiting burstiness characteristics of traffic while guaranteeing ultra-low latency and ultra-high reliability required?

It is challenging to answer the above questions, because a variety of delay components and packet loss factors should be considered, resulting from queueing [21], short packet transmissions [66], and random access [25]. Specifically, the delay components might include queueing delay, transmission delay, and access delay. The packet loss factors might include delay violations in queueing, decoding errors, collisions in random access, and classification errors. As such, we need a cross-layer design framework that takes different delay components and packet loss factors into consideration, especially the classification errors and their impacts on the packet loss probability. However, such a framework is still missing in the existing literature.

To address the above challenge, we will design and optimize bandwidth reservation for users in high and low traffic states subject to the delay and reliability constraints of all users, by taking into consideration the traffic state classification errors.

Recent studies in [42] indicated that the traffic of Tactile Internet is very bursty. The methods in [20, 21, 23–25] did not take burstiness into account in their resource allocation design. Although the effective bandwidth of some bursty arrival processes was used in resource allocation [22], the reserved resources were not adjusted according to traffic states. In a most relevant reference [42], the authors designed a radio access protocol in control-plane that was aware of burstiness. How to classify traffic states in computing systems and cognitive radio networks were studied in [67] and

[68], respectively. Since [67] and [68] did not consider URLLC, the impacts of classification errors on the reliability were not analyzed. Therefore, it is still not clear how to leverage burstiness in the data-plane for more effective URLLC design of tactile communications.

3.2 System Model and QoS Requirements

A Tactile Internet system is composed of three parts: the master device, the network domain and the slave device [40, 41, 64]. The master device is a tactile device, which converts human inputs to tactile inputs via various coding schemes and sends them to the network domain. The network domain couples the human to the remote environment and a local BS is considered in this chapter as the network domain. The slave device is a teleoperator, which interacts with various objects in the remote environment. The master device sends control commands (e.g., 3D locations and velocity of the joints) to the slave device and gets feedback (e.g., force or torques) from it.

In this chapter, we focus on the UL transmission in the air interface between N single-antenna tactile users and a BS with N_{r} antennas.[1] Our goal is to minimize the required bandwidth of URLLC by designing transmission schemes and optimizing bandwidth reservation.

[1]How to jointly design UL and downlink (DL) delay components has been studied in [69] and will not be discussed in this chapter.

3.2.1 Burstiness of Traffic

As observed in [42] and the references therein, burstiness is one of the major features of the packet arrival processes in Tactile Internet. Intuitively, the burstiness of Tactile Internet can be explained by the behavior of tactile sense. In most applications of Tactile Internet, the intense force feedback only happens when the slave device touches the surface of an object. Otherwise, the slave device just needs to send few short packets to inform the BS that it is associated with the BS. For the control commands from the master device, it only needs to update its real-time locations and velocity to the BS when it is moving. When it is static, the packet rate is very low. As a result, the packet arrival rate of a moving master device is much higher than a static one. Considering that the burstiness of the packet arrival processes of some applications in Tactile Internet may not be very high, we will illustrate the required bandwidth of the proposed methods with various burstiness levels in our simulations.

In the considered system, time is discretized into slots. The duration of each slot is denoted as T_{s}. The burstiness of the packet arrival process is characterized by the squared coefficient of variation (SCV), which is defined as $I_{\mathrm{s}} = \sigma^2/\nu$, where σ^2 and ν are the variance and the mean of the number of packets arriving within a slot, respectively [70]. The burstiness of an arrival process increases with SCV. As such, we will use burstiness and SCV interchangeably hereafter.

To capture the burstiness of the arrival process in Tactile Internet, we use the switched Poisson process (SPP), including a high traffic state and a low traffic state, in our model-based method [71]. In each state of SPP, the packet arrival process is a Poisson process with an average packet arrival rate λ_{H} (i.e., high traffic state) or λ_{L} (i.e., low traffic state). The durations of high and low traffic states follow exponential

distributions with the average durations μ_{H} and μ_{L}, respectively.

It is worth noting that for Tactile Internet, there is no well-established traffic model. SPP is a widely adopted model that can characterize the burstiness and the auto-correlation of a packet arrival process. When the model of the packet arrival process is unavailable, a data-driven method will be applied, and the burstiness can be estimated by calculating I_{s} from the historical packet arrival processes.

3.2.2 QoS requirements

We use a delay bound and a packet loss probability to characterize the UL delay and reliability requirements, i.e., $(D^{\mathrm{u}}, \varepsilon^{\mathrm{u}})$.

In the high traffic state, the packet arrival rate of each user can be higher than 1000 packets/s [41], so that the inter-arrival time between packets may be less than the delay bound requirement, i.e., 1 ms. As a result, there is a queue in the buffer of each user. Let D^{q} and D^{t} be the queueing and transmission delays, respectively. Then, the delay components should satisfy

$$D^{\mathrm{q}} + D^{\mathrm{t}} \leq D^{\mathrm{u}}. \tag{3.2.1}$$

For users in the low traffic state, the inter-arrival time between packets is much longer than the delay bound requirement. As a result, there is no queue at the user's buffer, and a user may stay silent for a relatively long time between the transmissions of two packets. To improve bandwidth usage efficiency, a resource pool is shared by all the users in the low traffic state. When a user has a packet to transmit, it randomly selects some time/frequency resources in the resource pool. To ensure the ultra-high reliability and avoid feedback overhead, M-Repetition scheme in [36] is applied, with which a packet is transmitted multiple times repetitively without acknowledgment

from the BS.[2] To exploit the frequency-diversity gain, and to avoid continuous transmission collisions, frequency-hopping is adopted. With frequency-hopping, different repetitions of one packet select different frequency resources randomly. Let D^{r} be the duration of each repetition, and M be the number of repetitions. Then, the delay requirement can be satisfied with the following constraint,

$$MD^{\mathrm{r}} \leq D^{\mathrm{u}}. \tag{3.2.2}$$

The factors that lead to packet loss depend on traffic states and bandwidth reservation schemes, which will be discussed in Section 3.4.

3.3 Traffic State Classification

Different users are assigned with orthogonal pilots for user detection and channel estimation at the BS [72]. When there are transmission collisions, the BS knows which users were sending packets according to their orthogonal pilots.[3] Besides, from the number of pilots, the BS knows how many packets were transmitted from users.

The BS classifies the packet arrival process of each user based on the number of packets arriving in the past sample window. As illustrated in Fig. 3.1, a sample window is defined as the past T_{w} slots. The number of packets arriving in the past sample window is referred to as a sample and is denoted as ℓ. The BS classifies a user in the high or low traffic states from ℓ. A prediction window follows the sample window. According to [42] and our experiment in Section 3.6-B, the durations of high

[2] In [36], the repetition scheme is referred to as K-Repetition. However, we will use the k-means method in our work. To avoid abuse of notations, the repetition scheme is referred to as M-Repetition.

[3] We assume that some time-frequency resources are reserved for pilots. How to optimize pilot overhead has been studied in [73], and will not be discussed in this work.

and low traffic states are in the order of hundreds of milliseconds. So we assume that the total duration of the sample window and the prediction window is much smaller than the average duration that a user stays in each traffic state. As such, the traffic state does not change within the adjacent sample and prediction windows.

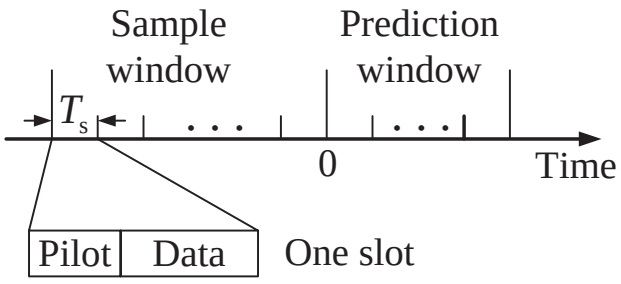

Figure 3.1: Illustration of sample and prediction windows.

3.3.1 Model-based Method

When the parameters of SPP are available, model-based methods are applicable. It should be noted that there are two types of errors from traffic state classification: classifying a user with low traffic into the high traffic state, and classifying a user with high traffic into the low traffic state. In URLLC, the first kind of error leads to conservative bandwidth reservation. While the second kind of error leads to packet loss or long delay, i.e., the QoS requirements cannot be satisfied due to this kind of error.

To address this issue, we utilize the N-P method to classify the traffic state, where the probability of classifying a high traffic state as a low traffic state is bounded by a threshold [43]. Following the N-P method, we denote H_0 and H_1 as the hypotheses that the sample is taken from the high and low traffic state, respectively. Denote D_0 and D_1 as the binary decisions that a user is classified into high and low traffic states,

respectively. Then, the probability of false alarm is defined as $P_{\rm f} = P(D_1|H_0)$, i.e., a user with high traffic is classified into low traffic state. Similarly, the probabilities of missing detection and successful detection are defined as $P_{\rm s} = P(D_0|H_1)$ and $P_{\rm d} = P(D_1|H_1)$, respectively.

The idea is to maximize the successful detection rate subject to the constraint on the false alarm probability. To guarantee the reliability requirement of URLLC, $P_{\rm f}$ should be less than a certain requirement $\varepsilon^{\rm f}$. In this way, the bandwidth for successfully detected users in low traffic state can be saved and the reliability requirement can be satisfied. A threshold $\hat{\ell}$ can be obtained as follows [43],

$$\begin{aligned} (\mathbf{P1}): \quad & \max_{\ell} P_{\rm d} \\ \text{s.t.} \quad & P_{\rm f} \leq \varepsilon^{\rm f}. \end{aligned} \tag{3.3.1}$$

According to [43], the threshold can be given as $\hat{\ell} \triangleq \frac{\ln(\gamma)-(\lambda_H-\lambda_L)}{\ln(\lambda_L)-\ln(\lambda_H)}$. When $\ell \leq \hat{\ell}$, it is classified into low traffic. Otherwise, it is classified into high traffic state. As such, we can rewrite the probability of false alarm as

$$P_{\rm f} = P(D_1|H_0) = P\left(\ell \leq \hat{\ell}|H_0\right). \tag{3.3.2}$$

When H_0 is true, ℓ follows a Poisson distribution with mean $T_{\rm w}\lambda_{\rm H}$. From the CDF of Poisson distribution, it is not hard to find the largest $\hat{\ell}$ that satisfies $P_{\rm f} \leq \varepsilon^{\rm f}$. When $\hat{\ell}$ is given, the missing detection rate can be calculated from $P_{\rm s} = P(D_0|H_1) = P\left(\ell > \hat{\ell}|H_1\right)$.

3.3.2 Data-driven Method

When the traffic model is unavailable, data-driven machine learning methods can be used [44]. Considering that the labels of training data are not available at the BS, supervised learning methods cannot be applied. In contrast, the k-means method

is an effective unsupervised learning method that can be applied without the labels of training data. Centroids of two clusters are trained offline by historical arrival processes, and used to classify a new sample online.

It is possible to further reduce classification error probability by applying more advanced machine learning algorithms, which deserves further study [44]. However, the performance limit of the classification accuracy is determined by the data. If the data in the two clusters are partly overlapped, classification errors are unavoidable.

3.4 Transmission Schemes for Different Traffic States

After traffic state classification, we will show how to design transmission schemes for users in high and low traffic states.

3.4.1 High Traffic State

To ensure QoS requirements, the dedicated bandwidth is reserved for each user in the high traffic state.

1) Queueing Analysis We use effective bandwidth[4] to characterize the queueing delay requirement. Effective bandwidth is defined as the minimal constant service rate (i.e., packets/slot) that is required to meet the requirements of maximum queueing delay D_m^{q} and maximum queueing delay violation probability $\varepsilon_m^{\mathrm{q}}$ for the mth user. It is widely believed that effective bandwidth is applicable when the delay bound is large.

[4]It should be noted that the concept of effective bandwidth is widely adopted in the community of computer networking [74], which is different from the concept of bandwidth of physical spectrum used in the community of telecommunications.

However, the studies in [22] validated that it is applicable in the short delay regime when the arrival process is more bursty than a Poisson process, i.e., the scenario we considered in this chapter. According to [22], the effective bandwidth of a Poisson process with average packet rate λ_{H} is given by

$$E_{\mathrm{B}}^{m} = \frac{T_{\mathrm{s}} \ln\left(1/\varepsilon_{m}^{\mathrm{q}}\right)}{D_{m}^{\mathrm{q}} \ln\left[\frac{T_{\mathrm{s}} \ln\left(1/\varepsilon_{m}^{\mathrm{q}}\right)}{\lambda_{\mathrm{H}} D_{m}^{\mathrm{q}}} + 1\right]} \text{ packets/slot.} \tag{3.4.1}$$

2) Transmission Mode and Bandwidth Reservation Denote the number of users that are classified in high traffic state as N_{H}. Orthogonal subchannels are assigned to the N_{H} users. Let B_{m}^{H} be the bandwidth reserved for the mth user. It is assumed that B_{m}^{H} is less than the coherent bandwidth W_{c}, so that each subchannel is frequency-flat fading. To avoid extra delay and overhead caused by feedback, the channel state information (CSI) is not available at the users, and the transmit power of each user is fixed as the maximal transmit power P_{t}.

According to (3.4.1), to guarantee the queueing delay bound and delay bound violation probability, we need to transmit bE_{B}^{m} bits in each slot, where b is the number of bits in each packet. Since the transmission delay of each coding block is D_{m}^{t}, $bE_{\mathrm{B}}^{m} D_{m}^{\mathrm{t}}/T_{\mathrm{s}}$ bits are transmitted in a block with length $D_{m}^{\mathrm{t}} \rho_{\mathrm{d}} B_{m}^{\mathrm{H}}$, where ρ_{d} denotes the fraction of time that is used for data transmission in each slot. In Tactile Internet, the packet size is much smaller than that of traditional video services. To transmit short packets with low latency, the blocklength of channel codes is short. As a result, the Shannon capacity is no longer applicable [75]. According to [66], the packet loss probability due to the decoding error over Rayleigh fading channel can be expressed as

$$\varepsilon_{m}^{\mathrm{c}} \approx \int_{0}^{\infty} f_{\mathrm{Q}}\left\{\sqrt{\frac{D_{m}^{\mathrm{t}} \rho_{\mathrm{d}} B_{m}^{\mathrm{H}}}{V_{m}^{\mathrm{H}}}}\left[\ln\left(1 + \frac{\alpha_{m} g_{m} P_{\mathrm{t}}}{\phi N_{0} B_{m}^{\mathrm{H}}}\right) - \frac{bE_{\mathrm{B}}^{m} \ln 2}{T_{\mathrm{s}} \rho_{\mathrm{d}} B_{m}^{\mathrm{H}}}\right]\right\} f_{g}(x) dx, \tag{3.4.2}$$

where α_{m} denotes the large-scale channel gain, g_{m} is the small-scale channel gain

with the probability density function $f_g(x) = \frac{1}{(N_\mathrm{r}-1)!}x^{N_\mathrm{r}-1}e^{-x}$, i.e., Rayleigh fading, $\phi > 1$ presents the signal-to-noise ratio loss due to inaccurate channel estimation at the BS, N_0 is the noise power spectral density, $V_m^\mathrm{H} = 1 - [1 + (\alpha_m g_m P_\mathrm{t})/(\phi N_0 B_m^\mathrm{H})]^{-2}$ [66], $f_\mathrm{Q}^{-1}(\cdot)$ is the inverse function of the Q-function, and ε_m^t is the decoding error probability (i.e., block error probability) of the mth user.

3) Packet Loss Probability The uplink packet loss comes from the queueing violation ε_m^q and the decoding error ε_m^c. To meet the reliability requirement, we have

$$1 - (1 - \varepsilon_m^\mathrm{q})(1 - \varepsilon_m^\mathrm{c}) \leq \varepsilon^\mathrm{u}. \tag{3.4.3}$$

Since ε_m^q and ε_m^c are small (i.e., in the order of $10^{-5} \sim 10^{-8}$), (3.4.3) can be accurately approximated by

$$\varepsilon_m^\mathrm{q} + \varepsilon_m^\mathrm{c} \leq \varepsilon^\mathrm{u}. \tag{3.4.4}$$

3.4.2 Low Traffic State

Reserving dedicated bandwidth for users in low traffic state results in low resource usage efficiency. To this end, we reserve a resource pool with K_p orthogonal subchannels that are shared by N_L users in the low traffic state. A synchronized multi-channel slotted ALOHA protocol is considered. Without scheduling, each packet randomly selects a subchannel to transmit its message. Transmission collisions happen if two or more packets try to access the same subchannel in the same slot. When the collisions happen, packets cannot be decoded successfully. To reduce the collision probability and improve the reliability, the repetition scheme is adopted [36], where multiple copies of each packet are transmitted without receiving ACKs. To exploit frequency diversity, frequency-hopping is applied, and different repetitions of each packet occupy different subchannels.

In our analysis, the worst case of large-scale channel gain is considered to ensure the QoS requirements, i.e., the users are located at the edge of the cell. We will find the minimal K_p and the bandwidth of each subchannel that are required to guarantee the QoS requirements of cell-edge users.

1) Collision Probability In this chapter, a multi-channel slotted ALOHA protocol is considered, where the resource pool is divided into multiple subchannels [25]. During each time slot, K_p subchannels in the resource pool are shared by N_{L} users in low traffic state that select subchannels randomly. Since M copies of each packet are transmitted, the equivalent packet arrival rate of each user is $M\lambda_{\mathrm{L}}$. In the multi-channel slotted ALOHA protocol, the probability that all the M repetitions of a packet collide with the other packets is [25]

$$P_{\mathrm{c}}^{0} = 1 - \left(\frac{e^{-M\lambda_{\mathrm{L}}} + K_p^M - 1}{K_p^M} \right)^{N_{\mathrm{L}}-1}. \tag{3.4.5}$$

Due to classification errors, some of the N_{L} users classified into low traffic state are high traffic users. Let n be the number of misclassified high traffic users. For each high traffic user, it may need to transmit multiple packets over multiple subchannels within the same slot. For example, when there are two packets generated by the user in one slot, it randomly selects two subchannels for the packets as if there were two users in low traffic state sending packets in the same slot.

With the above random access mechanism, there is no queueing delay, and each misclassified high traffic user can be approximated by $\lceil \lambda_{\mathrm{H}}/\lambda_{\mathrm{L}} \rceil$ low traffic users, where $\lceil x \rceil$ denotes the smallest integer that is larger than or equal to x. As a result, the equivalent number of low traffic users that share the K_p subchannels is given by $\hat{N}_{\mathrm{L}}(n) = n\lceil \lambda_{\mathrm{H}}/\lambda_{\mathrm{L}} \rceil + N_{\mathrm{L}} - n$. Similar to (3.4.5), the conditional collision probability

with n misclassified high traffic users is given by

$$P_{\mathrm{c}|n} = 1 - \left(\frac{e^{-M\lambda_{\mathrm{L}}} + K_p^M - 1}{K_p^M} \right)^{\hat{N}_{\mathrm{L}}(n)-1}. \tag{3.4.6}$$

Then, the probability that all the M repetitions of a packet collide with other packets can be obtained from the law of total probability, i.e.,

$$P_{\mathrm{c}} = \sum_{n=0}^{N_{\mathrm{L}}} P(n|N_L) P_{\mathrm{c}|n}, \tag{3.4.7}$$

where $P(n|N_{\mathrm{L}})$ is the probability that n of the N_{L} users classified into low traffic state are misclassified. $P(n|N_{\mathrm{L}})$ is given by

$$P(n|N_{\mathrm{L}}) = \binom{N_{\mathrm{L}}}{n} P_{\mathrm{h}}^n (1 - P_{\mathrm{h}})^{N_{\mathrm{L}}-n}, \tag{3.4.8}$$

where $\binom{N_{\mathrm{L}}}{n}$ is Binomial coefficient and P_{h} is the probability that a user classified into low traffic state is actually a high traffic user. It is not hard to derive that

$$P_{\mathrm{h}} = \frac{\mu_{\mathrm{H}} P_{\mathrm{f}}}{\mu_{\mathrm{H}} P_{\mathrm{f}} + \mu_{\mathrm{L}}(1 - P_{\mathrm{s}})}. \tag{3.4.9}$$

2) Decoding Error and Packet Loss Probabilities Now, we analyze the decoding error probabilities of a packet that is transmitted without collision. For each of the M repetitions, the decoding error probability is denoted as $\varepsilon_m^{\mathrm{r}}$. Similar to (4.3.13), $\varepsilon_m^{\mathrm{r}}$ is given by

$$\varepsilon_m^{\mathrm{r}} = \int_0^\infty f_{\mathrm{Q}} \left\{ \sqrt{\frac{D_m^{\mathrm{r}} \rho_{\mathrm{d}} B_{\mathrm{L}}}{V_m^{\mathrm{p}}}} \left[\ln\left(1 + \frac{\alpha_m^{\mathrm{p}} g_m P_{\mathrm{t}}}{\phi N_0 B_{\mathrm{L}}}\right) - \frac{b \ln 2}{D_m^{\mathrm{r}} \rho_{\mathrm{d}} B_{\mathrm{L}}} \right] \right\} f_g(x) dx, \tag{3.4.10}$$

where B_{L} is the bandwidth of each subchannel, and $D_m^{\mathrm{r}} \rho_{\mathrm{d}}$ is the data transmission duration of each repetition [66].

In the low traffic state, a packet will be successfully received if at least one of the repetitions is transmitted without collision and it is successfully decoded. Since P_{c} is the probability that all the M repetitions of a packet collide with other packets, the overall packet loss probability can be satisfied with the following constraint, given by

$$P_{\mathrm{c}} + (1 - P_{\mathrm{c}})\varepsilon_m^{\mathrm{r}} \leq P_{\mathrm{c}} + \varepsilon_m^{\mathrm{r}} \leq \varepsilon^{\mathrm{u}}, \tag{3.4.11}$$

where the upper bound is very tight since P_{c} is extremely small (i.e., ranges from 10^{-5} to 10^{-8}).

3.4.3 Error Correction Mechanism for False Alarm Errors

Classifying high traffic users into low traffic state leads to high collision probability. In the cases that the false alarm probability is much higher than the reliability requirement ε^{u}, it is very difficult to guarantee reliability. To handle this problem, except for taking into account the classification errors in our transmission scheme design, we propose an error correction mechanism.

As mentioned in Section II, the key difference between high and low traffic states is that only the high traffic users may need to transmit multiple packets in one slot. If the BS receives multiple packets from one user in one slot, then the user is misclassified and can be detected by the BS. Then, the BS reserves dedicated bandwidth to the user, and adjusts the number of subchannels in the shared resource pool.

Next, we analyze the collision probability with the proposed error correction mechanism. Before the detection of a misclassified high traffic user, it either stays silent or transmits one packet in a slot. This is because if more than one packet of a user is transmitted in one slot, the user can be detected by the BS. Then, the average packet arrival rate of a high traffic user before being detected can be obtained from

the following conditional expectation,

$$\begin{aligned}\lambda_{\mathrm{H}}^{e} &= \Pr\{\ell_f = 1 | \ell_f \leq 1\} \cdot 1 + \Pr\{\ell_f = 0 | \ell_f \leq 1\} \cdot 0 \\ &= \frac{\Pr\{\ell_f \leq 1\} - \Pr\{\ell_f \leq 0\}}{\Pr\{\ell_f \leq 1\}},\end{aligned} \tag{3.4.12}$$

where ℓ_f can be approximated by a Poisson distribution with the parameter $T_{\mathrm{w}}\lambda_{\mathrm{H}}$, and thus $\Pr\{\ell_f \leq 1\}$, $\Pr\{\ell_f \leq 0\}$ and $\Pr\{\ell_f \leq 1\}$ can be calculated by the corresponding CDF of the Poisson distribution.

Similar to (3.4.7) and (3.4.11), we can derive the collision probability of all the M repetitions and the packet loss probability. The decoding error probability without collision is the same as that with no correction scheme. It is not hard to see that $\lambda_{\mathrm{H}}^{e} < \lambda_{\mathrm{H}}$, and thus the overall packet loss probability with error correction mechanism is smaller.

3.5 Bandwidth Reservation Optimizations

Based on the transmission schemes in the previous section, we formulate an optimization problem to optimize bandwidth reservation that minimizes the required bandwidth with the constraints on delay and reliability.

3.5.1 Problem Formulation

The minimal bandwidth required to ensure the QoS requirements of URLLC can be obtained by solving the following optimization problem:

$$\min_{\substack{K_p, B_{\mathrm{L}}, B_{\mathrm{H}}, \\ M, D_m^{\mathrm{r}}, D_m^{\mathrm{q}}, D_m^{\mathrm{t}}, \\ \varepsilon_m^{\mathrm{q}}, \varepsilon_m^{\mathrm{c}}, P_{\mathrm{c}}, \varepsilon_m^{\mathrm{r}}}} \quad K_p B_{\mathrm{L}} + N_{\mathrm{H}} B_{\mathrm{H}}, \tag{3.5.1}$$

$$\text{s.t.} \quad 0 \leq B_{\mathrm{L}}, B_{\mathrm{H}} \leq W_{\mathrm{c}}, \tag{3.5.1a}$$

$$K_p \geq 1, K_p \in \mathbb{Z}, \tag{3.5.1b}$$

$$M D_m^{\mathrm{r}} \leq D^{\mathrm{u}}, M \in \mathbb{Z} \tag{3.5.1c}$$

$$D_m^{\mathrm{q}} + D_m^{\mathrm{t}} \leq D^{\mathrm{u}}, \tag{3.5.1d}$$

$$\varepsilon_m^{\mathrm{q}} + \varepsilon_m^{\mathrm{c}} \leq \varepsilon^{\mathrm{u}}, \tag{3.5.1e}$$

$$P_{\mathrm{c}} + \varepsilon_m^{\mathrm{r}} \leq \varepsilon^{\mathrm{u}}, \tag{3.5.1f}$$

$$(3.4.1), (4.3.13), (3.4.5), \text{ and } (3.4.10),$$

where N_{H} and N_{L} are the numbers of users classified in high and low traffic states, respectively. In the objective function (3.5.1), the first term is the bandwidth of the resource pool shared by low traffic users for random access. The second term is the bandwidth reserved for high traffic users.

Since (3.5.1) is a mixed-integer optimization problem, it is non-convex and hard to solve directly. To optimize bandwidth reservation, we set some optimization variables as constant system parameters. For the low traffic state, the duration of each repetition is set to be one slot and the number of repetitions M is fixed. To find the optimal value of M, we can search M in the range of $0 < M < D^{\mathrm{u}}/T_{\mathrm{f}}, M \in \mathbb{Z}$. Therefore, constraint (3.5.1c) is simplified as follows,

$$D_m^{\mathrm{r}} = T_{\mathrm{s}}. \tag{3.5.2}$$

For the high traffic state, to serve a queueing system that requires a fixed packet rate E_{B}^{m}, the optimal configuration of transmission delay is one slot [69]. According to this result, the constraint in (3.5.1d) can be replaced by

$$D_m^{\mathrm{t}} = T_{\mathrm{s}}, D_m^{\mathrm{q}} = D^{\mathrm{u}} - T_{\mathrm{s}}. \tag{3.5.3}$$

To further simplify the problem, the constraints in (3.5.1e) and (3.5.1f) are replaced by the following two constraints, given by

$$\varepsilon_m^{\mathrm{q}} = \varepsilon_m^{\mathrm{c}} = \varepsilon^{\mathrm{u}}/2, \tag{3.5.4}$$

$$P_c = \varepsilon_m^{\mathrm{r}} = \varepsilon^{\mathrm{u}}/2, \tag{3.5.5}$$

respectively. This is because the optimization results in [22] indicate that optimizing the value of packet loss probabilities (i.e., $\varepsilon_m^{\mathrm{q}}$, $\varepsilon_m^{\mathrm{c}}$, $\varepsilon_m^{\mathrm{r}}$ and P_{c} in problem (3.5.1)) is not necessary, and setting $\varepsilon_m^{\mathrm{q}} = \varepsilon_m^{\mathrm{c}} = \varepsilon^{\mathrm{u}}/2$ and $P_{\mathrm{c}} = \varepsilon_m^{\mathrm{r}} = \varepsilon^{\mathrm{u}}/2$ leads to minor performance loss.

With the above settings, the optimization problem (3.5.1) can be simplified as follows,

$$\begin{aligned} &\min_{K_p, B_{\mathrm{L}}, B_{\mathrm{H}}} K_p B_{\mathrm{L}} + N_{\mathrm{H}} B_{\mathrm{H}}, \\ &\text{s.t.} \quad (3.5.1a), (3.5.1b), (3.4.1), (4.3.13), (3.4.5), (3.4.10), \\ &\qquad (3.5.2), (3.5.3), (3.5.4) \text{ and } (3.5.5). \end{aligned} \tag{3.5.6}$$

3.5.2 Optimizations for Bandwidth Reservation

To solve optimization problem (3.5.6), a three-step method is proposed.

First, the minimal bandwidth B_{H}^{*} for a high traffic user can be obtained from (3.4.1) and (4.3.13). As we have discussed before, to ensure the delay and reliability requirements, we should set $D_m^{\mathrm{t}} = T_{\mathrm{s}}$, $D_m^{\mathrm{q}} = D^{\mathrm{u}} - T_{\mathrm{s}}$ and $\varepsilon_m^{\mathrm{q}} = \varepsilon_m^{\mathrm{c}} = \varepsilon^{\mathrm{u}}/2$. By

substituting the above values into (3.4.1) and (4.3.13), B_{H}^{*} is the solution of the following equation:

$$\Phi(B_{\mathrm{H}}) = (\varepsilon^{\mathrm{u}} - \varepsilon^{\mathrm{f}})/2 - \int_{0}^{\infty} f_{\mathrm{Q}}\left\{\sqrt{\frac{T_{\mathrm{s}}\rho_{\mathrm{d}}B_{\mathrm{H}}}{V_{m}^{\mathrm{H}}}}\right. \left.\left[\ln\left(1+\frac{\alpha_{m}g_{m}P_{\max}}{\phi N_{0}B_{\mathrm{H}}}\right) - \frac{bE_{\mathrm{B}}^{m}\ln 2}{T_{\mathrm{s}}\rho_{\mathrm{d}}B_{\mathrm{H}}}\right]\right\} f_{g}(x)dx = 0, \tag{3.5.7}$$

and E_{B}^{m} in (3.4.1) can be re-expressed as

$$E_{\mathrm{B}}^{m} = \frac{T_{\mathrm{s}}\ln\left(3/\varepsilon^{\mathrm{u}}\right)}{(D^{\mathrm{u}} - T_{\mathrm{s}})\ln\left[\frac{T_{\mathrm{s}}\ln\left(3/\varepsilon^{\mathrm{u}}\right)}{\lambda_{\mathrm{H}}(D^{\mathrm{u}}-T_{\mathrm{s}})}+1\right]}. \tag{3.5.8}$$

It should be noted that $\Phi(B_{\mathrm{H}})$ is an increasing function of B_{H}. This is because $\varepsilon_{m}^{\mathrm{t}}$ decreases as the bandwidth B_{H} increases [20]. Therefore, we can use binary search to find B_{H}^{*}.

Second, similar to searching B_{H}^{*} in the first step, by substituting $D_{m}^{\mathrm{r}} = T_{\mathrm{s}}$ and $\varepsilon_{m}^{\mathrm{r}} = \varepsilon^{\mathrm{u}}/2$ into (3.4.10), we can find B_{L}^{*} using binary search. The details are omitted for conciseness.

Third, K_{p} is an integer number, so we can exhaustively search $K_{p} \geq 1$ to get the minimal K_{p}^{*} that satisfies $P_{\mathrm{c}} \leq \varepsilon^{\mathrm{u}}/2$.

In summary, to ensure the latency and the reliability requirements during the queueing (i.e., D_{m}^{q} and $\varepsilon_{m}^{\mathrm{q}}$) and the transmission processes (i.e., D_{m}^{t} and $\varepsilon_{m}^{\mathrm{c}}$), the bandwidth reserved for a user in the high traffic state is B_{H}^{*}. For the users in the low traffic state, to ensure the latency and the reliability requirements during the random access and the transmission processes (i.e., MD_{m}^{p}, P_{c} and $\varepsilon_{m}^{\mathrm{r}}$), the bandwidth required for each subchannel is B_{L}^{*} and the number of subchannels in the resource pool is K_{p}^{*}. As such, the required minimal bandwidth is $B_{\min}^{*} = K_{p}^{*}B_{\mathrm{L}}^{*} + N_{\mathrm{H}}B_{\mathrm{H}}^{*}$. The optimal solution can be obtained by the three-step method because the optimal B_{L}^{*}, B_{H}^{*} and K_{p}^{*} can be obtained from three decoupled problems.

3.5.3 Implementation and Complexity Discussions

From the orthogonal pilots of different users, the BS records the number of packets arriving in the past sample window, i.e., ℓ. When the N-P method is applied, the BS only needs to compare ℓ with the threshold $\hat{\gamma}$, which was derived from SPP. For the k-means method, the BS only needs to compare the distance from ℓ to the two centroids ν_1^* and ν_2^*, which were obtained from the historical training data.

After classifications, the BS calculates the optimal B_{L}^*, B_{H}^* and K_p^* by solving (3.5.6). B_{L}^* and B_{H}^* are obtained via binary search for the user with the worst large-scale channel gain, and hence the searching complexity is low and does not increase with the number of users. K_p^* is obtained via exhaustive searching, and the searching complexity is linear with N, which is the number of users. Therefore, the complexity for solving problem (3.5.6) is $O(N)$.

At the beginning of each prediction window, the BS assigns bandwidth to each user that is classified into the high traffic state, and reserves bandwidth in the resource pool that is shared by the users classified into the low traffic state. During the prediction window, grant-free transmission is performed. It should be noted that the resource reservation is not updated in each slot. Instead, it is updated at the beginning of each prediction window, so that the signaling overheads will not be too large.

3.6 Performance Evaluation

In this section, simulations and experiments are conducted to verify the effectiveness of the proposed methods. The proposed model-based and data-driven methods

Table 3.1: Parameters [26]

Parameters	Values
Number of users N	20
Maximal transmit power of a user P_{t}	23 dBm
Single-sided noise spectral density N_0	-174 dBm/Hz
Coherence bandwidth W_{c}	0.5 MHz
Number of received antenna N_{r} at BS	16
Packet size b	32 bytes
Slot duration T_{s}	0.1 ms
Overall uplink packet loss probability ε^{u}	1×10^{-5}
Overall uplink latency D_{u}	0.5 ms
Sample window size N_{w}	100 T_{s}
Prediction window size N_{p}	100 T_{s}
Average packet rate generated by each user	1000 packets/s
Number of times for repetition M	4

are compared with another two methods. The baseline method is reserving dedicated bandwidth according to the high packet arrival rate for all the users, which can be considered as a direct extension of an existing method in [22]. The other method knows perfectly the traffic states of all the users. Such an idealistic method can obtain a lower bound of the required bandwidth.

3.6.1 Simulations

In simulations, we first show how to choose the upper bound of the false alarm probability with the N-P method. Then, we demonstrate the required bandwidth for different methods. Finally, we illustrate the delay and reliability achieved by the proposed methods.

Simulation settings are listed in Table 5.1. To ensure QoS requirements for all users, we consider the worst case of large-scale fading, i.e., the users are at the edge of the cell. The path loss model is $10\log_{10}(\alpha_m) = 35.3 + 37.6\log_{10}(d_m)$, where $d_m = 200$ m is the radius of the cell [76]. For the k-means method, we can obtain the empirical false alarm and missing detection probabilities from historical data by comparing if the classified traffic states within the sample window and prediction window are the same.

The packet arrival processes are generated according to the SPP model in simulations. Recall that the burstiness is defined as $I_{\rm s} = \sigma^2/\nu$. To investigate the impacts of burstiness on the required bandwidth, the average packet rate of each user and the sum of average durations of the high traffic state and the low traffic state are set to be constant, i.e., $\bar{\lambda} = (\lambda_{\rm H}\mu_{\rm H} + \lambda_{\rm L}\mu_{\rm L})/(\mu_{\rm H} + \mu_{\rm L}) = 1000$ packets/s [77], and $\mu_{\rm L} + \mu_{\rm H} = 1$ s. The packet arrival rate in low traffic state is set to be a constant, i.e., $\lambda_{\rm L} = 10$ packets/s. We change $\lambda_{\rm H}$ from 1000 packets/s to 4000 packets/s. To keep the average packet arrival rate constant, $\mu_{\rm H}$ decreases with $\lambda_{\rm H}$.

To show how to choose the value of $\varepsilon^{\rm f}$ in the N-P method, we illustrate the minimal bandwidth that is required to ensure the reliability and the latency requirements with different $\varepsilon^{\rm f}$. The results in Fig. 3.2 indicate that when the burstiness is given, e.g., 1.09, the minimal bandwidth first decreases and then increases with $\varepsilon^{\rm f}$. The optimal $\varepsilon^{\rm f}$ ranges from 10^{-3} to 10^{-2}, and is much larger than the reliability requirement $\varepsilon^{\rm u}$. Such an observation is counterintuitive. Since classification errors are considered in bandwidth reservation, the reliability can be satisfied in the case $\varepsilon^{\rm f} > \varepsilon^{\rm u}$. On the other hand, a small $\varepsilon^{\rm f}$ leads to a high missing detection probability. As a result, a lot of bandwidth is reserved for the low traffic users that are classified into high traffic

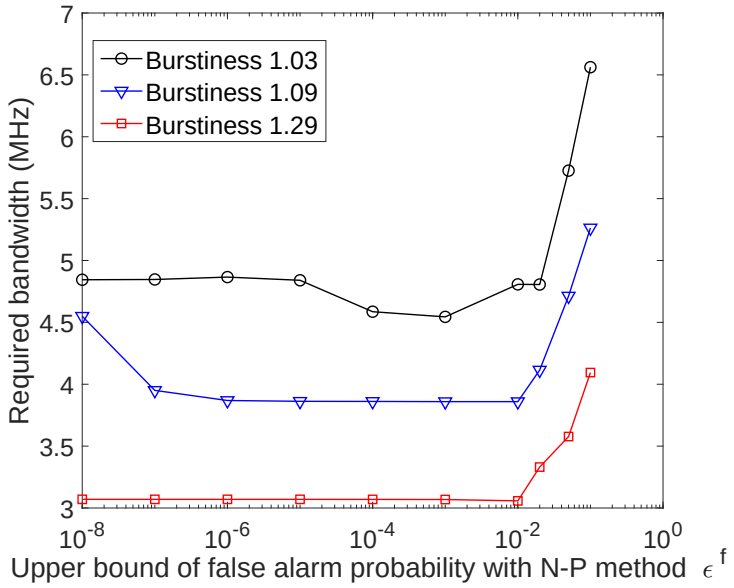

Figure 3.2: Required bandwidth vs. ε^{f}.

state, and the bandwidth usage efficiency is low. In this section, we set $\varepsilon^{\mathrm{f}} = 10^{-2}$.

The relation between the required bandwidth and burstiness is shown in Fig. 3.3. The reason why the curves in Fig. 3.3 are not smooth is because K_p is an integer, and is not due to insufficient number of Monte Carlo simulations. The results show that for the baseline method, the required bandwidth increases with the burstiness rapidly. This is because to guarantee the QoS in different traffic states, the BS needs to reserve bandwidth by assuming that all the users are in the high traffic state. While the proposed method without prediction errors provides the best performance, and the required bandwidth decreases with the burstiness. This is because the average duration of low traffic state increases with burstiness, and bandwidth is saved by sharing the resource pool among the users in the low traffic state. With the N-P method or the k-means method, the required bandwidth also decreases with the burstiness and is close to the lower bound when the burstiness is large. This demonstrates the

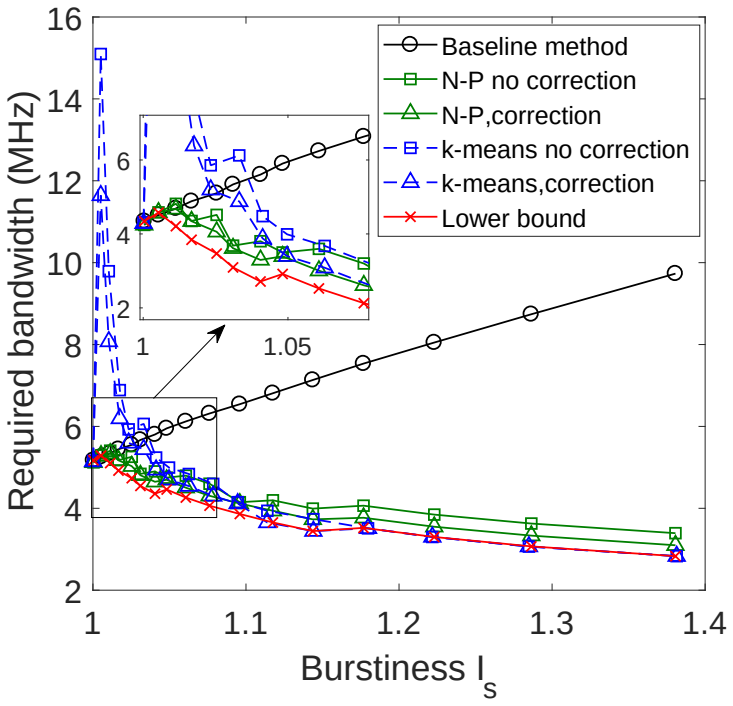

Figure 3.3: Minimal bandwidth required vs. burstiness.

effectiveness of the proposed methods. Moreover, the proposed methods with error correction mechanism require less bandwidth compared with the methods without error correction. Finally, the results also indicate that when the burstiness is less than 1.1, the k-means method is worse than the N-P method; when the burstiness is larger than 1.1, the k-means method outperforms the N-P method and is very close to the lower bound. This is because the gap between the average packet arrival rates in low and high traffic states increases with burstiness, and hence the classification error probability of the k-means method decreases with burstiness rapidly.

To investigate the delay and reliability achieved by the proposed methods, Fig. 3.4 shows the complementary cumulative distribution function (CCDF) of delay experienced by the users that are classified into the low traffic state. For the users that

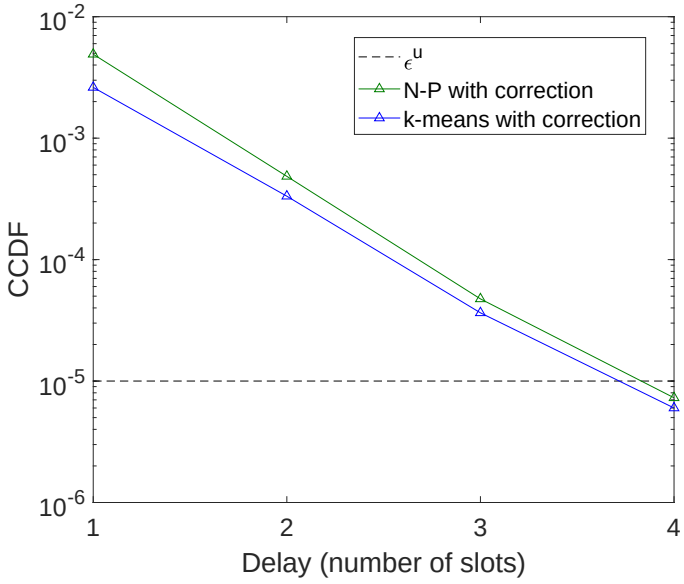

Figure 3.4: CCDF of the delay.

are classified into the high traffic state, the delay and reliability has been validated in [22], and hence is omitted in this work. In this simulation, the delay of a packet equals to the interval between the slot when the packet is generated by a user and the first slot when the packet is decoded at the BS. For example, if the first two repetitions of a packet fail, and the third repetition is successfully decoded, then the delay equals to 3 slots, where the duration of each repetition is one slot. The reliability requirement (i.e., $\varepsilon^{\mathrm{u}} = 10^{-5}$) is also provided as a reference. The results in Fig. 3.4 show that the probability that the delay of a packet is longer than 4 slots is less than the reliability requirement. In other words, with probability $1 - \varepsilon^{\mathrm{u}}$, a packet can be successfully received at the BS after 4 repetitions. Therefore, the UL delay and reliability requirements in Tactile Internet can be satisfied with the proposed methods.

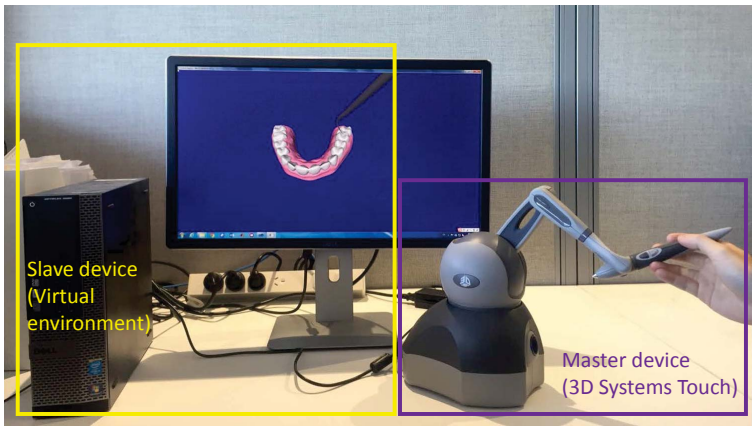

Figure 3.5: Experiment to gain real packet arrival process of Tactile Internet.

3.6.2 Experiments

Since the packet arrival processes in the simulation part are generated according to the SPP model, it is not clear whether our methods are still helpful when the real packet arrival processes do not match SPP perfectly. To further demonstrate the effectiveness of the proposed methods, we illustrate the required bandwidth with packet arrival processes that are generated from a real tactile hardware in Fig. 3.5. In this experiment, a typical application of Tactile Internet is considered (i.e., training dentists), where the dental students can use a probe to feel the hardness of the teeth. As shown in Fig. 3.5, a real 3D System Touch (also named Phantom Omni, Geomagic) tactile device is used as a master device. It is connected to a slave device in a virtual environment via a wire link. The slave device in the virtual environment is a probe that sends force feedback to the master device.

In the experiment, ten participants are invited to control the slave device in the virtual environment. The packet arrival process of force feedback from each participant is recorded in ten minutes. It can be observed that the traffic is very bursty,

which is similar to the observations from [42]. The recorded ten packet arrival processes are used in the optimization of bandwidth reservation for the scenario of ten users working simultaneously.

Next, we apply the N-P method and the k-means method in traffic state classifications. For the N-P method, we assume that the arrival process is SPP, and the corresponding λ_H and λ_L are set as the average packet arrival rates of the recorded real packet arrival processes. Then, the bandwidth is reserved for the users according to their traffic states. The minimal bandwidth that is required to ensure the delay and reliability requirements is illustrated in Table 3.2. The results in Table 3.2 indicate that the N-P method and the k-means method can save 33.9% and 43.2% of the bandwidth that is needed with the baseline method, respectively. Since the real packet arrival processes do not match SPP perfectly, the required bandwidth of the N-P method is higher than the k-means method, but is still much lower than the baseline method. The results indicate that the proposed methods outperform the baseline method with real packet arrival processes, while guaranteeing the delay and reliability requirements.

Table 3.2: Bandwidth Reservations

Applied Methods	Total Bandwidth (MHz)	Bandwidth Saving
Baseline	1.95	N/A
N-P	1.29	33.9%
k-means	1.11	43.2%
Lower bound	0.96	50.5%

3.7 Chapter Summary

In this chapter, we established a framework for designing burstiness aware bandwidth reservation for uplink transmissions of Tactile Internet in IIoT. We first classified packet arrival processes of Tactile Internet into high and low traffic states with the model-based method and the data-driven method. Then, we designed bandwidth reservation schemes according to the traffic states of users. Furthermore, the total bandwidth is minimized by optimizing bandwidth reservation under the delay and reliability requirements. Simulation results validate the effectiveness of the proposed methods and around 40% to 70% bandwidth can be saved compared with a baseline method. Besides, when the classification error probability is around 10^{-2}, our method can achieve 10^{-5} packet loss probability. Experiment results show that if the traffic model is inaccurate, the data-driven method outperforms the model-based method.

Chapter 4

Prediction based Bandwidth Optimization for URLLC of Long Distance Communications in IIoT

4.1 Chapter Introduction

In the last chapter, we mainly focus on a local area network with multiple IIoT devices and a local base station. In this chapter, we will extend the scenario into long distance communications. The long distance communications will enable the skill-set delivery globally. For example, the technical support teams located in different continents can work synchronously and seamlessly for a factory located in another continent. Achieving ultra-high reliability (e.g., 10^{-5} packet loss probability) and ultra-low E2E delay (e.g., 1 ms) is essential for such a global skill-set delivery network in IIoT [64].

The ultra-low delay and ultra-high reliability requirements are challenging to be met at the same time. The latency could be reduced by some existing techniques [34, 35, 78, 79], such as using "mini-slot" in 5G NR to reduce the delay in physical layer[34], or grant-free access to reduce the access delay [35]. However, the reliability

is severely compromised as the delay is reduced. This tradeoff relationship between delay and reliability has been revealed in various layers [22, 66, 80, 81]. To improve the reliability at the low latency domain, multiple forms of diversities are introduced, such as time diversity (e.g., K-repetition [36]), frequency diversity (e.g., frequency hopping [31]), space diversity (e.g., massive mimo [37]) or interface diversity (e.g., multiple communication interfaces [38]). By introducing diversities, the reliability is improved at the cost of reduced resource utilization efficiency. However, the resources shared by multiple devices for communications are quite limited. Moreover, even if diversities and thus more resources are used, the URLLC requirements still cannot be met by only designing and optimizing the air interface for many scenarios.

The E2E delay of a complete communication system not only includes transmission delay of the air interface, but also includes the queueing delay, the access delay, the computing processing delay. In long distance communications, it also includes the routing delay from the core network and backhauls, and inevitable propagation delay resulting from the propagation of the electromagnetic wave in the media of air in the air interface, or fibres or cables in the core network or backhaul. For example, when the distance is larger than 300 km, according to the speed light in vacuum which is 3×10^{-8} m/s, the propagation delay alone is larger than 1 ms. As such, ensuring 1 ms delay to the long distance communication seems to be an impossible mission by only designing and optimizing the communication system.

To overcome the above limitations, we propose to ensure the URLLC requirements by co-design of communications and predictions. The transmitter can predict and send the future system state, so that the users experience less delay at the receiver for a communication link with a given E2E delay. The most challenging part is

that the prediction is not error free. As a fact, when the prediction time becomes longer, The prediction tends to be more unreliable. Although predicting the future system state in a longer time may relax the E2E communication delay requirements, the larger prediction errors due to longer prediction time may cancel the benefits from relaxed E2E communication delay requirements. On the contrary, when the prediction time is small, the prediction could be very reliable. But the requested E2E communication delay is also small. The reliability of the communication system could be reduced due to the strict E2E communication delay requirement. As a result, there exists an optimal prediction time and E2E communication delay design. As such, it is necessary to jointly design the communication and prediction systems to reach an ultra-low delay with the ultra-high reliability requirement guaranteed. Specifically, in this chapter, we will answer the following questions: *1) how to jointly design the communication and prediction systems? 2) What is the performance gain of co-design of communication and prediction? 3) What is the situation when the promised performance gain can be achieved?*

The above questions are challenging to answer because it is difficult to quantitatively model the relationship between the prediction time and the corresponding prediction reliability. Moreover, complicated sources of delay and reliability should be considered.

In this chapter, we aim to ensure the requirements of URLLC by prediction and communication co-design. The basic idea is predicting the future system states, such as locations and forces, and sending them to the receiver in advance. In this way, the experienced delay can be reduced. To guarantee ultra-high reliability, the prediction errors and packet loss in communications are considered. We propose a framework

for prediction and communication co-design in URLLC. By optimizing the prediction time (or equivalently the communication delay), we minimize the required bandwidth to ensure the user experienced delay and reliability requirements. To evaluate the gain of the proposed method, we provide a case study for motion prediction in simulations, and the tradeoffs among bandwidth, reliability, and latency are revealed. With our method, it is possible to achieve zero-latency. This indicates that the tradeoffs can be fundamentally changed with prediction and communication co-design.

To overcome the above limitations by only designing and optimizing the communication system, we propose to introduce predictions into URLLC, and co-design and jointly optimize the communication and prediction systems. There are some existing research considering the usage of predictions in URLLC [40, 45–51]. In [45], the traffic is classified and predicted into either high or low state, based on which a bandwidth reservation scheme is proposed to improve the spectral efficiency with the reliability and latency requirements guaranteed. In [46], the outcome of the decoding is predicted before the end of the transmission, so that the latency could be reduced by an early feedback of Hybrid Automatic Repeat reQuest (HARQ). In [47], by exploiting the correlation of data acquisition and access behavior between nodes, the resource utilization for each user is thus predicted. As a result, the required resources are reserved in advance and thus the access delay is reduced. However, we are predicting the future system state in this chapter, such as location or force, which is different from the contents of predictions in [45–47]. Particularly, there are some research in Tactile Internet [48–50], which also predicts the system states. Their purpose is to compress the tactile data in the information source, which is different from ours. The idea of model-mediated teleoperation approach is mentioned in [40], where the tactile

experience is virtually emulated on both side of the master device and slave device. It is proposed to predict the movement or the force feedback to reduce latency. However, they do not quantitatively model it and do not jointly design communications and delay, so that a best effort service is provided. A most relevant work for us is [51], where prediction length is optimized to minimize the resource consumption. However, they do not consider and characterize the unavoidable prediction errors.

4.2 System Model

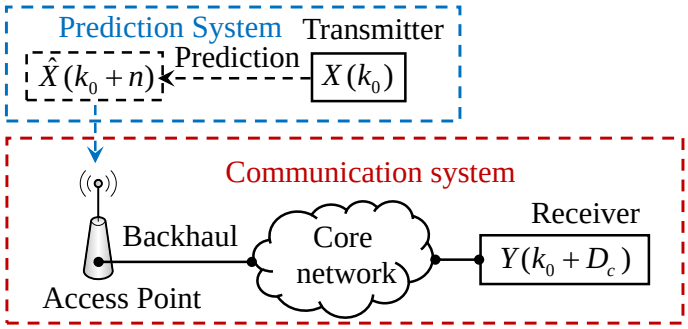

Figure 4.1: Illustration of network structure.

We consider a prediction and communication system shown in Fig. 4.1, where a transmitter sends its state to a target receiver. The state of the transmitter may be composed of multiple features, such as the location, velocity and acceleration of a device in remote driving or industrial automation, or the forces and torques in tactile internet. The communication system includes radio access networks, backhauls, and core networks. After predicting the future state of the transmitter with the prediction system, the transmitter can send its future state in advance. Thus, the user experienced latency can be reduced.

4.2.1 Reducing Experienced Latency by Prediction

Time is discretized into slots. The duration of each slot is denoted as T_s. Let $X(k) = [x_1(k), x_2(k), ..., x_N(k)]^T$ be the vector that denotes the state of the transmitter in the kth slot. The state of the transmitter that is received by the receiver in the kth slot is denoted as $Y(k)$. In traditional communication systems, there is no prediction. The transmitter can only send its current state $X(k)$ to the receiver. Let D_c (slots) be the E2E delay in the communication system. If the packet that conveys $X(k)$ is decoded successfully in the $(k + D_c)$th slot, then $Y(k + D_c) = X(k)$. This suggests that when there is no prediction, the delay experienced by the user is exactly the E2E delay in the communication system.

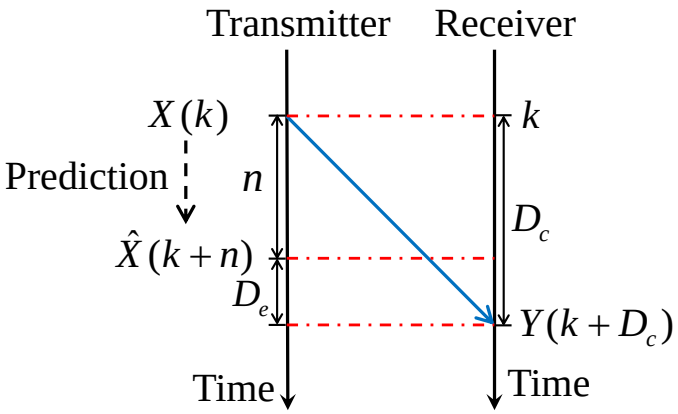

Figure 4.2: Illustration of prediction structure.

In this chapter, we leverage predictions to improve the delay experienced by a user as shown in Fig. 4.2. In the kth slot, the transmitter sends the predicted state $\hat{X}(k+n)$ to the receiver, where n is the number of prediction steps, which is referred to as prediction time. Since the communication delay is D_c, $\hat{X}(k+n)$ will arrive at the receiver in the $(k + D_c)$th slot. If the packet is decoded successfully, then

$Y(k + D_c) = \hat{X}(k + n)$. Therefore, the delay experienced by a user is $D_e = D_c - n$.

4.2.2 Delay and Reliability Requirements of URLLC

In this subsection, we present the requirements on the delay experienced by the user and the reliability of the system.

On the one hand, we need to ensure that the delay experienced by the user does not exceed a maximal delay bound, i.e.,

$$D_e = D_c - n \leq D_{\max}. \tag{4.2.1}$$

On the other hand, we need to ensure that the difference between the actual state of the transmitter and the received state does not exceed a required threshold. In tactile internet, there exists a minimum amount of variance of force stimulus intensity that a human can percept, which is named Weber's law of just noticeable differences (JND) [82]. This suggests that if the difference of force is less than the JND, a human can hardly notice it. In other words, JND can be used as the maximal tolerable difference of force. Alternatively, if the state is the location of a device, the tolerable difference depends on the specific applications. For example, it is in the order of 1 cm in remote driving, or in the order of 1 mm in industrial automation, or even smaller in the application of remote surgery [83].

The difference between $Y(k+D_e)$ and $X(k)$ is denoted as $E(k) = [e_1(k), e_2(k), ..., e_N(k)]^T$, where $e_j(k) = y_j(k + D_e) - x_j(k)$. Let $\Delta = [\delta_1, \delta_2, ..., \delta_N]^T$ be the required threshold. If $|e_j(k)| \leq \delta_j, \forall j = 1, 2, ..., N)$, the user cannot recognize the difference between $Y(k + D_e)$ and $X(k)$. Otherwise, the user can recognize the difference, and thus an error occurs.

We use the probability that the user can recognize the difference between $Y(k+D_e)$

and $X(k)$ as the metric for the overall reliability of the system, which is denoted as ε_{o}. Thus, the reliability requirement can be expressed as follows,

$$\varepsilon_{\mathrm{o}} \leq \varepsilon_{\max}. \tag{4.2.2}$$

4.2.3 Communication Reliability and Prediction Reliability

The overall reliability depends on the communication reliability and the prediction reliability. Denote the packet loss probability of the communication system as ε_{c}, which is used as the metric of communication reliability. If a packet is not decoded successfully at the receiver, then the state of the transmitter is not recovered at the receiver. We consider the worst case that the user can always notice the difference between $Y(k+D_{\mathrm{e}})$ and $X(k)$ if a packet is lost.

The prediction reliability is determined by the prediction error probability. If the difference between the predicted state $\hat{X}(k)$ and the actual state $X(k)$ exceeds the required threshold Δ, the the user can recognize the difference even if the packet is decoded successfully, i.e., $Y(k+D_{\mathrm{e}}) = \hat{X}(k)$. In this case, $E(k) = X(k) - \hat{X}(k)$, and the prediction error probability is given by

$$\varepsilon_{\mathrm{p}} = 1 - \prod_{j=1}^{N} \Pr\{|e_j(k)| \leq \delta_j\}. \tag{4.2.3}$$

If a packet is lost or the gap between the predicted state and the actual state exceeds the required threshold, then the difference between $Y(k+D_{\mathrm{e}})$ and $X(k)$ can be recognized by the user. The overall reliability can be re-expressed as follows,

$$\varepsilon_{\mathrm{o}} = 1 - (1-\varepsilon_{\mathrm{c}})(1-\varepsilon_{\mathrm{p}}). \tag{4.2.4}$$

To achieve ultra-high reliability, both ε_{c} and ε_{p} should be small (e.g., $10^{-5} \sim 10^{-8}$). Thus, (4.2.4) can be accurately approximated by $\varepsilon_{\mathrm{o}} \approx \varepsilon_{\mathrm{p}} + \varepsilon_{\mathrm{c}}$, and the reliability

requirement in (4.2.2) can be satisfied if

$$\varepsilon_{\mathrm{p}} + \varepsilon_{\mathrm{c}} \leq \varepsilon_{\max}. \tag{4.2.5}$$

4.3 Analyses of Prediction and Communication

In this section, we first consider a prediction method, and derive the relation between the prediction error probability and the prediction time in closed-form. Then, we characterize the tradeoff between communication reliability and E2E delay for short packet transmissions in closed-form. Based on the closed-form expressions, we study how to minimize the resource usage to ensure the reliability and latency requirements.

4.3.1 State Transition Function

We assume that the state of the transmitter can be modelled as a discrete time stochastic process $X(k), k = 1, 2, 3, .., \infty$. It varies according to the following state transition function [84]:

$$X(k+1) = \Phi X(k) + W(k), \tag{4.3.1}$$

where $\Phi = [\phi_{i,j}]_{N\times N}, i, j = 1, 2, \cdots, N$ is a $N \times N$ state transition matrix, and $W(k) = [w_1(k), w_2(k), ..., w_N(k)]^T$ is the transition noise. We assume that the stochastic process is stationary, and thus Φ is constant over time, which can be obtained from training data or the physical laws. The elements of $W(k)$ are independent random variables that follow Gaussian distributions with zero mean and variances $\sigma_1^2, \sigma_2^2, \cdots, \sigma_N^2$, respectively. Such a model is widely adopted in kinematics systems or control systems [84, 85].

According to (4.3.1), the state in the $(k+n)$th slot is given by

$$X(k+n) = \Phi^n X(k) + \sum_{i=1}^{n} \Phi^{n-i} W(k+i-1), \tag{4.3.2}$$

where the $(N \times N)$ matrix $\Phi^n = [\phi_{i,j,n}], (i,j = 1,2,\cdots,N)$ is the n-th power of the matrix Φ.

4.3.2 Prediction Time and Prediction Error Probability

Inspired by Kalman filter, we consider a general linear prediction method [84]. Based on the system state in the kth slot, we can predict the state in the $(k+1)$th slot according to following expression,

$$\hat{X}(k+1) = \Phi X(k). \tag{4.3.3}$$

From (4.3.3), we can further predict the state in the $(k+n)$th slot,

$$\hat{X}(k+n) = \Phi^n X(k). \tag{4.3.4}$$

After n steps of prediction, the difference between $X(k+n)$ and $\hat{X}(k+n)$ can be derived as follows,

$$\begin{aligned} E(k+n) &\triangleq X(k+n) - \hat{X}(k+n) \\ &= W(k+n-1) + \sum_{i=1}^{n-1} \Phi^{n-i} W(k+i-1). \end{aligned} \tag{4.3.5}$$

The jth element of $E(k+n)$ is given by

$$e_j(k+n) = w_j(k+n-1) + \sum_{i=1}^{n-1} \sum_{m=1}^{N} \phi_{j,m,n-i} w_m(k+i-1), \tag{4.3.6}$$

where $\phi_{j,m,n-i}$ is the element of Φ^{n-i} at the jth row and the mth column.

Since the state transition noises follow independent Gaussian distributions, and $e_j(k+n)$ is a linear combination of them, $e_j(k+n)$ follows a Gaussian distribution

with zero mean. The variance of $e_j(k+n)$ is denoted as $\rho_j^2(n)$, which is given by

$$\rho_j^2(n) = \sigma_j^2 + \sum_{i=1}^{n-1}\sum_{m=1}^{N}(\phi_{j,m,n-i})^2\sigma_m^2. \tag{4.3.7}$$

Therefore, $\Pr\{|e_j(k+n)| \le \delta_j\}$ can be derived as follows,

$$\begin{aligned}\Pr\{|e_j(k+n)| \le \delta_j\} =& 1 - \Pr\{|e_j(k+n)| > \delta_j\}\\ =& 1 - \psi_{n,j}\left(-\delta_j\right)\\ =& 1 - \psi\left(\frac{-\delta_j}{\rho_j(n)}\right),\end{aligned} \tag{4.3.8}$$

where $\psi_{n,j}(\cdot)$ is the CDF of $e_j(k+n)$, and $\psi(\cdot)$ is the CDF of standard Gaussian distribution with zero mean and unit variance.

By substituting (4.3.8) into (4.2.3), ε_{p} can be expressed as follows,

$$\varepsilon_{\mathrm{p}} = 1 - \prod_{j=1}^{N}\left[1 - \psi\left(\frac{-\delta_j}{\rho_j(n)}\right)\right]. \tag{4.3.9}$$

With the closed-form expression in (4.3.9), we can verify the monotonicity ε_{p}.

Property 1. *ε_{p} strictly increases with the prediction time n.*

Proof. Please see Appendix A.1. □

4.3.3 Delay-Reliability Tradeoff for Short Packet Transmissions

1) E2E Delay in the Communication System

As shown in Fig. 4.1, the distance between the transmitter and the receiver can be large. In this case, the E2E delay includes transmission delays and queueing delays in radio access networks, routing delays in backhauls and core networks, propagation delays, and processing delays in multiple equipments.

Here we assume that the inter-arrival time between packets is longer than the transmission delay. As a result, there is no queue in the buffers of the system. We

mainly focus on optimizing the transmission delay in the radio interface, which is denoted as D_{t}. The sum of all the other delays in the backhaul and the core network is assumed to be a constant D_{r}. As such, the E2E delay of a communication system is

$$D_{\mathrm{c}} = D_{\mathrm{r}} + D_{\tau}. \tag{4.3.10}$$

From (4.2.1), we can see that given prediction time n, the requirement on E2E communication delay is $D_{\mathrm{c}} \leq D_{\max} + n$. With predictions, the communication delay can be longer than the $D_{\max}$ (e.g., 1 ms). As such, retransmissions or repetitions become possible. If retransmissions are applied, the receiver needs to send acknowledgements back to the transmitter, and hence causes extra delay. To reduce latency, we apply K-Repetitions [36], i.e., the transmitter sends K copies of each packet no matter whether the first few copies are successfully decoded at the receiver or not. Let D_{τ} and ε_{τ} be the transmission duration of each copy and the decoding error probability, respectively. Then, the transmission delay is

$$D_{\mathrm{t}} = KD_{\tau}, \tag{4.3.11}$$

2) Packet Loss Probability

We assume that the packet loss probability in the core network and backhaul is much smaller than packet loss probability in radio access networks. In this section, we mainly focus on deriving the packet loss probability in the radio interface.

In the typical URLLC applications, the packet size is much smaller than that of traditional audio or video services. To transmit small packets with low transmission duration D_{τ}, the blocklength of channel coding is short. In the short blocklength

regime, the Shannon channel capacity is no longer applicable [75]. We consider flat-fading quasi-static wireless channels.[1] The achievable rate (bits/block) in the short blocklength regime can be accurately approximated by [66]

$$b \approx \frac{D_\tau T_s B}{\ln 2}\left[\ln\left(1+\frac{agP_{\mathrm{t}}}{\phi N_0 B}\right)-\sqrt{\frac{V}{D_\tau T_s B}}f_{\mathrm{Q}}^{-1}(\varepsilon_\tau)\right] \tag{4.3.12}$$

where B is the bandwidth, P_{t} represents the transmit power, N_0 denotes the noise power spectral density, $\gamma = \frac{agP_{\mathrm{t}}}{\phi N_0 B}$ represents the received SNR, a denotes the large-scale channel gain, g is the small-scale channel gain, $\phi > 1$ is the SNR loss that reflects the gap between the approximation in (4.3.12) and the achievable rate of practical coding schemes[2]. $V = 1 - [1+\gamma]^{-2}$ [66], $f_{\mathrm{Q}}^{-1}(\cdot)$ is the inverse function of the Q-function, and ε_τ is the decoding error probability. $D_\tau T_s B$ is the blocklength of channel codes. When the blocklength is large, (4.3.10) approaches to the Shannon capacity.

To avoid overhead and extra delay caused by channel estimation at the transmitter, we assume that the transmitter does not have channel state information. Only the AP has channel state information. According to (4.3.12), the expected decoding error probability of each transmission over a wireless channel is given by [66]

$$\bar{\varepsilon}_\tau = \int_0^\infty f_{\mathrm{Q}}\left\{\sqrt{\frac{D_\tau T_s B}{V}}\left[\ln\left(1+\frac{agP_{\mathrm{t}}}{\phi N_0 B}\right)-\frac{b\ln 2}{D_\tau T_s B}\right]\right\}\cdot f_g(x)dx, \tag{4.3.13}$$

where $f_g(x)$ is the distribution of the instantaneous channel gain [66]. For Rayleigh fading channel, we have $f_g(x) = \frac{1}{(N_{\mathrm{r}}-1)!}x^{N_{\mathrm{r}}-1}e^{-x}$, where N_{r} is the number of antennas at the AP and each transmitter only has one antenna.

After K repetitions, the packet loss probability in the communication system is

[1] The transmission duration D_τ is smaller than channel coherence time and the bandwidth for each transmission is smaller than coherence bandwidth [21].

[2] According to [86], when the decoding error probability ranges from 10^{-3} to 10^{-7}, ϕ ranges lies in $(0.1, 2)$ dB.

given by

$$\varepsilon_{\mathrm{c}} = (\bar{\varepsilon}_{\tau})^{K}. \tag{4.3.14}$$

According to (4.3.14), we can verify the monotonicity ε_{c}.

Property 2. *ε_{c} strictly decreases with repetition time K, or the E2E communication delay D_{c}.*

Proof. According to (4.3.14), it is obvious that ε_{c} decreases with K since $\bar{\varepsilon}_{\tau} < 1$, and thus decreases with the E2E delay D_{c} since $D_{\mathrm{c}} = D_{\mathrm{r}} + KD_{\tau}$. □

4.4 Prediction and Communication Co-design

4.4.1 Optimization problem formulation and solution

Based on the prediction and communication models in the previous subsections, we formulate an optimization problem to minimize the required bandwidth to ensure certain delay and reliability requirements, i.e., $(D_{\max}, \varepsilon_{\max})$. The optimization problem can be formulated as follows,

$$\min_{n,B,K} \quad B \tag{4.4.1}$$

$$\text{s.t.} \quad KD_{\tau} + D_{\mathrm{r}} - n \leq D_{\max}, \tag{4.4.1a}$$

$$\varepsilon_{\mathrm{p}} + \varepsilon_{\mathrm{c}} \leq \varepsilon_{\max}, \tag{4.4.1b}$$

$$(4.3.7), (4.3.9), (4.3.13) \text{ and } (4.3.14),$$

where (4.4.1a) is the combination of (4.2.1), (4.3.10) and (4.3.11).

It is very challenging to find the optimal solution of problem (4.4.1). This is because both of the optimization variables n and K are integers, and the expressions of ε_{c} given by (4.3.7) and (4.3.9), and ε_{p} given by (4.3.13) and (4.3.14) are non-convex.

To solve this problem, we decompose the original problem into two subproblems. In the first subproblem, we find the optimal prediction time n that minimizes overall error probability for a given B. By solving this problem, we can obtain the optimal bandwidth-reliability tradeoff in the co-design system, denoted as $\varepsilon_{\mathrm{o}}^{\min}(B)$. In the second subproblem, we find a minimal bandwidth B^* to ensure $\varepsilon_{\mathrm{o}}^{\min}(B^*) \leq \varepsilon_{\max}$ by binary search.

1) Subproblem 1

When B is given, the minimal overall error probability can be achieved by optimizing n as follows,

$$\begin{aligned} \varepsilon_{\mathrm{o}}^{\min}(B) = \min_{n} \quad & \varepsilon_{\mathrm{p}} + \varepsilon_{\mathrm{c}} && (4.4.2) \\ \text{s.t.} \quad & KD_{\tau} + D_{\mathrm{r}} - n = D_{\max}, && (4.4.2\text{a}) \\ & (4.3.7), (4.3.9), (4.3.13) \text{ and } (4.3.14), \end{aligned}$$

where K has been removed from the optimization variables. This is because the optimal solution is obtained when the equality in (4.4.1a) holds, and hence the value of K is determined by n. Problem (4.4.2) is still a non-convex optimization problem. According to property 2 and (4.4.2a), ε_{p} increases with n, and ε_{c} decreases with n. Thus, we can use binary search to find $\tilde{n}$ that satisfies $\varepsilon_{\mathrm{p}} \leq \varepsilon_{\mathrm{c}}$ when $n \leq \tilde{n}$, and $\varepsilon_{\mathrm{p}} > \varepsilon_{\mathrm{c}}$ when $n > \tilde{n}$. The correponding reliability is denoted as $\hat{\varepsilon}_{\mathrm{o}}^{\min}(B)$. Denote the optimal solution of problem (4.4.2) as n^*. We have the following proposition in terms of the error of $\hat{\varepsilon}_{\mathrm{o}}^{\min}(B)$.

Proposition 4.4.1. *The gap between $\hat{\varepsilon}_{\mathrm{o}}^{\min}(B)$ and $\varepsilon_{\mathrm{o}}^{\min*}(B)$ is less than $\varepsilon_{\mathrm{o}}^{\min*}(B)$, where $\varepsilon_{\mathrm{o}}^{\min*}(B)$ is the reliability achieved by the optimal solution.*

Proof. Please see Appendix A.2. □

We will further validate the accuracy of the near optimal solution via simulations.

2) Subproblem 2

The required minimal bandwidth to guarantee the overall reliability can be obtained from the following optimization problem,

$$\min_{B} B \tag{4.4.3}$$

$$\text{s.t. } \hat{\varepsilon}_{\text{o}}^{\min}(B) \leq \varepsilon_{\max}. \tag{4.4.3a}$$

Since the packet loss in the communication system decreases with bandwidth, the optimal solution of problem (4.4.3) is achieved when the equality in (4.4.3a) holds. Thus, the minimal bandwidth can be obtained via binary search.

4.4.2 Discussions on Complexity and Optimality

Denote the feasible region of bandwidth and prediction time as $[0, B_{\max}]$ and $[0, n_{\max}]$. Then, the complexity of binary search algorithm is in the order of $\log_2(B_{\max}) \log_2(n_{\max})$.

If we can obtain the global optimal solution of the two subproblems, then it is the global optimal solution of problem (4.4.1).

4.5 Performance Evaluation

In this section, we evaluate the effectiveness of the proposed co-design method via simulations and experiments.

4.5.1 Simulations

In the simulations, we consider one dimensional movement prediction as an example to evaluate the proposed co-design method. With this example, we show how

Table 4.1: Simulation Parameters

Parameters	**Values**
Maximal transmit power of a user P_{t}	23 dBm
Single-sided noise spectral density N_0	-174 dBm/Hz
Slot duration T_{s}	0.1 ms
Transmission duration T_τ	0.5 ms
Delay of core network and backhaul D_{r}	50 ms

the proposed method helps improving the reliability with given delay requirement. For comparison, the reliability achieved by a traditional transmission scheme without prediction is provided. Furthermore, we illustrate the tradeoff between bandwidth and reliability when the user experienced latency is zero. The simulations parameters are listed in Table 4.1. To ensure the reliability and latency requirements, we consider the worst case of the large-scale channel fading, i.e., the transmitter is located at the edge of a cell. The path loss model is $10\log_{10}(\delta_m) = 35.3 + 37.6\log_{10}(d_m)$, where $d_m = 100$ m.

We take one dimensional movement as an example, with which the state transition function in (4.3.1) can be simplified as follows [84],

$$\begin{bmatrix} r(k+1) \\ v(k+1) \\ a(k+1) \end{bmatrix} = \begin{bmatrix} 1 & T_s & \frac{T_s^2}{2} \\ 0 & 1 & T_s \\ 0 & 0 & 1 \end{bmatrix} \begin{bmatrix} r(k) \\ v(k) \\ a(k) \end{bmatrix} + \begin{bmatrix} 0 \\ 0 \\ w(k) \end{bmatrix},$$

where $X(k+1) = [r(k+1), v(k+1), a(k+1)]^T$, $X(k) = [r(k), v(k), a(k)]^T$, $r(k), v(k), a(k)$ are the location, velocity and acceleration in the kth slot, respectively. $W(k) = [0, 0, w(k)]^T$, and Φ is given by

$$\Phi = \begin{bmatrix} 1 & T_s & \frac{T_s^2}{2} \\ 0 & 1 & T_s \\ 0 & 0 & 1 \end{bmatrix}. \tag{4.5.1}$$

With given delay requirement (i.e., $D_{\max} = 0$ ms), the packet loss probability in

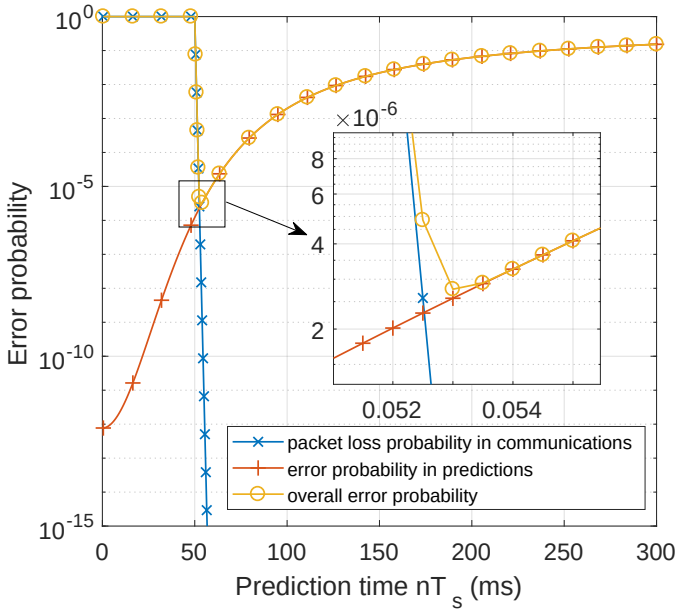

Figure 4.3: Joint optimization of predictions and communications: the packet loss probability ε_c in communications, the prediction error probability ε_p, and the over error probability ε_o are drawn as functions of prediction time n.

communications ε_{c}, the prediction error probability ε_{p}, and the overall error probability ε_{o} are shown in Fig. 4.3. The value of bandwidth B has impacts on the communication reliability, but does not change the trend of the overall reliability. To provide low packet loss probability ε_c, the bandwidth B is set as 55 KHz, packet size $b = 256$ bits, and $N_{\mathrm{r}} = 1$ to achieve 10^{-5} reliability. In predictions, the standard derivative of the transition noise of acceleration is $\sigma_w = 0.01$ m/s^2, and the required threshold is δ_l=0.1 m. The standard derivative of the initial error vector of location, velocity and acceleration are set to be 0.01 m, 0.3 m/s, and 0.3 m/s^2, respectively. The values of initial errors depend on the accuracy of observation and residual filter errors [84].

In Fig. 4.3, according to (4.2.1), the communication delay equals to the prediction

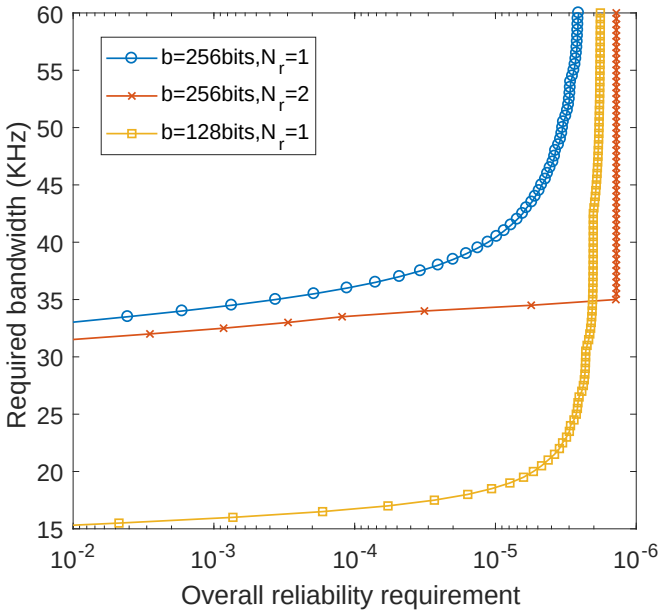

Figure 4.4: Bandwidth-reliability tradeoff curve with different packet sizes b and the numbers of received antenna N_{r}.

time, i.e., $D_{\mathrm{c}} = n$, since delay experienced by the user is set to be zero. The results in Fig. 4.3 show that when the E2E communication delay $D_{\mathrm{c}} = n < 50$ ms, i.e., less than the delays in the core network and the backhaul D_{r}, it is impossible to achieve zero latency with ultra-high reliability by using communication systems alone. When $D_{\mathrm{c}} = n > 50$ ms, the required transmission duration KD_{τ} increases with prediction time n. As a result, the overall error probability, ε_{o}, is first dominated by ε_{c} and then by ε_{p}. As such, ε_{o} first decreases and then increases with n. The proposed method obtained by binary search is $\varepsilon_{\mathrm{o}}^{\min} = 4.7 \times 10^{-6}$ with $n = 55$ ms and $K^* = 10$, which is the same as the solution obtained by exhaustive search. It implies that we can obtain the minimal $\varepsilon_{\mathrm{o}}^{\min}$ by the proposed heuristic method.

To illustrate the tradeoff between bandwidth and reliability, the required bandwidth to achieve different overall reliability requirements $\varepsilon_{\max}$ is shown in Fig. 4.4,

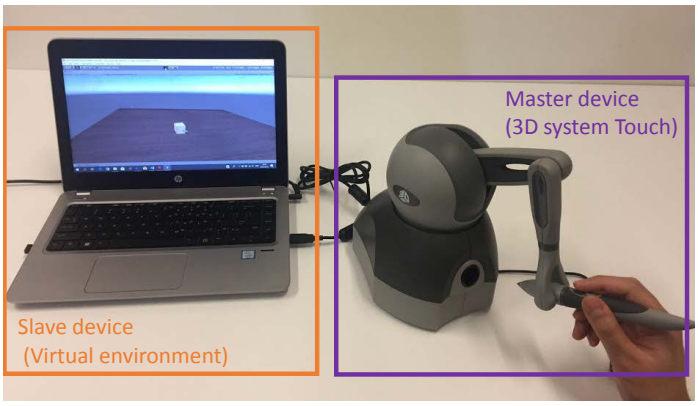

Figure 4.5: Experiment to obtain real movement data in tactile internet.

where zero user experienced latency is always ensured. It can be seen from Fig. 4.4 that when the reliability is large enough, i.e., $\varepsilon_{\max}$ is small enough, further increasing bandwidth cannot help improve reliability. This is because the overall error probability is dominated by the prediction error, while increasing bandwidth can only improve communication reliability. Moreover, the results also indicate that increasing the number of received antennas and compressing the size of packets with better source coding are helpful for achieving better tradeoff between bandwidth and reliability.

4.5.2 Experiments

To verify the feasibility of predictions in practice, we record the real movement data from the experiment shown in Fig. 4.5. In this experiment, a typical application of tactile internet is implemented in a virtual environment, where a box of hazardous chemicals or radioactive substances is dragged to move on the floor by a virtual slave device. A tactile hardware device named 3D System Touch (previously named Phantom Omni, or Geomagic) is used as a master device, which sends real time location information to the virtual slave device. A cable is used to connect the

master device to the virtual slave device in a virtual environment. The slave device in the virtual environment receives the locations from the master device, so it can move synchronously with the master device.

Human operators are invited to drag the virtual box from one corner to another corner of the floor in the virtual environment. In this experiment, we are mainly interested in the motion prediction, so the location information on the x-axis produced by the tactile hardware device is recorded and used to verify the predictions. A general linear prediction method in (4.3.4) is used to predict the future state system. Since only location information is available from the hardware, the velocity and acceleration are obtained from the first and the second order differences of locations [87]. Moreover, due to the limitation of the hardware, the duration of each slot is $T_{\mathrm{s}} = 1ms$.

The prediction error probability ε_{p} with different prediction time nT_{s} and the required location threshold δ are shown in Table 4.2. It can be seen from Table 4.2 that for $\delta = 0.002$ m, the prediction error probability ε_{p} increases with prediction time nT_{s}, which verifies Property 1 in section 4.3. Moreover, for the constant prediction time $nT_{\mathrm{s}} = 5$ ms, ε_{p} decreases with the required threshold δ. When the required threshold is larger, e.g., $\delta = 0.1$ m in remote driving, we can achieve the target reliability with longer prediction time, e.g., tens of milliseconds. This implies that prediction and communication co-design has the potential to achieve zero-latency in practice. It should be noted that the results from the experiment are generally worse than those of the simulations. This is because we only have the location information of the device, and extra estimation errors are introduced during the estimation of the velocity and acceleration.

Table 4.2: Prediction Error Probability

nT_{s}(ms)	δ (m)	ε_{p}
1	0.002	3.00×10^{-6}
2	0.002	1.62×10^{-5}
5	0.002	2.95×10^{-4}
5	0.005	3.73×10^{-5}
5	0.01	1.62×10^{-5}
10	0.01	6.55×10^{-5}
30	0.1	5.17×10^{-5}

4.6 Chapter Summary

In this chapter, we established a framework for prediction and communication co-design, where the prediction errors are taken into account when we analyze the reliability of URLLC. We first derived the relationship between prediction error and prediction time in closed-form. Then, we analyzed the relationship between packet loss probability, bandwidth usage and end-to-end communication delay. Based on these results, we formulated an optimization problem to minimize the required bandwidth for ensuring the delay and reliability requirements. Simulation results validate the effectiveness of the proposed methods, and show that it is possible to achieve zero-latency with ultra-high reliability. Thus, the tradeoff among bandwidth-reliability-latency is fundamentally changed.

Chapter 5

Incentive Mechanism Design for Wireless Energy Harvesting-Based IIoT

5.1 Chapter Introduction

In the last two chapters, we focus on minimizing bandwidth usage while ensuring the stringent latency and reliability requirements in mission critical applications. In this chapter, we will address the issue of energy supply, i.e., the long standing bottleneck of limited battery capabilities for IIoT.

The limited lifetime of traditional battery-powered sensors is one of the major hurdles for implementing fully wireless connections for IIoT, which are costly and hard to maintain [88, 89]. For example, frequent recharging or battery replacement is inconvenient in deserts or remote areas, and is even impossible for some scenarios, such as toxic environment or implanted medical applications [90]. To tackle this problem, RFEH has recently been proposed as an attractive technology to prolong the operational lifetime of sensors, enhance the deployment flexibility, and reduce the maintenance costs [90, 91].

In this chapter, we consider a radio frequency energy harvesting based IoT system consisting of a DAP and several EAPs. The DAP collects information from its associated sensors. EAPs can provide wireless charging services to sensors via the RF energy transfer technique. The sensors are assumed to have no embedded energy supply, but they can harvest energy from radio frequency signals radiated by the surrounding EAPs to transmit the data to the DAP [92].

There are some research considering the deployment of dedicated EAPs in the existing cellular network, such that the upgraded network can provide both wireless access and wireless charging services [93–100]. However, it was assumed that the EAPs are deployed by the same operator of the existing network. In practice, the DAP and EAPs may be operated by different operators[1]. To effectively motivate these third-party and self-interested EAPs to help charge the sensors, effective incentive mechanisms are required to improve the payoff of the DAP as well as that of EAPs. While there is several initial work designing the incentive mechanism [101–103] for the EAPs belonging to different operators, complete information was considered in these schemes. Specifically, it was assumed that the EAPs will truthfully report their private information to the DAP, e.g., their energy costs and channel gains between EAPs and sensors. This happens when there exists a *supervising entity* in the network, which is capable of monitoring and sharing all behaviours and network conditions of the DAP and EAPs to ensure that they always report the trustful information. However, without such a supervising entity, EAPs' private information might not be aware to the DAP, which is normally called *information asymmetry* in the literature

[1]This could happen when a resource-limited operator cannot provide radio frequency energy charging service in some certain area due to limited budgets, or lack of site locations, or lack of licensed spectrum for energy harvesting. Therefore, it has to resort to third-party operators.

[52]. A rational EAP may provide misleading information maliciously and pretend to be an EAP with better channel condition and/or higher energy cost to cheat for more rewards. A malicious EAP can succeed in cheating to get more benefits because of *information asymmetry* in the RF energy trading process.

To address the above issues, in this chapter, we will design effective incentive mechanisms to maximize the utilities of the DAP and EAPs under scenarios with asymmetric information. To this end, the following important questions should be addressed under asymmetric information:

Which EAPs the DAP should hire, how much energy should be requested from the hired EAPs, and how many rewards should be given to the hired EAPs?

The above questions are non-trivial to answer because the hierarchical interactions between multiple parities should be modeled and analyzed: the cooperation between the DAP, the DAP's sensors and the EAPs, and the competition among EAPs with heterogeneous private information. Moreover, the information asymmetry makes the problem even more challenging, because it is difficult for the DAP to hire the effective EAPs without knowing EAPs' private information, such as energy costs and channel condition towards its sensors.

To answer the above questions, we apply the well-established economic theories to model the conflicted interests among the multiple parities in the considered RFEH-based IoT system. Specifically, we first extend the existing Stackelberg game-based approach with complete information to the considered case with asymmetric information, such that we can evaluate the performance degradation caused by information asymmetry to this approach. More specifically, due to lack of the complete information, the expected utility function of the DAP is defined and optimized in the

Stackelberg game with asymmetric information. Considering that contract theory is a powerful tool originating from economics to deal with information asymmetry in a monopoly market, we apply contract theory to develop an optimal contract to effectively motivate the EAPs under asymmetric information. In our contract, the RF energy trading market is analogous as a monopoly labor market in economics. The DAP is modeled as the employer who offers a contract to each EAP. The contract is composed of a serious of contract items, which are combinations of energy-reward pairs. Each contract item is an agreement about how many rewards an EAP will get by contributing a certain amount of RF energy. Various heterogeneous EAPs are classified into different types according to their energy costs and instantaneous channel conditions. The EAPs are regarded as labors in the market, which will choose a contract item best meeting their interests. By properly designing the contract, an EAP's type will be revealed through its selection. Thus the DAP can capture each EAP's private information to a certain extent and thus relieve the issue of information asymmetry.

The idea of deploying a dedicated wireless energy network, which can provide wireless charging service to the terminals by using RFEH technology, was originally proposed by Huang *et al.* [93, 94]. The dedicated power transmitters are called power beacons or EAPs. Using stochastic geometry, the tradeoff between the densities of the base stations and EAPs was analyzed in [93]. There are many works exploiting EAPs to enable services of both wireless information and energy access in existing cellular networks [95–100]. Stochastic geometry was used to analyze the network performance with the EAPs in [95–97]. In [98], beamforming was introduced in the EAPs assisted cellular network to reduce the interference resulting from the EAPs. Leveraging

finite-length information theory, the system performance in the finite blocklength regime was analyzed in [99]. The security issue with EAP in the presence of a passive eavesdropper was investigated in [100]. In all the above works, the DAP and EAPs were assumed to belong to the same operator. In such a network, the devices belonging to the same operator with extra energy were assumed to voluntarily assist other devices. However, in practice, the DAP and EAPs may be operated by different operators. To successfully motivate self-interested EAPs to provide help, effective incentive mechanisms are required. There are several prior research works in designing the incentive mechanism [101–103] for the EAPs, where [101, 102] adopted Stackelberg game and [103] used auction to design the incentive mechanism. However, the existing incentive mechanisms only considered complete information scenario.

The contract theory has been employed to address incentive design problems in wireless communication areas, such as mobile edge computing [61], D2D communications [62] and cooperative spectrum sharing [63]. To our best knowledge, we are the first to apply contract theory in the RF energy trading process in RFEH-based IoT systems. To design the incentive mechanism in such a scenario is challenging because the DAP needs to choose and reward the most efficient EAPs without knowing their channel conditions and energy costs.

Stackelberg game has been widely used in wireless communications to model the interactions of steatitic parties, such as physical layer security [104], resource management for LTE-unlicensed [105], cognitive radio [106] and wireless energy harvesting [101, 102, 107, 108]. In [107], the authors considered cooperative spectrum sharing with one primary user and one secondary user), which harvests energy from ambient radio signal. The Stackelberg game was used to design the secondary user's

optimal cooperation strategy. In [108], simultaneous wireless information and power transfer (SWIPT) in relay interference channels was considered, where multiple source-destination pairs communicate through their dedicated energy harvesting relays. The optimal power splitting ratios for all relays were derived by the formulated Stackelberg game. There is a recent paper addressing the EAP assisted wireless energy harvesting by using Stackelberg game [102], but their system settings are different from those in our work. Only one EAP with multiple antennas is considered in this paper, and the EAP acts as the seller and the base station (BS) as the buyer on behalf of its sensors. A more relevant work is [101], where an incentive mechanism was designed for the system with the similar setup where monetary reward with unified pricing provided by the DAP to motivate third-party EAPs to assist the charging process. Here the unified pricing means prices per unit energy for different EAPs are the same. However, in this paper, we consider discriminative pricing scheme of Stackelberg game for the heterogeneous EAPs in our work, including unified pricing scheme as a special case. Here discriminative pricing means that we set different energy prices for different EAPs to fully exploit their potentials for the enery charging service. Moreover, we extend the Stackelberg game to asymmetric information scenarios by optimizing expected utility function of the DAP, instead of optimizing instantaneous utility function of the DAP in the classical Stackelberg game.

5.2 System Model

Consider a wireless energy harvesting-based IoT system consisting of one DAP and N EAPs belonging to different operators, which are connected to constant power supplies and connected to the server by backhauls, as shown in Fig. 5.1. The DAP is

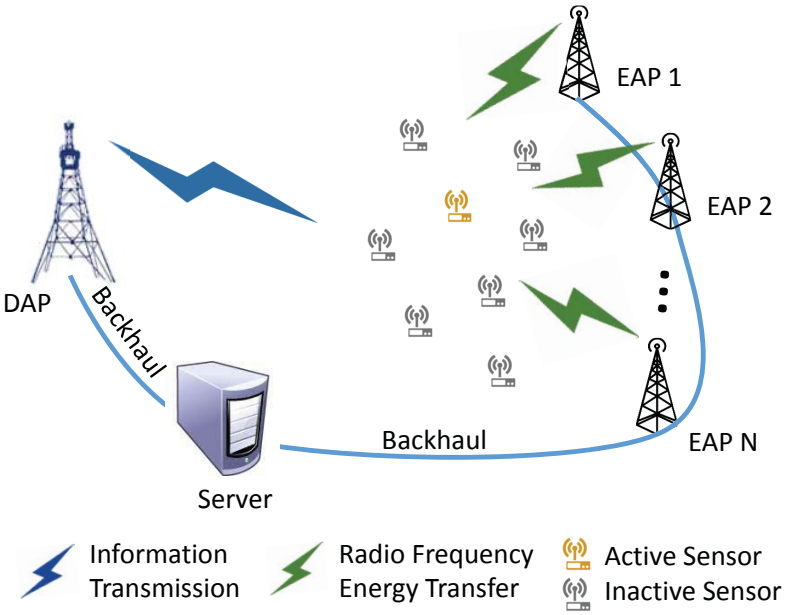

Figure 5.1: System model for the radio frequency energy harvesting assisted Internet of Things network

responsible for collecting various data from several wireless-powered sensors within its serving region. Without embedded energy supplies, the wireless-powered sensors fully rely on the energy harvested from the RF signals emitted by the EAPs to transmit its information to the DAP. For simplicity, we consider that the RF energy transfer and information transmission are performed over orthogonal bandwidth. For analytical tractability, time division-based transmission among sensors is adopted, i.e., there is only one active sensor during each transmission block. Hereafter, we refer to this active sensor as the information source. Besides, all the nodes in the system are assumed to be equipped with a single antenna and operate in the half-duplex mode.

We consider that the energy-carrying signals sent by the EAPs are independent and identically distributed (i.i.d.) random variables with zero mean and unit variance. Note that no coordination between the EAPs is needed since independent signals

are transmitted. All channels are assumed to experience independent slow and flat fading, where the channel gains remain constant during each transmission block and change independently from one block to another[2]. The information source rectifies the RF signals received from the EAPs and uses the harvested energy to transmit its information. The time duration of every transmission block is normalized to one. So we use "energy" and "power" interchangeably hereafter. The amount of energy harvested by the information source during one transmission block can be expressed as

$$E_s = \eta \sum_{m=1}^{N} p_m G_{m,s}, \tag{5.2.1}$$

where $0 < \eta < 1$ is the energy harvesting efficiency, p_m is the charging power of the mth EAP, and $G_{m,s}$ is the channel power gain between the mth EAP and the information source. Note that the noise is ignored in (5.2.1) [101] since it is practically negligible at the energy receiver.

The harvest-use protocol is considered in this chapter [109]. More specifically, the information source will use the harvested energy to perform instantaneous information transmission to the DAP. We consider a battery-free design which indicates that the sensor only has a storage device like supercapacitor to hold the harvested energy for a short period of time, e.g., among its scheduled transmission block. Hence the sensor exhausts all the harvested energy in each transmission block, so the sensor's energy storage device is emptied at the beginning of the transmission block. This battery-free design can reduce the complexity and cost of the sensors, which is particularly suitable for the considered IoT sensing applications and has been adopted by other

[2]Pilots are broadcasted by the active sensor to allow the DAP and EAPs to estimate the channels. So the DAP is aware of the channel gain from the DAP to the sensor and each EAP is aware of the channel gain from this EAP to the sensor. But the DAP generally is not aware of the channel gains from the EAPs to the active sensor. The energy consumption of channel estimation is ignored.

applications [110, 111]. The transmit power of the information source is thus given by

$$P_s = E_s. \tag{5.2.2}$$

Then, the received SNR at the DAP is given by

$$\beta = \frac{P_s G_{a,s}}{N_0}, \tag{5.2.3}$$

where N_0 is the noise power at the DAP, and $G_{a,s}$ is the channel power gain from the information source to the DAP. Note that the time duration for each transmission block is normalized as one, such that the channel capacity and throughput can be used interchangeably. Hence the achievable throughput (bps) from the information source to the DAP can be expressed by

$$\begin{aligned} R_{SD} &= W \log_2(1+\beta) \\ &= W \log_2 \left(1 + \frac{\eta G_{a,s}}{N_0} \sum_{m=1}^{N} p_m G_{m,s}\right), \end{aligned} \tag{5.2.4}$$

where W is the bandwidth. We define the received signal power at the active sensor contributed by the mth EAP[3] as $q_m = p_m G_{m,s}$, and set $\gamma = \eta G_{a,s}/N_0$ for notation simplicity. We can thus simplify (4) as

$$R_{SD} = W \log_2 \left(1 + \gamma \sum_{m=1}^{N} q_m\right). \tag{5.2.5}$$

As we mentioned before, the EAPs considered in the system belong to different operators and act strategically, so they would not help the DAP voluntarily. To address this issue, the DAP needs to provide rewards to motive the EAPs to charge its sensors. In this work, we mainly focus on monetary rewards as the incentive between operators. Other forms of rewards, such as physical resources (e.g., spectrum), or free offloading data between operators can also be used. To efficiently exploit the

[3]Note that the received power contributed by each EAP is assumed to be distinguishable by considering that the EAPs work in disjoint narrow bandwidth.

EAPs to achieve a good throughput, the following questions need to be answered in asymmetric information: *Which EAPs the DAP should hire, how much energy should be requested from the hired EAPs, and how many rewards should be given to the hired EAPs?*

5.3 Incentive Mechanisms with Asymmetric Information

To answer the above questions in the practical scenario with asymmetric information, we first model the strategic interactions between the DAP and EAPs as a Stackelberg game. We will first re-design and re-analyze the existing Stackelberg game into the considered scenario by defining and optimizing expected utility of the DAP. In economic theories, contract theory is a powerful tool to design incentive mechanisms in information asymmetry. As such, we will then reformulate the incentive mechanism problem into an optimal contract design problem.

5.3.1 Stackelberg Game with Asymmetric Information

In this part, we will first explore how to design a Stackelberg game to model the interactions between the DAP and the EAPs, and then derive the optimal energy prices under asymmetric information. In the proposed Stackelberg game with asymmetric information, the DAP provides rewards to the EAPs for charging its sensors. The DAP is the leader of the formulated Stackelberg game, which imposes energy prices for the EAPs. The DAP optimizes the energy prices to maximize its expected utility function defined as the difference between the benefits obtained from the achievable

throughput and its total payment to the EAPs. The EAPs are the followers which optimize their utility functions defined as the payment received from the DAP minus its energy cost.

1) Stackelberg Game Formulation

The channel conditions and energy costs of EAPs are different, so the efficiencies of EAPs to charge the sensor are distinct. To fully exploit the potential of the EAPs, a discriminative pricing strategy is considered, i.e., the DAP can impose different prices per unit energy harvested from different EAPs. Let $\boldsymbol{q} = [q_1, q_2, \ldots, q_N]^T$ as the vector of the active sensor's received power from EAPs, with q_m denoting the received power from the mth EAP, and let $\boldsymbol{\lambda} = [\lambda_1, \lambda_2, \ldots, \lambda_N]^T$ as the vector of prices per unit energy harvested from EAPs, with $\lambda_m \geq 0$ denoting the price per unit energy harvested from the mth EAP. The total payment of the DAP to the EAPs is

$$\Lambda(\boldsymbol{\lambda}, \boldsymbol{q}) = \sum_{m=1}^{N} \lambda_m q_m, \tag{5.3.1}$$

where q_m is the received energy from mth EAP. Since the aim of the DAP is to achieve higher throughput at the cost of less rewards to the EAPs, the utility function of the DAP can be defined as

$$U_{DAP}^{S}(\boldsymbol{\lambda}, \boldsymbol{q}) = R_{SD} - c\Lambda(\boldsymbol{\lambda}, \boldsymbol{q}), \tag{5.3.2}$$

where R_{SD} is the achievable throughput defined in (5.2.4) and (5.2.5), and c is the unit cost of the DAP, which is normalized as $c = 1$ without loss of generality hereafter.

Each EAP is modeled as a follower which would like to maximize its individual profit, the utility of which is defined as

$$U_k^S(\lambda_k, q_k) = \lambda_k q_k - \mathcal{C}_k(p_k), \tag{5.3.3}$$

where $p_k = q_k / G_{k,s}$ is the transmit power of the kth EAP, and $\mathcal{C}_k(\cdot)$ is used to model

the energy cost of the kth EAP, given by

$$\mathcal{C}_k(x) = a_k x^2, \tag{5.3.4}$$

where $a_k > 0$ is the energy cost coefficient. Note that the above quadratic function has been widely adopted in the energy trading market to model the energy cost [112]. The utility function of the kth EAP becomes

$$U_k^S(\lambda_k, q_k) = \lambda_k q_k - \frac{a_k}{G_{k,s}^2} q_k^2. \tag{5.3.5}$$

Since the DAP is not aware of each EAP's exact energy cost coefficient and channel gain, it can sort EAPs into some discrete types and use the statistical distributions of the types of EAPs from historical data to optimize the expected utility of the DAP. Specifically, we define the type of the kth EAP as

$$\theta_k := \frac{G_{k,s}^2}{a_k}, \tag{5.3.6}$$

which suggests that the larger the channel gain $G_{k,s}$ between the EAP and the information source, and/or the lower the unit energy cost coefficient a_k, the higher the type of the EAP. Without loss of generality, we assume that there are totally K types of EAPs with $\theta_1 < \theta_2 < \cdots < \theta_K$. In this definition, the higher type EAP has better channel quality and/or lower energy cost coefficient. Note that since $a_k > 0$ and $G_{k,s} > 0$, $\theta_i > 0$ holds for $i = 1, 2, \cdots, K$. Using (5.3.6), the EAP's utility can be rewritten as

$$U_k^S(\lambda_k, q_k) = \lambda_k q_k - \frac{q_k^2}{\theta_k}. \tag{5.3.7}$$

Assume that there are N_k EAPs belonging to the kth type, we thus have $\sum_{k=1}^{K} N_k = N$. We then can rewrite the DAP's utility according to the types of EAPs as

$$U_{DAP}^S(\lambda_k, q_k) = W \log_2 \left(1 + \gamma \sum_{k=1}^{K} N_k q_k\right) - \sum_{k=1}^{K} N_k \lambda_k q_k. \tag{5.3.8}$$

In this section, we consider a scenario with strong information asymmetry. In

such a scenario, the DAP is only aware of the total number of EAPs (i.e., N) and the distribution of each type. But it does not know each EAP's private type and thus it does not know the exact number of EAPs belonging to each type k (i.e., N_k). As such, the DAP needs to optimize its expected utility over the possibilities of all possible combinations of N_k. The expected utility of the DAP with N EAPs is given by

$$\begin{aligned}\mathbb{E}\{U_{DAP}^{S}(\boldsymbol{\lambda},\boldsymbol{q})\} = &\sum_{n_1=0}^{N}\sum_{n_2=0}^{N-n_1}\cdots\sum_{n_{K-1}=0}^{N-\sum_{i=0}^{K-2}n_i} \\ &\left\{\Phi_{n_1,\ldots,n_K}\left[W\log_2\left(1+\gamma\sum_{k=1}^{K}n_k q_k\right)-\sum_{k=1}^{K}n_k\lambda_k q_k\right]\right\},\end{aligned} \tag{5.3.9}$$

where $n_K = N-\sum_{i=0}^{K-1} n_i$ is known after giving $n_1, n_2, \ldots, n_{K-1}$ since the DAP knows the total number N of EAPs, and $\Phi_{n_1,\ldots,n_K}$ is the probability of a certain combination of the number of EAPs belonging to each type (i.e., $N_k, \{k = 1, 2, \ldots, K\}$). We assume that all types are uniformly distributed. The probability of one EAP belonging to each type is the same, which is $1/K$. In this case, $\Phi_{n_1,\ldots,n_K}$ can be calculated as

$$\begin{aligned}\Phi_{n_1,\ldots,n_K} &= \mathbf{Pr}\left(N_1 = n_1, N_2 = n_2, \ldots, N_k = n_k\right) \\ &= \frac{N!}{n_1! n_2! \ldots n_K! K^N}.\end{aligned} \tag{5.3.10}$$

Since the DAP is not aware of the EAPs' private information, it can only optimize the expectation of DAP's utility function by using the statistical knowledge of the EAP's private information. So the optimization problem for the DAP or the leader-level game can be formulated as

$$\begin{aligned}(\mathbf{P4.1}): \quad &\max_{\boldsymbol{\lambda}} \mathbb{E}\{U_{DAP}^{S}(\boldsymbol{\lambda},\boldsymbol{q})\} \\ s.t. \quad &\boldsymbol{\lambda} \geq \mathbf{0}.\end{aligned} \tag{5.3.11}$$

Accordingly, the optimization problem for the EAP with kth type or the follower-level

game can be formulated as

$$\begin{aligned} (\mathbf{P4.2}): \quad & \max_{q_k} U_k^S(\lambda_k, q_k) \\ s.t. \quad & q_k \geq 0. \end{aligned} \tag{5.3.12}$$

Note that although the DAP does not know the EAP's exact type, it knows the type set of EAPs.

The Stackelberg game for the considered system has been formulated by combining problems (P4.1) and (P4.2). In this game, the DAP is the leader who aims to solve problem (P4.1), while the EAPs are the followers who aim to solve their individual problem (P4.2). Once a game is formulated, the subsequent task is to find its equilibrium point(s). For the solution of the formulated game, the most well-known concept is the Stackelberg equilibrium (SE), which can be formally defined as follows:

Definition 5.3.1 (**Stackelberg equilibrium (SE)**). We use $\boldsymbol{\lambda}^* = [\lambda_1^*, \lambda_2^*, \ldots, \lambda_N^*]^T$ and $\boldsymbol{q}^* = [q_1^*, q_2^*, \ldots, q_N^*]^T$ to denote the solutions of problems (P4.1) and (P4.2), respectively. Then, $(\boldsymbol{\lambda}^*, \boldsymbol{q}^*)$ is a SE of the formulated game if the following conditions are satisfied:

$$U_{DAP}^S(\boldsymbol{\lambda}^*, \boldsymbol{q}^*) \geq U_{DAP}^S(\boldsymbol{\lambda}, \boldsymbol{q}^*), \tag{5.3.13}$$

$$U_m^S(q_m^*, \lambda_m^*) \geq U_m^S(q_m, \lambda_m^*), \tag{5.3.14}$$

for all $\boldsymbol{\lambda} \geq \mathbf{0}$ and $\boldsymbol{q} \geq \mathbf{0}$.

2) Analysis of the Proposed Game

In this part, we will analyze the SE of the proposed Stackelberg game with asymmetric information.

It can be observed from (5.3.5) that for given values of λ_k, the utility function of the EAP with the kth type is a quadratic function of its contributed power q_k to the active sensor and the constraint is affine, which indicates that the problem (P4.2)

is a convex optimization problem. Thus, it is straightforward to obtain its optimal solution given in the following lemma:

Lemma 5.3.1. *For given values of λ_k, the optimal q_k^* of the EAP with kth type for problem (P4.2) is given by*

$$q_k^* = \frac{\theta_k \lambda_k}{2}. \tag{5.3.15}$$

Proof. The proof of this lemma follows by noting that the objective function of problem (P4.2) given in (5.3.12) is a quadratic function in terms of q_k. So when $q_k^* = \frac{\theta_k \lambda_k}{2}$, the quadratic function is maximized. □

It can be observed from Lemma 5.3.1 that for the same energy price, an EAP with better channel gain and/or less energy cost would like to contribute more power to the sensors.

Then we replace q_k with q_k^* in problem (P4.1), so the optimization problem at the DAP side can be expressed as

$$\begin{aligned} (\mathbf{P4.3}): \quad & \max_{\boldsymbol{\lambda}} \mathbb{E}\{U_{DAP}^S(\boldsymbol{\lambda}, \boldsymbol{q}^*)\} \\ & s.t. \quad \boldsymbol{\lambda} \geq \mathbf{0}. \end{aligned} \tag{5.3.16}$$

where $\mathbb{E}\{U_{DAP}^S(\boldsymbol{\lambda}, \boldsymbol{q}^*)\}$ is given by

$$\begin{aligned} \mathbb{E}\{U_{DAP}^S(\boldsymbol{\lambda}, \boldsymbol{q}^*)\} = & \sum_{n_1=0}^{N} \sum_{n_2=0}^{N-n_1} \cdots \sum_{n_{K-1}=0}^{N-\sum_{i=0}^{K-2} n_i} \\ & \left\{ \Phi_{n_1,\ldots,n_K} \left[W \log_2 \left(1 + \frac{\gamma}{2} \sum_{k=1}^{K} n_k \theta_k \lambda_k \right) - \frac{1}{2} \sum_{k=1}^{K} n_k \theta_k \lambda_k^2 \right] \right\}, \end{aligned} \tag{5.3.17}$$

where $\Phi_{n_1,\ldots,n_K}$ is given in (5.3.10).

We can observe that problem (P4.3) is a concave function in terms of vector $\boldsymbol{\lambda}$. This is because each term in the summation is composed by a logarithm function (concave) and quadratic functions (concave), and the summation of concave functions

is still a concave function. Moreover, the constraint is affine. Problem (P4.3) is then a convex optimization problem. So we can numerically solve the system of equations given by the KKT conditions to get the solution of problem (P4.3). According to the KKT conditions, we can also get some insight about the structure of the solution and thus have the following proposition.

Proposition 5.3.1. *The optimal solution to problem (P4.3) has the following structure:*

$$\lambda_1^* = \lambda_2^* = \cdots = \lambda_N^*. \tag{5.3.18}$$

Proof. See Appendix B.1. □

We surprisingly find that the optimal energy prices for different EAPs are the same, even if we impose discriminative prices for different EAPs in the original design of the Stackelberg game. This is because the energy price of unit received power is used in our pricing scheme. The DAP has no motivation to treat the received power from EAPs differently, so a unified pricing per unit received power is achieved.

Lack of complete information, the performance of the Stackelberg game with asymmetric information is worse than that with complete information. Note that in the considered scenario, there are N EAPs in the market. In each channel realization, each EAP in the market selects one EAP type from an EAP type set randomly. In each channel realization, the Stackelberg game under complete information can adapt to the instantaneous combination of EAP types and calculate an optimal price for each instantaneous combination of EAP types by optimizing the instantaneous utility function. However, the Stackelberg game under asymmetric information cannot adapt to instantaneous combination of EAP types, since it can only calculate a single price

for all possible combinations of EAP types. Therefore, the reason why Stackelberg game under asymmetric information is worse than Stackelberg game under complete information is that it fails to adapt to the change of the instantaneous combinations of EAP types, i.e., the change of wireless channel conditions. This deduction will be verified later in the simulation part.

5.3.2 Optimal Contract with Asymmetric Information

As we mentioned above, the performance of the Stackelberg game is degraded under asymmetric information. To improve the performance under asymmetric information, the DAP could design and offer a contract to effectively motivate the EAPs to charge its sensors. Note that in the Stackelberg game, the EAP has the freedom to optimize its own utility by choosing any amount of received signal power at the active sensor when the DAP imposes some given energy price. Different from the Stackelberg game, limited options are allowed for EAPs to select in contract theory. Specifically, a group of energy-reward pairs (referred to as contract items) are designed. A contract consisting of a group of contract items is provided to the EAPs. The EAPs will choose a contract item at its discretion to maximize its benefit. By properly designing the contract item, the DAP can induce the EAP to expose its type by its selection of the contract item and thus relieve the information asymmetry.

In the following, we will formulate the optimal contract, characterize its feasibility conditions and provide the optimal solution for the formulated contract.

1) Contract Formulation In this part, we will formulate a contract for the RF energy trading between the DAP and EAPs, characterize its feasibility conditions, and derive the optimal contract subject to the feasibility conditions.

A contract including a series of energy-reward pairs (q_k, π_k) is designed to maximize the expectation of the DAP's utility. For the kth type EAP, q_k is the received power contributed by the kth EAP and π_k is the reward paid to the kth EAP as the incentive for the corresponding contribution.

We first rewrite the utility functions of the DAP and EAPs according to contract items. The DAP's utility function is thus given by

$$U_{DAP}^{C}(\boldsymbol{\pi}, \boldsymbol{q}) = W \log_2 \left(1 + \gamma \sum_{k=1}^{K} N_k q_k\right) - \sum_{k=1}^{K} N_k \pi_k, \tag{5.3.19}$$

where $\boldsymbol{\pi} = [\pi_1, \pi_2, \ldots, \pi_K]^T$ is the reward paid by the DAP to the EAP with the kth type for its corresponding contribution $\boldsymbol{q} = [q_1, q_2, \ldots, q_K]^T$. Similar to (5.3.9), the expectation of $U_{DAP}^{C}(\boldsymbol{\pi}, \boldsymbol{q})$ can be represented as

$$\begin{aligned} \mathbb{E}\{U_{DAP}^{C}(\boldsymbol{\pi}, \boldsymbol{q})\} = & \sum_{n_1=0}^{N} \sum_{n_2=0}^{N-n_1} \cdots \sum_{n_{K-1}=0}^{N-\sum_{i=0}^{K-2} n_i} \\ & \left\{ \Phi_{n_1,\ldots,n_K} \left[W \log_2 \left(1 + \gamma \sum_{k=1}^{K} n_k q_k\right) - \sum_{k=1}^{K} n_k \pi_k \right] \right\}, \end{aligned} \tag{5.3.20}$$

where $n_K = N - \sum_{i=0}^{K-1} n_i$ is known after giving $n_1, n_2, \ldots, n_{K-1}$ since the DAP knows the total number N of EAPs, and $\Phi_{n_1,\ldots,n_K}$ is the probability of a certain combination of the number of EAPs belonging to each type (i.e., $N_k, \{k = 1, 2, \ldots, K\}$), which is given by (5.3.10). And then the utility function of the EAP with the kth type is rewritten as

$$U_k^C(\pi_k, q_k) = \pi_k - \frac{q_k^2}{\theta_k}. \tag{5.3.21}$$

The social welfare is defined as the summation of the utilities of the DAP and all N

EAPs, given by

$$\begin{aligned}\Gamma(\boldsymbol{\pi},\boldsymbol{q}) &= U_{DAP}^{C}(\boldsymbol{\pi},\boldsymbol{q}) + \sum_{k=1}^{K} N_k U_k^C(\pi_k, q_k) \\ &= W\log_2\left(1+\gamma\sum_{k=1}^{K} N_k q_k\right) - \sum_{k=1}^{K}\frac{N_k q_k^2}{\theta_k}.\end{aligned} \tag{5.3.22}$$

It can be seen that the internal transfers, i.e., rewards, are cancelled in the social welfare, which is consistent with the aim to maximize the efficiency of the whole system, i.e., achieving more throughput at the cost of less energy consumptions.

Next, we will figure out the feasibility conditions. In our design, to encourage the EAPs to participate in the charging process and ensure that each EAP only chooses the contract item designed for its type, the following IR and IC constraints should be satisfied [52].

Definition 5.3.2 (**Individual Rationality (IR)**)**.** The contract item that an EAP chooses should ensure a nonnegative utility, i.e.,

$$U_k^C(\pi_k, q_k) = \pi_k - \frac{q_k^2}{\theta_k} \geq 0, \forall k \in \{1,\ldots,K\}. \tag{5.3.23}$$

Definition 5.3.3 (**Incentive Compatibility (IC)**)**.** An EAP of any type k prefers to choose the contract item (q_k, π_k) designed for its type, instead of any other contract item $(q_j, \pi_j), \forall j \in \{1,\ldots,K\}$ and $j \neq k$, given by

$$\pi_k - \frac{q_k^2}{\theta_k} \geq \pi_j - \frac{q_j^2}{\theta_k}, \forall k, j \in \{1,\ldots,K\}. \tag{5.3.24}$$

The IR condition requires that the received reward of each EAP should compensate the cost of its consumed energy when it participates in the energy trading. If $U_k \leq 0$, the EAP will choose not to charge the information source for the DAP. We define this case as $(q_k = 0, \pi_k = 0)$. The IC condition ensures that each EAP automatically selects the contract item designed for its corresponding type. The type

of each EAP is thus revealed to the DAP, which is called "self-reveal". If a contract satisfies the IR and IC constraints, we refer to the contract as a feasible contract.

Following the idea of contract theory[52], the DAP aims at maximizing its expected utility subject to the constraints of IR and IC given in (5.3.23) and (5.3.24). Thus, the optimal contract is the solution to the following optimization problem:

$$\begin{aligned}(\mathbf{P4.4}): \quad & \max_{(\boldsymbol{\pi},\boldsymbol{q})} \mathbb{E}\{U_{DAP}^{C}(\boldsymbol{\pi},\boldsymbol{q})\} \\ s.t. \quad & \pi_k - \frac{q_k^2}{\theta_k} \geq 0, \forall k \in \{1,\ldots,K\}, \\ & \pi_k - \frac{q_k^2}{\theta_k} \geq \pi_j - \frac{q_j^2}{\theta_k}, \forall k,j \in \{1,\ldots,K\}, \\ & q_k \geq 0, \pi_k \geq 0, \theta_k \geq 0, \forall k \in \{1,\ldots,K\}.\end{aligned} \tag{5.3.25}$$

The first two constraints correspond to IR and IC, respectively. Note that the EAP will reveal its private type truthfully with the IR and IC constraints. Specifically, the IR condition ensures the EAP's participation and the IC condition ensures that each EAP selects the contract item designed for its corresponding type to gain the highest payoff.

2) Constraint Reduction There are K IR constraints and $K(K-1)$ IC constraints in (5.3.25), which are non-convex and couple different EAPs together. It is hard to solve (5.3.25) directly due to the complicated constraints. Motivated by this, in the subsection, we first reduce the constraints of (5.3.25) and transform it.

We first realize that the following necessary conditions can be derived from the IR and IC constraints.

Lemma 5.3.2. *For any feasible contract, $\pi_i > \pi_j$ if and only if $q_i > q_j$, $\forall i,j \in \{1,\ldots,K\}$.*

Proof. See Appendix B.2. □

Lemma 5.3.2 shows that the EAP contributing more received power at the information source will receive more reward.

Lemma 5.3.3. *For any feasible contract, $\pi_i = \pi_j$ if and only if $q_i = q_j$, $\forall i, j \in \{1, \ldots, K\}$.*

Lemma 5.3.3 can be proved by using similar procedures as Lemma 5.3.2, which is omitted for brevity. Lemma 5.3.3 indicates that the EAPs providing the same received power will get the same amount of reward.

Lemma 5.3.4. *For any feasible contract, if $\theta_i > \theta_j$, then $\pi_i > \pi_j$, $\forall i, j \in \{1, \ldots, K\}$.*

Proof. See Appendix B.3. □

Lemma 3 shows that a higher type EAP should be given more reward. Together with Lemma 1 and Lemma 2, it can be deduced that a higher type EAP also contributes more energy to the information source. We define this feature as monotonicity.

Definition 5.3.4 (**Monotonicity**). If $\theta_i \geq \theta_j, \forall i, j \in \{1, \ldots, K\}$ and then $\pi_i \geq \pi_j$.

Based on the above analysis, we can now use the IC condition to reduce the IR constraints and have the following lemma.

Lemma 5.3.5. *With the IC condition, the IR constraints can be reduced as*

$$\pi_1 - \frac{q_1^2}{\theta_1} \geq 0. \tag{5.3.26}$$

Proof. Due to the IC condition, $\forall k \in \{2, \ldots, K\}$, we have

$$\pi_k - \frac{q_k^2}{\theta_k} \geq \pi_1 - \frac{q_1^2}{\theta_k}. \tag{5.3.27}$$

Since we have defined that $\theta_1 < \theta_2 < \cdots < \theta_K$, we also have

$$\pi_1 - \frac{q_1^2}{\theta_k} \geq \pi_1 - \frac{q_1^2}{\theta_1}. \tag{5.3.28}$$

Combining (5.3.27) and (5.3.28), we have

$$\pi_k - \frac{q_k^2}{\theta_k} \geq \pi_1 - \frac{q_1^2}{\theta_1} \geq 0. \tag{5.3.29}$$

Note that (5.3.29) shows that with the IC condition, if the IR condition of the EAP with type θ_1 holds, the IR condition of the other $K-1$ types will also hold. So the other $K-1$ IR conditions can be bound into the IR condition of the EAP with type θ_1. □

We can also reduce the IC constraints and attain the following lemma.

Lemma 5.3.6. *With monotonicity, the IC condition can be reduced as the local downward incentive compatibility (LDIC), given by*

$$\pi_i - \frac{q_i^2}{\theta_i} \geq \pi_{i-1} - \frac{q_{i-1}^2}{\theta_i}, \forall i \in \{2, \ldots, K\}, \tag{5.3.30}$$

and the local upward incentive compatibility (LUIC), given by

$$\pi_i - \frac{q_i^2}{\theta_i} \geq \pi_{i+1} - \frac{q_{i+1}^2}{\theta_i}, \forall i \in \{1, \ldots, K-1\}. \tag{5.3.31}$$

Proof. There are $K(K-1)$ IC constraints in (5.3.25), which can be divided into $K(K-1)/2$ downward incentive compatibility (DIC)[4], given by

$$\pi_i - \frac{q_i^2}{\theta_i} \geq \pi_j - \frac{q_j^2}{\theta_i}, \forall i, j \in \{2, \ldots, K\}, i > j, \tag{5.3.32}$$

and $K(K-1)/2$ upward incentive compatibility (UIC), given by

$$\pi_i - \frac{q_i^2}{\theta_i} \geq \pi_j - \frac{q_j^2}{\theta_i}, \forall i, j \in \{2, \ldots, K\}, i < j. \tag{5.3.33}$$

Let us first prove that the DIC can be reduced as the LDIC. By using the LDIC

[4]Note that $K(K-1)/2$ is still an integer, because $K(K-1)$ is the multiplication of two continuous integers, which must be an even number. So it is divisible by two.

for three continuous types, $\theta_{i-1} < \theta_i < \theta_{i+1}, \forall i \in \{2, \ldots, K-1\}$, we have

$$\pi_{i+1} - \frac{q_{i+1}^2}{\theta_{i+1}} \geq \pi_i - \frac{q_i^2}{\theta_{i+1}}, \tag{5.3.34}$$

$$\pi_i - \frac{q_i^2}{\theta_i} \geq \pi_{i-1} - \frac{q_{i-1}^2}{\theta_i}, \forall i. \tag{5.3.35}$$

By applying the monotonicity, i.e., if $\theta_i > \theta_j$, then $\pi_i > \pi_j$, $\forall i, j \in \{1, \ldots, K\}$, we have

$$(\theta_{i+1} - \theta_i)(\pi_i - \pi_{i-1}) \geq 0, \tag{5.3.36}$$

$$\theta_{i+1}(\pi_i - \pi_{i-1}) \geq \theta_i(\pi_i - \pi_{i-1}). \tag{5.3.37}$$

Combining (5.3.35) and (5.3.37), we have

$$\theta_{i+1}(\pi_i - \pi_{i-1}) \geq \theta_i(\pi_i - \pi_{i-1}) \geq q_i^2 - q_{i-1}^2. \tag{5.3.38}$$

Equally, (5.3.38) becomes

$$\pi_i - \frac{q_i^2}{\theta_{i+1}} \geq \pi_{i-1} - \frac{q_{i-1}^2}{\theta_{i+1}}. \tag{5.3.39}$$

Combining (5.3.39) and (5.3.34), we have

$$\pi_{i+1} - \frac{q_{i+1}^2}{\theta_{i+1}} \geq \pi_{i-1} - \frac{q_{i-1}^2}{\theta_{i+1}}. \tag{5.3.40}$$

So far, we have proved that type θ_{i+1} will prefer contract item (q_{i+1}, π_{i+1}) rather than contract item (q_{i-1}, π_{i-1}). By using (5.3.40), it can be extended downward until type θ_1, and thus all DIC holds.

$$\pi_{i+1} - \frac{q_{i+1}^2}{\theta_{i+1}} \geq \pi_{i-1} - \frac{q_{i-1}^2}{\theta_{i+1}} \geq \ldots \geq \pi_1 - \frac{q_1^2}{\theta_1}, \forall i. \tag{5.3.41}$$

So we conclude that with the monotonicity and the LDIC, the DIC holds. Similarly, we can prove that with the monotonicity and the LUIC, the UIC holds. □

By using the reduced IR and IC constraints, the optimization problem (5.3.25)

can be transformed as

$$
\begin{aligned}
(\mathbf{P4.5}): \quad & \max_{(\boldsymbol{\pi},\boldsymbol{q})} \mathbb{E}\{U_{DAP}^{C}(\boldsymbol{\pi},\boldsymbol{q})\} \\
s.t. \quad & \pi_1 - \frac{q_1^2}{2\theta_1} \geq 0, \\
& \pi_i - \frac{q_i^2}{\theta_i} \geq \pi_{i-1} - \frac{q_{i-1}^2}{\theta_i}, \forall i \in \{2,\ldots,K\}, \\
& \pi_i - \frac{q_i^2}{\theta_i} \geq \pi_{i+1} - \frac{q_{i+1}^2}{\theta_i}, \forall i \in \{1,\ldots,K-1\}, \\
& \pi_K \geq \pi_{K-1} \geq \cdots \geq \pi_1, \\
& q_k \geq 0, \pi_k \geq 0, \theta_k \geq 0, \forall k \in \{1,\ldots,K\}.
\end{aligned}
\tag{5.3.42}
$$

The LDIC and the LUIC in (5.3.42) can be combined as shown in Lemma 8.

Lemma 5.3.7. *Since the optimization objective function is an increasing function of q_k and a decreasing function of $\pi_k, \forall k \in \{1,\ldots,K\}$, the above optimal problem can be further simplified as*

$$
\begin{aligned}
(\mathbf{P4.6}): \quad & \max_{(\boldsymbol{\pi},\boldsymbol{q})} \mathbb{E}\{U_{DAP}^{C}(\boldsymbol{\pi},\boldsymbol{q})\} \\
s.t. \quad & \pi_1 - \frac{q_1^2}{\theta_1} = 0, \\
& \pi_k - \frac{q_k^2}{\theta_k} = \pi_{k-1} - \frac{q_{k-1}^2}{\theta_k}, \forall k \in \{2,\ldots,K\}, \\
& \pi_K \geq \pi_{K-1} \geq \cdots \geq \pi_1, \\
& q_k \geq 0, \pi_k \geq 0, \theta_k \geq 0, \forall k \in \{1,\ldots,K\}.
\end{aligned}
\tag{5.3.43}
$$

Proof. We will first prove that the LDIC can be simplified as $\pi_k - q_k^2/\theta_k = \pi_{k-1} - q_{k-1}^2/\theta_k$, which together with monotonicity can ensure the LUIC hold.

For the reduced IR constraint $\pi_1 - q_1^2/\theta_1 \geq 0$ in (5.3.42), the DAP will lower the π_1 as possible as it can to improve the optimization objective function $\mathbb{E}\{U_{DAP}\}$, until $\pi_1 - q_1^2/\theta_1 = 0$. As for the LDIC, which is $\pi_i - q_i^2/\theta_i \geq \pi_{i-1} - q_{i-1}^2/\theta_i, \forall i \in \{2,\ldots,K\}$. Notice that the LDIC will still hold if both π_i and π_{i-1} are lowered

by the same amount. To maximize the optimization objective function, the DAP will lower all $\pi - j$ as much as possible until $\pi_i - q_i^2/\theta_i = \pi_{i-1} - q_{i-1}^2/\theta_i$. Note that this process will not affect other type's LDIC. So the LDIC can be reduced to $\pi_i - q_i^2/\theta_i = \pi_{i-1} - q_{i-1}^2/\theta_i, \forall k \in \{2, \ldots, K\}$.

Next, we show that if $\pi_i - q_i^2/\theta_i = \pi_{i-1} - q_{i-1}^2/\theta_i, \forall k \in \{2, \ldots, K\}$ and the monotonicity holds, the LUIC holds. Since we have $\pi_i - q_i^2/\theta_i = \pi_{i-1} - q_{i-1}^2/\theta_i, \forall k \in \{2, \ldots, K\}$, and equally it becomes

$$\theta_i(\pi_i - \pi_{i-1}) = q_i^2 - q_{i-1}^2. \tag{5.3.44}$$

Because of monotonicity, i.e., if $\theta_i \geq \theta_{i-1}$, then $\pi_i \geq \pi_{i-1}$, we further have

$$\theta_i(\pi_i - \pi_{i-1}) \geq \theta_{i-1}(\pi_i - \pi_{i-1}). \tag{5.3.45}$$

Combining (5.3.44) and (5.3.45), we have

$$\theta_i(\pi_i - \pi_{i-1}) = q_i^2 - q_{i-1}^2 \geq \theta_{i-1}(\pi_i - \pi_{i-1}), \tag{5.3.46}$$

and equally we have

$$\theta_{i-1}\pi_i - q_i^2 \leq \theta_{i-1}\pi_{i-1} - q_{i-1}^2, \tag{5.3.47}$$

$$\pi_i - \frac{q_i^2}{\theta_{i-1}} \leq \pi_{i-1} - \frac{q_{i-1}^2}{\theta_{i-1}}, \tag{5.3.48}$$

which is exactly the LUIC condition. So the LUIC can be removed from the constraints in (5.3.42). □

3) Solution to Optimal Contract We now solve the optimization problem (5.3.43) to attain the optimal contract in the subsequent way: a standard method is first applied to resolve the relaxed problem without monotonicity and the solution is then verified to satisfy the condition of the monotonicity. By iterating the first and

second constraints in (5.3.43), we have

$$\begin{aligned}\pi_k &= \frac{q_1^2}{\theta_1} + \sum_{n=2}^{k} \frac{q_n^2 - q_{n-1}^2}{\theta_n} \\ &= \frac{1}{\theta_k} q_k^2 + \sum_{n=2}^{k} \left(\frac{1}{\theta_{n-1}} - \frac{1}{\theta_n} \right) q_{n-1}^2,\end{aligned} \tag{5.3.49}$$

where $\forall k \in \{2, \ldots, K\}$. Substitute (5.3.49) into $\mathbb{E}\{U_{DAP}^{C}(\boldsymbol{\pi}, \boldsymbol{q})\}$, and all $\pi_k, \forall k \in \{1, \ldots, K\}$ are removed from the optimization problem (5.3.43), which becomes

$$\begin{aligned}\max_{\boldsymbol{q}} & \sum_{n_1=0}^{N} \sum_{n_2=0}^{N-n_1} \cdots \sum_{n_{K-1}=0}^{N-\sum_{i=0}^{K-2} n_i} \Phi_{n_1,\ldots,n_K} \\ & \times \left[W \log_2 \left(1 + \gamma \sum_{k=1}^{K} n_k q_k \right) \right. \\ & \left. - \sum_{k=1}^{K-1} \left(\frac{1}{\theta_k} \sum_{i=k}^{K} n_i - \frac{1}{\theta_{k+1}} \sum_{i=k+1}^{K} n_i \right) q_k^2 - \frac{n_K}{\theta_K} q_K^2 \right], \\ s.t. \quad & q_k \geq 0, \forall k \in \{1, \ldots, K\}.\end{aligned} \tag{5.3.50}$$

Note that (5.3.50) is composed of logarithmic functions and quadratic functions, both of which are concave functions. And the positive summation of all these concave functions is still a concave function. Besides, the constraint set is a convex set. So we can leverage standard convex optimization tools in [113] to solve it to get q_k, and then π_k can be calculated by (5.3.49). Moreover, monotonicity is met automatically when the type is uniformly distributed [52]. So far, we have derived the optimal contract (q_k, π_k), $\forall k \in \{1, \ldots, K\}$, which can maximize the utility of the DAP and satisfy the constraints of IR and IC.

5.3.3 Practical Implementation

To implement the proposed approach in a practical radio frequency energy harvesting-based IoT system, the following steps should be followed.

First, the DAP needs to collect the information it requires by the computation of the optimal contract. The active sensor will broadcast pilots to allow the DAP and EAPs to estimate the channels such that the DAP is aware of the channel gain from the DAP to the sensor. From historical data, the DAP can obtain empirical values of the energy harvesting efficiency factor and noise power, and thus it can attain the value of parameter γ. With the known values of other public system parameters including the channel bandwidth, the user number, and the set of EAP types, the DAP can calculate the optimal contract.

Next, the DAP will broadcast the optimal contract to the candidate EAPs via the corresponding backhauls. By evaluating the contract, the EAPs will decide whether to participate in the cooperation. If it decides to participate in the current energy trading, it will send a feedback to the DAP. After the DAP receives the feedback, it will sign a contract with the EAP.

Finally, after the contracts are signed, the EAPs will perform the contracts by establishing an energy transfer link towards the active sensor and charge it according to the agreed transmit power. When the DAP detects that the EAPs have fulfilled its contractual obligation, the DAP will pay the EAP with agreed amount of rewards via the backhaul connecting the operators.

5.4 Benchmark Schemes with Complete Information

To investigate the impacts from information scenarios and compare the proposed schemes with the existing schemes under complete information, we first extend existing Stackelberg game from a unified pricing strategy into a discriminative pricing strategy. And then we present the centralized optimization scheme under complete information as the reference for the proposed incentive mechanisms.

5.4.1 Stackelberg Game Formulation

To fully exploit the potentials of EAPs with distinct channel conditions and energy costs, a discriminative pricing strategy is considered, i.e., the DAP can impose different prices per unit energy harvested from different EAPs. The utility function of the DAP can be rewritten as

$$U_{DAP}^{S}(\boldsymbol{\lambda}, \boldsymbol{q}) = R_{SD} - \sum_{m=1}^{N} \lambda_m q_m, \tag{5.4.1}$$

where $\boldsymbol{q} = [q_1, q_2, \ldots, q_N]^T$ is the vector of the active sensor's received power from EAPs, with q_m denoting the received power from the mth EAP, $\boldsymbol{\lambda} = [\lambda_1, \lambda_2, \ldots, \lambda_N]^T$ is the vector of prices per unit energy harvested from EAPs, with $\lambda_m \geq 0$ denoting the price per unit energy harvested from m EAP, and R_{SD} is the achievable throughput defined in (5.2.4) and (5.2.5). The optimization problem for the DAP or the leader-level game can be formulated as

$$\begin{aligned} (\mathbf{P5.1}): \quad & \max_{\boldsymbol{\lambda}} U_{DAP}^{S}(\boldsymbol{\lambda}, \boldsymbol{q}) \\ s.t. \quad & \boldsymbol{\lambda} \geq \mathbf{0}. \end{aligned} \tag{5.4.2}$$

Note that the optimization problem (P5.1) is different from (P4.1) under asymmetric information, and the instantaneous utility of the DAP is optimized here, instead of expected utility of the DAP in asymmetric information.

Each EAP is modeled as a follower which would like to maximize its individual profit, the utility of which is rewritten as

$$U_m^S(\lambda_m, q_m) = \lambda_m q_m - \frac{a_m}{G_{m,s}^2} q_m^2, \tag{5.4.3}$$

where $a_m > 0$ and $G_{m,s}$ are the energy cost coefficient and channel gain of the mth EAP, respectively. Thus, the optimization problem for the EAP m or the follower-level game is given by

$$\begin{aligned} (\mathbf{P5.2}): \quad & \max_{q_m} U_m^S(\lambda_m, q_m) \\ s.t. \quad & q_m \geq 0. \end{aligned} \tag{5.4.4}$$

5.4.2 Analysis of the Formulated Stackelberg Game

In this subsection, we will derive the SE of the formulated game by analyzing the optimal strategies for the DAP and EAPs to maximize their own utility functions. A closed-form solution is derived by using Karush-Kuhn-Tucker (KKT) conditions.

First, the optimal q_m^* of the mth EAP is similar to that in (5.3.15), which is given by the following Lemma:

Lemma 5.4.1. *For given λ_m, the optimal solution for problem (P5.2) is given by*

$$q_m^* = \frac{G_{m,s}^2 \lambda_m}{2a_m}. \tag{5.4.5}$$

Proof. The proof of this lemma follows by noting that the objective function of problem (P5.2) given in (5.4.4) is a concave function in terms of q_m. □

It can be observed from Lemma 5.4.1 that for the same energy price, an EAP with

better channel gain and/or less energy cost would like to contribute more power to the active sensor.

Subsequently, we need to solve problem (P5.1) by replacing q_m with q_m^* given in (5.4.5). The optimization problem at the DAP side can be expressed as

$$\begin{aligned} (\mathbf{P5.3}): \quad & \max_{\boldsymbol{\lambda}} U_{DAP}^S(\boldsymbol{\lambda}, \boldsymbol{q}^*) \\ & s.t. \quad \boldsymbol{\lambda} \geq \mathbf{0}, \end{aligned} \tag{5.4.6}$$

where $U_{DAP}^S(\boldsymbol{\lambda}, \boldsymbol{q}^*)$ is given by

$$U_{DAP}^S(\boldsymbol{\lambda}, \boldsymbol{q}^*) = W \log_2 \left(1 + \gamma \sum_{m=1}^{N} \frac{G_{m,s}^2}{2a_m} \lambda_m\right) - \sum_{m=1}^{N} \frac{G_{m,s}^2}{2a_m} \lambda_m^2. \tag{5.4.7}$$

We can observe that problem (P5.3) is a concave function in terms of vector $\boldsymbol{\lambda}$ since the former part in (5.4.7) is a logarithm function (concave) and the latter part in (5.4.7) is the summation of quadratic functions (concave), and the constraint is affine. So problem (P5.3) is a convex optimization problem. By using KKT conditions to solve problem (P5.3), the closed-form solution for $\boldsymbol{\lambda}$ is derived in the following proposition.

Proposition 5.4.1. *The optimal solution to problem (P5.3) is given by*

$$\lambda_1^* = \lambda_2^* = \cdots = \lambda_N^* = \frac{\sqrt{\log_2(e)\gamma^2 W \Theta + 1} - 1}{\gamma \Theta}, \tag{5.4.8}$$

where e is the base of the natural logarithm, and Θ is given by

$$\Theta = \sum_{m=1}^{N} \frac{G_{m,s}^2}{a_m}. \tag{5.4.9}$$

Proof. See Appendix B.4. □

Proposition 5.4.1 shows that the optimal prices for the Stackelberg game with complete information are the same. This result is consistent with that of the Stackelberg game with asymmetric information. As we explained before, this is because the received power price is used in the Stackelberg games with complete and asymmetric

information. The DAP has no motivation to treat the received power from EAPs differently.

Note that the Stackelberg game under complete information can calculate an optimal price for each instantaneous channel realization and equivalently the combination of EAPs' types. As such, it can adapt to the change of channel conditions. As a comparison, the Stackelberg game under asymmetric information can only calculate a single price no matter of the change of the channel conditions, i.e., the change of the combinations of the EAPs' types.

5.4.3 Centralized Optimization

In this part, the performance of centralized optimization scheme, i.e., the optimal contract with complete information, where the DAP knows exactly the types of the EAPs, is presented. The centralized optimization problem is given as follows.

$$\begin{aligned} (\mathbf{P5.4}): \quad & \max_{(\boldsymbol{\pi},\boldsymbol{q})} \mathbb{E}\{U_{DAP}^{C}(\boldsymbol{\pi},\boldsymbol{q})\} \\ & s.t. \quad \pi_k - \frac{q_k^2}{\theta_k} \geq 0, \forall k \in \{1,\ldots,K\}, \end{aligned} \tag{5.4.10}$$

where $\mathbb{E}\{U_{DAP}^{C}(\boldsymbol{\pi},\boldsymbol{q})\}$ is given in (5.3.20).

Since the DAP knows exactly the types of the EAPs, the optimal prices are given by

$$\pi_k^* = \frac{q_k^2}{\theta_k}, \forall k \in \{1,\ldots,K\}. \tag{5.4.11}$$

We substitute π_k in (5.4.10) with π_k^* and get

$$\begin{aligned} (\mathbf{P5.5}): \quad & \max_{\boldsymbol{q}} \mathbb{E}\{U_{DAP}^{C}(\boldsymbol{\pi}^*,\boldsymbol{q})\} \\ & s.t. \quad \boldsymbol{q} \geq \mathbf{0}, \end{aligned} \tag{5.4.12}$$

where $\mathbb{E}\{U_{DAP}^{C}(\boldsymbol{\pi}^*, \boldsymbol{q})\}$ is given by

$$\mathbb{E}\{U_{DAP}^{C}(\boldsymbol{\pi}^*, \boldsymbol{q})\} = \sum_{n_1=0}^{N} \sum_{n_2=0}^{N-n_1} \cdots \sum_{n_{K-1}=0}^{N-\sum_{i=0}^{K-2} n_i} \left\{ \Phi_{n_1,\ldots,n_K} \left[W \log_2 \left(1 + \gamma \sum_{k=1}^{K} n_k q_k \right) - \sum_{k=1}^{K} n_k \frac{q_k^2}{\theta_k} \right] \right\}. \tag{5.4.13}$$

Note that (5.4.13) is exactly the expectation of the social welfare, which is defined in (5.3.22). Although we originally optimize the utility function of the DAP in problem (P5.4), it is consistent with the optimization of the social welfare, which is a similar case in the design of contract theory as we mentioned before.

It can also be observed that problem (P5.5) is a convex optimization problem. This is because each term in the summation is composed of a logarithm function (concave) and quadratic functions (concave), the summation of concave functions is still a concave function, and the constraint is affine. We can get the solution of problem (P5.5) by solving the system of equations given by KKT conditions, which is omitted here as it is similar to that in Appendix B.1.

5.5 Performance Evaluations

In this section, we first evaluate the feasibility of the proposed contract, and then compare the performance of the proposed incentive mechanisms. The performance of centralized optimization scheme is also simulated as the upper bound.

The main system parameters are shown in Table 5.1. Since $\theta = G_{m,s}^2/a_m$ and $\gamma = \eta G_{a,s}/N_0$, the practical ranges of θ and γ can be determined by the parameters shown in Table 5.1. In the simulations, K types of EAPs are first generated randomly and used as the set of EAP types. Then each of N EAPs in the market will choose one

Table 5.1: System Settings

Parameters	Values
Energy harvesting efficiency η	0.5
Bandwidth W	1MHz
Energy cost coefficient a_m	[0.1,1]
$d_{m,s}$	[5m,10m]
$d_{a,s}$	[15m,25m]
Path-loss coefficient α	2
Power attenuation at reference distance of 1m	30dB
Noise power N_0	$10^{-8}mW$

type from the set of EAP types uniformly, and thus the DAP's type θ is uniformly distributed. The unit of achievable throughput is set as Mbps.

To verify the feasibility (i.e., IR and IC) of the proposed scheme under information asymmetry, the utilities of EAPs with type 3, type 6 and type 9 are plotted in Fig. 5.2 as functions of all contract items $(q_k, \pi_k), k \in 1, 2, \ldots, K$. We can see from Fig. 5.2 that each of the utility achieves its peak value only when it chooses the contract item designed for its corresponding type, which indicates that the IC constraint is satisfied. For example, for the type 6 EAP, its utility achieves the peak value only when it selects the contract item (q_6, π_6), which is exactly designed for its type. If the type 6 EAP selects any other contract item $(q_k, \pi_k), k \in 1, 2, \ldots, K$ and $k \neq 6$, its utility will reduce. Moreover, when each of above type EAPs (i.e., type 3, type 6 and type 9) chooses the contract item designed for its corresponding type, the utilities are nonnegative. Note that similar phenomenon can be observed for all other types of EAPs when they select the contract item designed for their corresponding types, which are not shown in Fig. 5.2 for brevity. In this sense, the IR condition is satisfied. It

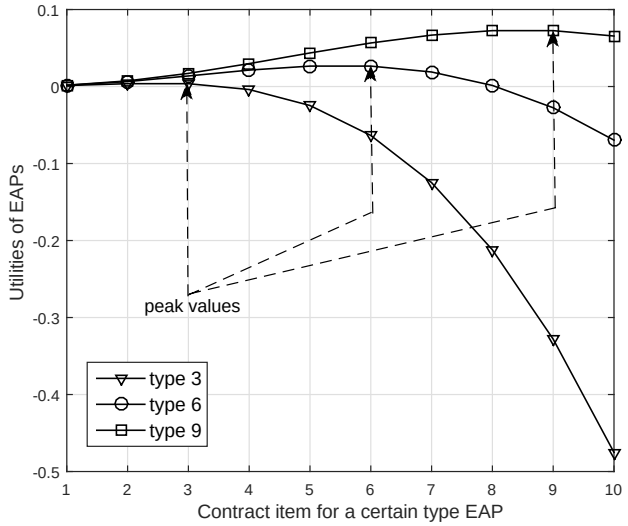

Figure 5.2: Utilities of EAPs with type 3, type 6 and type 9 as functions of contract items designed for all kinds of EAPs from type 1 to type 10. We set $N = 5$ and $K = 10$.

can be concluded that utilizing the proposed scheme, EAPs will automatically reveal its type to the DAP after selecting the contract item. This means that using the proposed scheme, the DAP can capture the EAPs' private information (i.e., its type), and thus effectively address the problem of information asymmetry.

To evaluate the performance of the proposed schemes, we compare the social welfare of the contract, Stackelberg games and the upper bound. Fig. 5.3 plots the social welfare of these schemes as a function of γ. It can be observed from Fig. 5.3 that the utilities achieved by all schemes increase with γ. This is because with the same $\sum_{m=1}^{N} q_m$, the larger the value of γ, the larger the achievable throughput R_{sa} (refer to (5.2.5)), and thus the larger social welfare (refer to (5.3.22)). The performance of the optimal scheme with complete information providing the best performance serves as the upper bound. The performance of contract scheme is generally better than

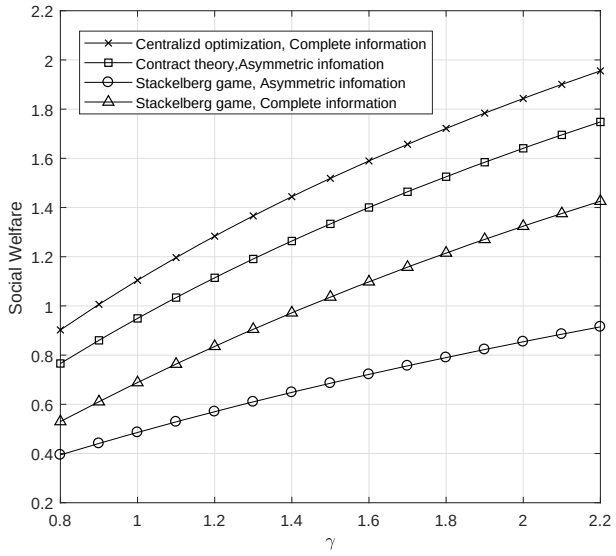

Figure 5.3: Social welfare as a function of γ. We set $N = 2$ and $K = 5$.

that of two Stackelberg games. This is because in contract theory, the EAPs have limited contract items to choose from and thus by using the contract theory, the DAP extracts more benefits from the EAPs and leave less surplus for the EAPs. However, in Stackelberg games, the EAPs have the freedom to optimize its individual utility function and thus can reserve more surplus. So the performance of the Stackelberg games is inferior than that of the contract scheme. We can also observe that the Stackelberg game with asymmetric information is inferior than that with complete information. This is because without complete information, the Stackelberg game fails to adapt to the change of the channel, and thus the performance becomes worse.

Fig. 5.4 shows the normalized social welfare as a function of γ, where social welfare of the contract and Stackelberg games is normalized by the upper bound. It can be seen in Fig. 5.4 that when γ is small, the social welfare of contract can initially achieve

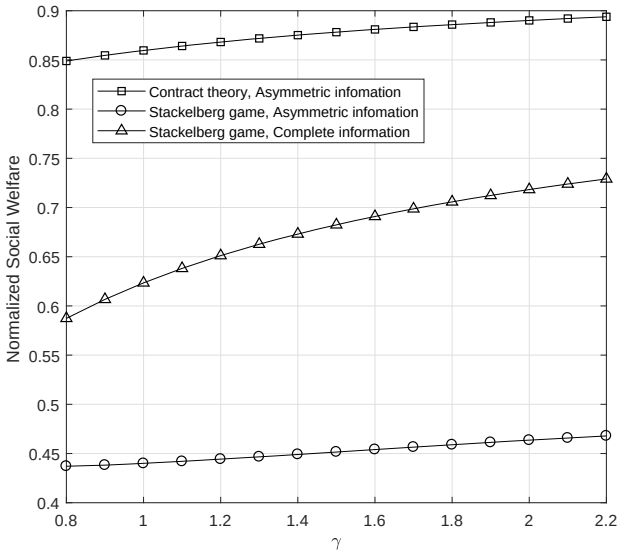

Figure 5.4: Normalized social welfare as a function of γ. We set $N = 2$ and $K = 5$.

more than 85% of that of the centralized optimization scheme with complete information, and gradually approach to it with the increase of γ. This demonstrates that the proposed incentive mechanism can effectively mitigate the effects of information asymmetry by leveraging contract theory, while the performance of the Stackelberg game with complete information is generally less than 75% of that of the optimal scheme with complete information. Moreover, the performance of the Stackelberg game with asymmetric information is even worse, which is generally less than 50% of that of the optimal scheme with complete information. The above results show that by using the monopoly position in contract theory to provide limited contract items, the contract can achieve good performance close to the optimal centralized optimization with complete information. However, in Stackelberg games, the DAP grants some freedom for the EAPs to do optimizations, which is selfish and does not care about social welfare. As such, its performance in terms of social welfare is

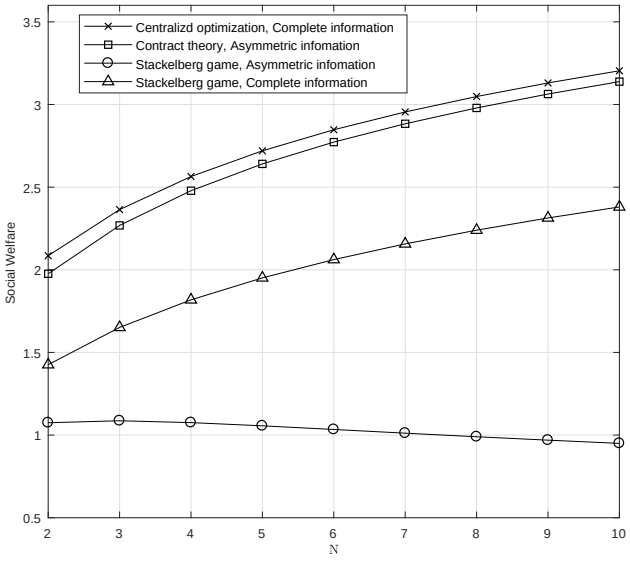

Figure 5.5: Social welfare as a function of N. We set $K = 2$, $\gamma = 2.2$ and $N = 2, 3, \ldots, 10$.

degraded.

To explore the impact of the total EAP number N in the market, we plot the curves of the social welfare and the normalized social welfare of the contract, Stackelberg games and the upper bound in Fig. 5.5 and Fig. 5.6. In Fig. 5.5, the social welfare of these schemes is plotted as a function of N. We can observe from Fig. 5.5 that the utility functions achieved by all three schemes of upper bound, contract, Stackelberg with complete information increase with N. This is because the overall social welfare increases with the number of EAPs in the market. The more EAPs in the market, the larger the summation of utility functions of all the DAP and EAPs. However, the Stackelberg game under asymmetric information decreases slightly as N increases. This is because the Stackelberg game under asymmetric information fails to adapt to the change of the combinations of the EAPs' types. As we mentioned before, it can

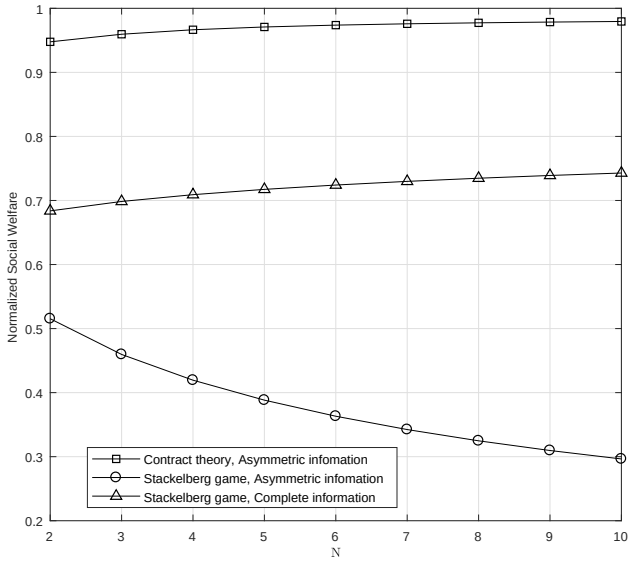

Figure 5.6: Normalized social welfare as a function of N. We set $K = 2$, $\gamma = 2.2$ and $N = 2, 3, \ldots, 10$.

only calculate one single price for all the combinations of EAPs' types. The more EAPs in the market, the more diverse combinations of the EAPs' types. As such, the performance of the Stackelberg under asymmetric information becomes worse. As a comparison, the Stackelberg game with complete information can calculate a price targeting a certain combination of EAPs' types in the market. So it provides better performance than that of its asymmetric counterpart, while the contract leverages its monopoly status in the market structure to provide a limited group of contract items for the EAPs to choose from. Therefore, contract theory-based scheme provides the better performance than that of both Stackelberg games and close to the performance of the upper bound.

In Fig. 5.6, the normalized social welfare of these schemes is plotted as a function of N, where social welfare of the contract and Stackelberg games is normalized by

the upper bound. It can be seen in Fig. 5.6 that when $N = 2$, the social welfare of contract can initially gain more than 95% of that of the centralized optimization scheme with complete information, and gradually approach to it with the increase of N. This proves that the effects of information asymmetry can be mitigated successfully by leveraging contract theory, while the Stackelberg game with complete information can only provide the normalized social welfare of less than 75%. Besides, the performance of the Stackelberg game with asymmetric information is even worse, which is generally less than 50% of that of the optimal scheme with complete information and decreases significantly with the increase of N in the market. This is because the more EAPs in the market, the more diverse the combinations of EAPs' types will be. The Stackelberg game under asymmetric information cannot adapt to the change of the combinations of EAPs' types as it can only calculate a single price for all possible combinations of EAPs' types.

5.6 Chapter Summary

In this chapter, we developed incentive mechanisms under complete and asymmetric information to unveil the impact of information asymmetry and market structure. Specifically, we developed a contract based incentive mechanism for the wireless energy trading in RFEH based IIoT systems under asymmetric information. In the asymmetric information scenario, a Stackelberg game based scheme was also formulated as a comparison. In complete information, the existing Stackelberg game was extended from unified pricing into discriminative pricing as a comparison. In the simulations, it was shown that the Stackelberg game degrades significantly without complete information, and the performance of the contract scheme under asymmetric

information is better than that of the Stackelberg scheme with complete information. It can be concluded that the performance of the considered system depends largely on the market structure (i.e., whether the EAPs are allowed to optimize their received power at the IIoT devices with full freedom or not) than on the information scenarios (i.e., the complete or asymmetric information).

Chapter 6

Conclusions and Future Work

In this thesis, we focus on the designs, analyses and optimizations of wireless resources to meet the stringent performance challenges of machine type communications in terms of latency, reliability, spectrum usage and energy supply for wireless communications in IIoT. The key results and insights are first summarized in this chapter, and then the potential future extensions are discussed.

6.1 Summary of Results and Insights

In Chapter 3, we first studied the problem of ensuring ultra-reliable and low-latency communications with limited bandwidth for local area network in IIoT. We established a cross-layer framework for designing burstiness-aware bandwidth reservation for UL transmission. The traffic state classification errors are taken into account when we design transmission schemes and optimize bandwidth reservations. Simulation results show that with around 10^{-2} classification error probability, our method can achieve 10^{-5} packet loss probability. Meanwhile, 40% to 70% bandwidth can be saved compared with the baseline method. Experiment results show that if the traffic model is inaccurate, the data-driven method outperforms the model-based method

by 14%.

Then, in Chapter 4, we extended the scenario from local area network into long distance communications in IIoT. We established a co-design framework of communication and prediction, where the future system states, such as locations and forces, are predicted and sent to the receiver in advance. We formulated an optimization problem to minimize the required bandwidth for ensuring the delay and reliability requirements. By using the proposed algorithm, we can achieve zero user experienced delay for both local and long distance communication scenarios. Simulation results verify the effectiveness of the proposed method, and show that the tradeoffs among bandwidth, reliability, and latency can be fundamentally improved with prediction and communication co-design. The results are further evaluated by practical motion data acquired from experiments by a real hardware device.

In the above two chapters, we studied bandwidth minimizations while ensuring stringent latency and reliability requirements. Finally, in Chapter 5, we further addressed the long standing energy supply problem in IIoT. Radio frequency energy harvesting is introduced to charge the IIoT devices wirelessly. We developed a contract based incentive mechanism for the wireless energy trading in radio frequency energy harvesting based IIoT systems under asymmetric information. Numerical simulation results show that information asymmetry can lead to severe performance degradation for the Stackelberg game-based framework, while the proposed contract theory-based scheme using asymmetric information outperforms the Stackleberg game-based approach with complete information. This implies that *the performance of the considered system depends largely on the market structure (i.e., whether the*

EAPs are allowed to optimize their received power at the IoT devices with full freedom or not) than on the information availability (i.e., the complete or asymmetric information).

6.2 Future Work

We will provide some possible extensions of the presented work in this thesis as follows.

The traffic arrival processes are classified into two traffic states, i.e., high and low traffic states, in Chapter 3. It would be interesting to check if it is beneficial to classify them into multiple levels, so that the classifications can reflect the real traffic arrival process more accurately. Moreover, in the current work, two types of classification methods are applied in the traffic state classification: a model-based Neyman-Pearson method and a data-driven unsupervised learning method, i.e., k-means method. It would be possible to use more sophisticated machine learning method to classify the traffic state, such as deep learning. The training process for deep learning will need a large data set and longer time for training. In this case, we can explore if the improvement of the traffic state classifications will lead to how much performance gain.

The queueing delay is ignored in Chapter 4 for tractability, which happens in the scenario without intense traffic. So the packet arrival interval is larger than the E2E delay requirement, i.e., 1 ms. However, there will be queue when the traffic arrival process is random and the arrival rate is high, such as the typical scenario in Tactile Internet. In our future work, we will include the queueing delay and queueing delay bound violation probability into our analyses framework. Moreover, in our current

work, we use K-repetitions to improve the reliability in the short packet domain. Since the prediction is introduced, larger E2E delay of communications is feasible. As a result, retransmissions with acknowledgements (ACKs) would be possible. There are many possible options for ACK settings. It would be interesting to evaluate the performance of different ACK settings, and choose the suitable settings in different scenarios.

In the scenario of Chapter 5, only information asymmetry is considered. In our future work, we could consider both information asymmetry as well as hidden action. In this scenario, the DAP is not aware of the private information of EAPs and it cannot distinguish the actions taken by different EAPs, i.e., the received power contributed by different EAPs. Because the actions of EAPs are hidden from the DAP, some EAPs may get the reward of the group without paying any efforts, which leads to the free-rider problem. In this case, another mathematical tool from the economics, known as the moral hazard [52] in teams, has a good potential to design effective incentive mechanisms for this new scenario.

Appendix A

Proofs for Chapter 4

A.1 Proof of Property 2

Proof. To prove this proposition, we need to prove that for any $n_1 < n_2$, $\varepsilon_{\mathrm{p}}(n_1) < \varepsilon_{\mathrm{p}}(n_2)$ holds.

From (4.3.7), we have

$$\sigma_j^2(n+1) - \sigma_j^2(n) = \sum_{m=1}^{N} \phi_{j,m,n}\sigma_m^2 > 0.$$

As such, we can conclude that $\sigma_j(n), j = 1, 2, \cdots, N$, increases with n.

Moreover, from (4.3.9), we can see that ε_{p} increases with $\sigma_j(n), j = 1, 2, \cdots, N$. Therefore, ε_{p} increases with the prediction time n. This completes the proof. □

A.2 Proof of Proposition 4.4.1

Proof. To prove this proposition, we first introduce an upper bound of $\varepsilon_{\mathrm{o}}(n) = \varepsilon_{\mathrm{c}}(n + D_{\max}) + \varepsilon_{\mathrm{p}}(n)$, i.e., $\varepsilon_{\mathrm{o}}^{\mathrm{ub}}(n) = 2\max\{\varepsilon_{\mathrm{c}}(n + D_{\max}), \varepsilon_{\mathrm{p}}(n)\}$.

Suppose $\tilde{n}$ is the maximal prediction time that satisfies $\varepsilon_{\mathrm{c}}(n + D_{\max}) - \varepsilon_{\mathrm{p}}(n) > 0$ for all $0 \le n \le \tilde{n}$, and hence $\varepsilon_{\mathrm{o}}^{\mathrm{ub}}(n) = 2\varepsilon_{\mathrm{c}}(n + D_{\max})$, which strictly decreases with n.

On the other hand, when $n > \tilde{n}$, $\varepsilon_{\mathrm{c}}(n+D_{\max})-\varepsilon_{\mathrm{p}}(n) < 0$, and hence $\varepsilon_{\mathrm{o}}^{\mathrm{ub}}(n) = 2\varepsilon_{\mathrm{p}}(n)$, which strictly increases with n. In other words, $\varepsilon_{\mathrm{o}}^{\mathrm{ub}}(n)$ strictly decreases with n when $n \leq \tilde{n}$ and strictly increases with n when $n > \tilde{n}$. Therefore, the upper bound $\varepsilon_{\mathrm{o}}^{\mathrm{ub}}(n)$ is minimized at $\hat{n} = \tilde{n}$ or $\hat{n} = \tilde{n} + 1$.

Let $\varepsilon_{\mathrm{c}}(\hat{n} + D_{\max}) - \varepsilon_{\mathrm{p}}(\hat{n}) = \Delta$, where Δ is the small gap between ε_c and ε_p at $\hat{n}$, which is very closed to zero. We have

$$\varepsilon_{\mathrm{o}}(\hat{n}) \approx \varepsilon_{\mathrm{o}}^{\mathrm{ub}}(\hat{n}). \tag{B.1}$$

Besides, $\varepsilon_{\mathrm{o}}^{\mathrm{ub}}(\hat{n})$ is the minimum of $\varepsilon_{\mathrm{o}}^{\mathrm{ub}}(n), \forall n \in [0, \infty)$, and hence

$$\varepsilon_{\mathrm{o}}^{\mathrm{ub}}(\hat{n}) \leq \varepsilon_{\mathrm{o}}^{\mathrm{ub}}(n^*), \tag{B.2}$$

where n^* is the optimal prediction time that minimizes $\varepsilon_{\mathrm{o}}(n)$. According to the definition of $\varepsilon_o^{\mathrm{ub}}(n)$, we have

$$\begin{aligned}
\varepsilon_{\mathrm{o}}^{\mathrm{ub}}(n^*) &= 2\max\{\varepsilon_{\mathrm{c}}(n^* + D_{\max}), \varepsilon_{\mathrm{p}}(n^*)\} \\
&< 2\left[\varepsilon_{\mathrm{c}}(n^* + D_{\max}) + \varepsilon_{\mathrm{p}}(n^*)\right] \\
&= 2\varepsilon_{\mathrm{o}}(n^*).
\end{aligned} \tag{B.3}$$

From (B.1), (B.2) and (B.3), we have $\varepsilon_{\mathrm{o}}(\hat{n}) < 2\varepsilon_{\mathrm{o}}(n^*)$, i.e., $\varepsilon_{\mathrm{o}}(\hat{n}) - \varepsilon_{\mathrm{o}}(n^*) < \varepsilon_{\mathrm{o}}(n^*)$. For the given bandwidth B, $\varepsilon_{\mathrm{o}}(\hat{n})$ and $\varepsilon_{\mathrm{o}}(n^*)$ are redefined as $\hat{\varepsilon}_{\mathrm{o}}^{\min}(B)$ and $\varepsilon_{\mathrm{o}}^{\min*}(B)$, respectively. So we have $\hat{\varepsilon}_{\mathrm{o}}^{\min}(B) - \varepsilon_{\mathrm{o}}^{\min*}(B) < \varepsilon_{\mathrm{o}}^{\min*}(B)$. □

Appendix B

Proofs for Chapter 5

B.1 Proof of Proposition 5.3.1

$$\begin{cases} \sum\limits_{n_1,\ldots,n_K} \Phi_{n_1,\ldots,n_K} \left[\dfrac{-W\log_2(e)\gamma n_1\theta_1}{2+\gamma\sum\limits_{k=1}^{K} n_k\theta_k\lambda_k} + n_1\theta_1\lambda_1 \right] - \mu_1 = 0 \\ \sum\limits_{n_1,\ldots,n_K} \Phi_{n_1,\ldots,n_K} \left[\dfrac{-W\log_2(e)\gamma n_2\theta_2}{2+\gamma\sum\limits_{k=1}^{K} n_k\theta_k\lambda_k} + n_2\theta_2\lambda_2 \right] - \mu_2 = 0 \\ \qquad\qquad\qquad\qquad\qquad\qquad\qquad\qquad \vdots \\ \sum\limits_{n_1,\ldots,n_K} \Phi_{n_1,\ldots,n_K} \left[\dfrac{-W\log_2(e)\gamma n_N\theta_N}{2+\gamma\sum\limits_{k=1}^{K} n_k\theta_k\lambda_k} + n_N\theta_N\lambda_N \right] - \mu_N = 0 \end{cases} \tag{B.1}$$

In this part, we will prove the proposition 5.3.1. Because the problem (P4.3) is a convex optimization problem, KKT conditions are the sufficient and necessary conditions for the optimal solution. The KKT conditions of problem (P4.3) are given as follows.

The first-order necessary condition is given by (B.1), where $\theta_k \geq 0$ are the types of EAPs, $\mu_k \geq 0$ are KKT multipliers, $\lambda_m \geq 0$ are the prices, and $k = 1, 2, \ldots, K$. The complementary slackness condition is given by

$$\mu_1\lambda_1 + \mu_2\lambda_2 + \cdots + \mu_K\lambda_K = 0. \tag{B.2}$$

Since $\mu_k \geq 0$ and $\lambda_k \geq 0$, $k = 1, 2, \ldots, K$ hold, (B.2) becomes

$$\begin{cases} \mu_1\lambda_1 = 0 \\ \mu_2\lambda_2 = 0 \\ \quad\vdots \\ \mu_K\lambda_K = 0 \end{cases} \tag{B.3}$$

To get the optimal solution of the KKT conditions, we need to solve the equation system consisting of (B.1) and (B.3) in terms of $\mu_k \geq 0$ and $\lambda_k \geq 0$, $k = 1, 2, \ldots, N$, which is a system of quadratic equations.

Now we will discuss the combinations of active or inactive constraints in KKT conditions. Let first test if $\mu_1 = \mu_2 = \cdots = \mu_K = 0$ leads to a valid solution. By substituting $\mu_1, \mu_2, \ldots, \mu_K$ with $\mu_1 = \mu_2 = \cdots = \mu_K = 0$ in (B.1), we have

$$\begin{cases} \lambda_1\Delta = W\log_2(e)\gamma\Omega(\boldsymbol{\lambda}) \\ \lambda_2\Delta = W\log_2(e)\gamma\Omega(\boldsymbol{\lambda}) \\ \qquad\vdots \\ \lambda_K\Delta = W\log_2(e)\gamma\Omega(\boldsymbol{\lambda}) \end{cases} \tag{B.4}$$

where Δ is given by

$$\Delta = \sum_{n_1,\ldots,n_K} \Phi_{n_1,\ldots,n_K} = 1, \tag{B.5}$$

and $\Omega(\boldsymbol{\lambda})$, $\boldsymbol{\lambda} = [\lambda_1, \lambda_2, \ldots, \lambda_K]^T$ is given by

$$\Omega(\boldsymbol{\lambda}) = \sum_{n_1,\ldots,n_K} \frac{\Phi_{n_1,\ldots,n_K}}{2 + \gamma \sum_{k=1}^{K} n_k\theta_k\lambda_k}. \tag{B.6}$$

The above system of equations in (B.4) can be solved numerically. Note that the right term of each equation in (B.4) are the same, so we can conclude that

$$\lambda_1 = \lambda_2 = \cdots = \lambda_K = W \log_2(e)\gamma\Omega(\boldsymbol{\lambda}). \tag{B.7}$$

Because problem (P4.3) is a convex optimization problem, we can conclude that this solution given by KKT conditions is the solution of the original optimization problem.

B.2 Proof of Lemma 5.3.2

The proof is conducted in two parts. First, we prove if $q_i > q_j$, then $\pi_i > \pi_j$. Due to the IC constraints in (5.3.25), we have

$$\pi_i - \frac{q_i^2}{\theta_i} \geq \pi_j - \frac{q_j^2}{\theta_i}, \tag{B.1}$$

and equivalently,

$$\theta_i(\pi_i - \pi_j) \geq q_i^2 - q_j^2 = (q_i + q_j)(q_i - q_j). \tag{B.2}$$

Since $q_i > q_j$, we have

$$\theta_i(\pi_i - \pi_j) \geq q_i^2 - q_j^2 = (q_i + q_j)(q_i - q_j) > 0, \tag{B.3}$$

and thus $\pi_i > \pi_j$.

Next we prove if $\pi_i > \pi_j$, then $q_i > q_j$. Due to the IC constraints in (5.3.25), we have

$$\pi_j - \frac{q_j^2}{\theta_j} \geq \pi_i - \frac{q_i^2}{\theta_j}, \tag{B.4}$$

and equivalently,

$$(q_i + q_j)(q_i - q_j) = q_i^2 - q_j^2 \geq \theta_i(\pi_i - \pi_j). \tag{B.5}$$

Since $\pi_i > \pi_j$, then we have

$$(q_i + q_j)(q_i - q_j) = q_i^2 - q_j^2 \geq \theta_i(\pi_i - \pi_j) > 0, \tag{B.6}$$

and thus $q_i > q_j$. This completes the proof.

B.3 Proof of Lemma 5.3.4

We prove this by contradiction. Suppose that there exists $\pi_i < \pi_j$ when $\theta_i > \theta_j$. We have

$$(\pi_i - \pi_j)(\theta_i - \theta_j) < 0. \tag{B.1}$$

Due to the IC constraints, we also have

$$\pi_i - \frac{q_i^2}{\theta_i} \geq \pi_j - \frac{q_j^2}{\theta_i}, \tag{B.2}$$

and

$$\pi_j - \frac{q_j^2}{\theta_j} \geq \pi_i - \frac{q_i^2}{\theta_j}. \tag{B.3}$$

Combine (B.2) and (B.3), we have

$$(\pi_i - \pi_j)(\theta_i - \theta_j) \geq 0, \tag{B.4}$$

which is in contradiction with (B.1). So if $\theta_i > \theta_j$, then $\pi_i > \pi_j$.

B.4 Proof of Proposition 5.4.1

In this part, we will prove the proposition 5.4.1. Since the problem (P5.3) is a convex optimization problem, KKT conditions will be the sufficient and necessary conditions for the optimal solution. To solve problem (P5.3), the KKT conditions are given as follows.

The first-order necessary condition is given by

$$\begin{cases} \dfrac{-W\log_2(e)\gamma\theta_1}{2+\gamma\sum\limits_{m=1}^{N}\theta_m\lambda_m}+\theta_1\lambda_1-\mu_1=0 \\ \dfrac{-W\log_2(e)\gamma\theta_2}{2+\gamma\sum\limits_{m=1}^{N}\theta_m\lambda_m}+\theta_2\lambda_2-\mu_2=0 \\ \qquad\qquad\vdots \\ \dfrac{-W\log_2(e)\gamma\theta_N}{2+\gamma\sum\limits_{m=1}^{N}\theta_m\lambda_m}+\theta_N\lambda_N-\mu_N=0 \end{cases} \tag{B.1}$$

where $\theta_m=\frac{G_{m,s}^2}{a_m}$, $\mu_m\geq 0$ are KKT multipliers, and $\lambda_m\geq 0, m=1,2,\ldots,N$.

The complementary slackness condition is given by

$$\mu_1\lambda_1+\mu_2\lambda_2+\cdots+\mu_N\lambda_N=0. \tag{B.2}$$

Since $\mu_m\geq 0$ and $\lambda_m\geq 0, m=1,2,\ldots,N$ hold, (B.2) becomes

$$\begin{cases} \mu_1\lambda_1=0 \\ \mu_2\lambda_2=0 \\ \qquad\vdots \\ \mu_N\lambda_N=0 \end{cases} \tag{B.3}$$

To get the optimal solution of the KKT conditions, we need to solve the equation system consisting of (B.1) and (B.3) in terms of $\mu_m\geq 0$ and $\lambda_m\geq 0, m=1,2,\ldots,N$, which is a system of quadratic equations.

Now we will discuss the combinations of active or inactive constraints in KKT condition. Let first test if $\mu_1=\mu_2=\cdots=\mu_N=0$ leads to a valid solution. By

substituting $\mu_1, \mu_2, \ldots, \mu_N$ with $\mu_1 = \mu_2 = \cdots = \mu_N = 0$ in (B.1), we have

$$\begin{cases} \lambda_1 \left(2 + \gamma \sum_{m=1}^{N} \theta_m \lambda_m\right) = W \log_2(e) \gamma \\ \lambda_2 \left(2 + \gamma \sum_{m=1}^{N} \theta_m \lambda_m\right) = W \log_2(e) \gamma \\ \vdots \\ \lambda_N \left(2 + \gamma \sum_{m=1}^{N} \theta_m \lambda_m\right) = W \log_2(e) \gamma \end{cases} \tag{B.4}$$

By solving the system of equations of (B.4), we can get a solution as given by

$$\lambda_1 = \lambda_2 = \cdots = \lambda_N = \frac{\sqrt{\log_2(e)\gamma^2 W \Theta + 1} - 1}{\gamma \Theta}, \tag{B.5}$$

where e is the base of the natural logarithm, and Θ is given by

$$\Theta = \sum_{m=1}^{N} \theta_m. \tag{B.6}$$

Because problem (P5.3) is a convex optimization problem, we can conclude that this solution given by KKT conditions is the solution of the original optimization problem.

Bibliography

[1] R. Drath and A. Horch, "Industrie 4.0: Hit or hype?" *IEEE Industrial Electronics Magazine*, vol. 8, no. 2, pp. 56–58, 2014.

[2] D. Lukač, "The fourth ICT-based industrial revolution" Industry 4.0"," in *Telecommunications Forum Telfor (TELFOR)*. IEEE, 2015, pp. 835–838.

[3] M. Wollschlaeger, T. Sauter, and J. Jasperneite, "The future of industrial communication: Automation networks in the era of the internet of things and industry 4.0," *IEEE Industrial Electronics Magazine*, vol. 11, no. 1, pp. 17–27, 2017.

[4] Y. Lu, "Industry 4.0: A survey on technologies, applications and open research issues," *Journal of Industrial Information Integration*, vol. 6, pp. 1–10, 2017.

[5] J. Posada, C. Toro, I. Barandiaran, D. Oyarzun, D. Stricker, R. De Amicis, E. B. Pinto, P. Eisert, J. Döllner, and I. Vallarino, "Visual computing as a key enabling technology for industrie 4.0 and industrial internet," *IEEE computer graphics and applications*, vol. 35, no. 2, pp. 26–40, 2015.

[6] J. Lin, W. Yu, N. Zhang, X. Yang, H. Zhang, and W. Zhao, "A survey on internet of things: Architecture, enabling technologies, security and privacy, and applications," *IEEE Internet of Things Journal*, vol. 4, no. 5, pp. 1125–1142, 2017.

[7] H. Boyes, B. Hallaq, J. Cunningham, and T. Watson, "The industrial internet of things (IIoT): An analysis framework," *Computers in Industry*, vol. 101, pp. 1–12, 2018.

[8] M. W. Condry and C. B. Nelson, "Using smart edge IoT devices for safer, rapid response with industry IoT control operations," *Proceedings of the IEEE*, vol. 104, no. 5, pp. 938–946, 2016.

[9] S. Jeschke, C. Brecher, T. Meisen, D. Özdemir, and T. Eschert, "Industrial internet of things and cyber manufacturing systems," in *Industrial Internet of Things*. Springer, 2017, pp. 3–19.

[10] T. Heer, O. Kleineberg, and S. Bagchi, "Communication for the Industrial Internet of Things," *White paper, http://theinternetofthings.report/Resources/White-papers/ed2fcb92-5ca6-426c-86bd-0b985e91983b_Belden-WP-Communication-for-the-Industrial-Internet-of-Things.pdf*, 2015.

[11] T. Sauter, "The three generations of field-level networks-evolution and compatibility issues," *IEEE Transactions on Industrial Electronics*, vol. 57, no. 11, pp. 3585–3595, 2010.

[12] ——, "Fieldbus systems: history and evolution," pp. 7–1, 2005.

[13] P. Danielis, J. Skodzik, V. Altmann, E. B. Schweissguth, F. Golatowski, D. Timmermann, and J. Schacht, "Survey on real-time communication via ethernet in industrial automation environments," in *Emerging Technology and Factory Automation (ETFA), 2014 IEEE*. IEEE, 2014, pp. 1–8.

[14] F. Tramarin and S. Vitturi, "Strategies and services for energy efficiency in real-time Ethernet networks," *IEEE Transactions on Industrial Informatics*, vol. 11, no. 3, pp. 841–852, 2015.

[15] T. Müller, A. Walz, M. Kiefer, H. D. Doran, and A. Sikora, "Challenges and prospects of communication security in real-time ethernet automation systems," in *IEEE International Workshop on Factory Communication Systems (WFCS)*. IEEE, 2018, pp. 1–9.

[16] M. Schumacher, J. Jasperneite, and K. Weber, "A new approach for increasing the performance of the industrial Ethernet system PROFINET," in *Factory Communication Systems, 2008. WFCS 2008. IEEE International Workshop on*. IEEE, 2008, pp. 159–167.

[17] F. Tramarin, S. Vitturi, M. Luvisotto, and A. Zanella, "On the use of IEEE 802.11n for industrial communications," *IEEE Transactions on Industrial Informatics*, vol. 12, no. 5, pp. 1877–1886, 2016.

[18] E. Toscano and L. L. Bello, "Comparative assessments of IEEE 802.15. 4/ZigBee and 6LoWPAN for low-power industrial WSNs in realistic scenarios," in *Factory Communication Systems (WFCS), 2012 9th IEEE International Workshop on*. IEEE, 2012, pp. 115–124.

[19] G. Patti, L. Leonardi, and L. L. Bello, "A Bluetooth low energy real-time protocol for industrial wireless mesh networks," in *Industrial Electronics Society, IECON 2016-42nd Annual Conference of the IEEE*. IEEE, 2016, pp. 4627–4632.

[20] S. Xu, T.-H. Chang, S.-C. Lin, C. Shen, and G. Zhu, "Energy-efficient packet scheduling with finite blocklength codes: Convexity analysis and efficient algorithms," *IEEE Trans. Wireless Commun.*, vol. 15, no. 8, pp. 5527–5540, Aug. 2016.

[21] Y. Hu, A. Schmeink, and J. Gross, "Blocklength-limited performance of relaying under quasi-static Rayleigh channels," *IEEE Trans. Wireless Commun.*, vol. 15, no. 7, pp. 4548–4558, Jul. 2016.

[22] C. She, C. Yang, and T. Q. S. Quek, "Cross-layer optimization for ultra-reliable and low-latency radio access networks," *IEEE Trans. Wireless Commun.*, vol. 17, no. 1, pp. 127–141, Jan. 2018.

[23] J. J. Nielsen, R. Liu, and P. Popovski, "Ultra-reliable low latency communication (URLLC) using interface diversity," *IEEE Trans. Commun.*, vol. 66, no. 3, pp. 1322–1334, Mar. 2017.

[24] M. Takeya, Y. Kawamura, and S. Katsura, "Data reduction design based on delta-sigma modulator in quantized scaling-bilateral control for realizing of haptic broadcasting," *IEEE Trans. Ind. Electron.*, vol. 63, no. 3, pp. 1962–1971, Mar. 2016.

[25] B. Singh, O. Tirkkonen, Z. Li, and M. A. Uusitalo, "Contention-based access for ultra-reliable low latency uplink transmissions," *IEEE Wireless Commun. Lett.*, Oct. 2017.

[26] 3GPP TSG RAN TR38.913 R14, "Study on scenarios and requirements for next generation access technologies," Jun. 2017.

[27] M. Shafi, A. F. Molisch, P. J. Smith, T. Haustein, P. Zhu, P. Silva, F. Tufvesson, A. Benjebbour, and G. Wunder, "5G: A tutorial overview of standards, trials, challenges, deployment, and practice," *IEEE Journal on Selected Areas in Communications*, vol. 35, no. 6, pp. 1201–1221, 2017.

[28] J. G. Andrews, S. Buzzi, W. Choi, S. V. Hanly, A. Lozano, A. C. Soong, and J. C. Zhang, "What will 5G be?" *IEEE Journal on selected areas in communications*, vol. 32, no. 6, pp. 1065–1082, 2014.

[29] P. Schulz, M. Matthe, H. Klessig, M. Simsek, G. Fettweis, J. Ansari, S. A. Ashraf, B. Almeroth, J. Voigt, I. Riedel *et al.*, "Latency critical iot applications

in 5G: Perspective on the design of radio interface and network architecture," *IEEE Communications Magazine*, vol. 55, no. 2, pp. 70–78, 2017.

[30] P. Popovski, J. J. Nielsen, C. Stefanovic, E. de Carvalho, E. Strom, K. F. Trillingsgaard, A.-S. Bana, D. M. Kim, R. Kotaba, J. Park *et al.*, "Wireless access for ultra-reliable low-latency communication: Principles and building blocks," *IEEE Network*, vol. 32, no. 2, pp. 16–23, 2018.

[31] C. She, C. Yang, and T. Q. S. Quek, "Radio resource management for ultra-reliable and low-latency communications," *IEEE Communications Magazine*, vol. 55, no. 6, pp. 72–78, 2017.

[32] Z. Dawy, W. Saad, A. Ghosh, J. G. Andrews, and E. Yaacoub, "Toward massive machine type cellular communications," *IEEE Wireless Communications*, vol. 24, no. 1, pp. 120–128, 2017.

[33] Z. Sheng, S. Yang, Y. Yu, A. Vasilakos, J. Mccann, and K. Leung, "A survey on the ietf protocol suite for the internet of things: Standards, challenges, and opportunities," *IEEE Wireless Communications*, vol. 20, no. 6, pp. 91–98, 2013.

[34] X. Lin, J. Li, R. Baldemair *et al.*, "5G New Radio: unveiling the essentials of the next generation wireless access technology," 2018. [Online]. Available: https://arxiv.org/abs/1806.06898

[35] T. Jacobsen, R. Abreu, G. Berardinelli *et al.*, "System level analysis of uplink grant-free transmission for URLLC," in *IEEE Globecom Workshops*, 2017, pp. 1–6.

[36] 3GPP TR 38.802 V2.0.0, "Study on new radio (NR) access technology; physical layer aspects (release 14)," 2017.

[37] T. K. Vu, C.-F. Liu, M. Bennis *et al.*, "Ultra-reliable and low latency communication in mmwave-enabled massive MIMO networks," *IEEE Commun. Letters*, vol. 21, no. 9, pp. 2041–2044, Sep. 2017.

[38] J. J. Nielsen, R. Liu, and P. Popovski, "Ultra-reliable low latency communication using interface diversity," *IEEE Transactions on Communications*, vol. 66, no. 3, pp. 1322–1334, March 2018.

[39] C. She, Z. Chen, C. Yang *et al.*, "Improving network availability of ultra-reliable and low-latency communications with multi-connectivity," *IEEE Trans. Commun., early access*, 2018.

[40] M. Simsek, A. Aijaz, M. Dohler, J. Sachs, and G. Fettweis, "5G-enabled tactile internet," *IEEE J. Sel. Areas Commun.*, vol. 34, no. 3, pp. 460–473, Mar. 2016.

[41] A. Aijaz, M. Dohler, A. H. Aghvami, V. Friderikos, and M. Frodigh, "Realizing the Tactile Internet: haptic communications over next generation 5G cellular networks," *IEEE Wireless Commun.*, vol. 24, no. 2, pp. 82–89, Apr. 2017.

[42] M. Condoluci, T. Mahmoodi, E. Steinbach, and M. Dohler, "Soft resource reservation for low-delayed teleoperation over mobile networks," *IEEE Access*, vol. 5, pp. 10 445–10 455, May 2017.

[43] S. M. Kay, *Fundamentals of statistical signal processing, Volume II: Detection theory*. Prentice Hall, 1998.

[44] M. B. Christopher, *Pattern Recognition and Machine Learning*. Springer-Verlag New York, 2016.

[45] Z. Hou, C. She, Y. Li *et al.*, "Burstiness aware bandwidth reservation for ultra-reliable and low-latency communications (URLLC) in Tactile Internet," *IEEE J. Sel. Areas Commun.(early access)*, 2018.

[46] N. Strodthoff, B. Göktepe, T. Schierl *et al.*, "Enhanced machine learning techniques for early HARQ feedback prediction in 5G," *arXiv preprint arXiv:1807.10495*, 2018.

[47] M. Li, X. Guan, C. Hua, C. Chen, and L. Lyu, "Predictive pre-allocation for low-latency uplink access in industrial wireless networks," *arXiv preprint arXiv:1801.06451*, 2018.

[48] K. Antonakoglou, X. Xu, E. Steinbach *et al.*, "Towards haptic communications over the 5G tactile internet," *IEEE Communications Surveys & Tutorials*, 2018.

[49] N. Sakr, J. Zhou, N. D. Georganas, and J. Zhao, "Prediction-based haptic data reduction and transmission in telementoring systems," *IEEE Transactions on Instrumentation and Measurement*, vol. 58, no. 5, pp. 1727–1736, 2009.

[50] N. Sakr, N. D. Georganas, and J. Zhao, "Human perception-based data reduction for haptic communication in six-dof telepresence systems," *IEEE Transactions on Instrumentation and Measurement*, vol. 60, no. 11, pp. 3534–3546, 2011.

[51] X. Tong, G. Zhao, M. A. Imran *et al.*, "Minimizing wireless resource consumption for packetized predictive control in real-time cyber physical systems," in *2018 IEEE ICC Workshops*, May 2018.

[52] P. Bolton and M. Dewatripont, *Contract theory*. MIT press, 2005.

[53] G. Durisi, T. Koch, and P. Popovski, "Toward massive, ultrareliable, and low-latency wireless communication with short packets," *Proceedings of the IEEE*, vol. 104, no. 9, pp. 1711–1726, 2016.

[54] C. E. Shannon, "A mathematical theory of communication," *Bell system technical journal*, vol. 27, no. 3, pp. 379–423, 1948.

[55] R. A. Costa, M. Langberg, and J. Barros, "One-shot capacity of discrete channels," in *Information Theory Proceedings (ISIT), 2010 IEEE International Symposium on*. IEEE, 2010, pp. 211–215.

[56] Y. Polyanskiy, H. V. Poor, and S. Verdú, "Channel coding rate in the finite blocklength regime," *IEEE Transactions on Information Theory*, vol. 56, no. 5, pp. 2307–2359, 2010.

[57] T. M. Mitchell *et al.*, "Machine learning. 1997," *Burr Ridge, IL: McGraw Hill*, vol. 45, no. 37, pp. 870–877, 1997.

[58] M. Chen, U. Challita, W. Saad, C. Yin, and M. Debbah, "Machine learning for wireless networks with artificial intelligence: A tutorial on neural networks," *arXiv preprint arXiv:1710.02913*, 2017.

[59] C. Bellavitis, D. S. Kamuriwo, and U. Hommel, "Mitigation of moral hazard and adverse selection in venture capital financing: The influence of the country's institutional setting," *Journal of Small Business Management*, 2018.

[60] O. A. Rud, J. P. Rabanal, and J. Horowitz, "Does competition aggravate moral hazard? a multi-principal-agent experiment," *Journal of Financial Intermediation*, vol. 33, pp. 115–121, 2018.

[61] T. Liu, J. Li, F. Shu, M. Tao, W. Chen, and Z. Han, "Design of contract-based trading mechanism for a small-cell caching system," *IEEE Trans. Wireless Commun.*, vol. 16, no. 10, pp. 6602–6617, Oct 2017.

[62] Y. Zhang, L. Song, W. Saad, Z. Dawy, and Z. Han, "Contract-based incentive mechanisms for device-to-device communications in cellular networks," *IEEE J. Sel. Areas Commun.*, vol. 33, no. 10, pp. 2144–2155, May 2015.

[63] L. Duan, L. Gao, and J. Huang, "Cooperative spectrum sharing: A contract-based approach," *IEEE Trans. Mobile Commun.*, vol. 13, no. 1, pp. 174–187, Nov. 2014.

[64] G. P. Fettweis, "The Tactile Internet: applications & challenges," *IEEE Veh. Technol. Mag.*, vol. 9, no. 1, pp. 64–70, Mar. 2014.

[65] 3GPP TR 36.881 V0.5.0, "Evolved universal terrestrial radio access(E-UTRA)," Nov. 2015.

[66] W. Yang, G. Durisi, T. Koch, and Y. Polyanskiy, "Quasi-static multiple-antenna fading channels at finite blocklength," *IEEE Trans. Inf. Theory*, vol. 60, no. 7, pp. 4232–4265, Jul. 2014.

[67] S. Zhang, Z. Qian, Z. Luo, J. Wu, and S. Lu, "Burstiness-aware resource reservation for server consolidation in computing clouds," *IEEE Trans. Parallel Distrib. Syst.*, vol. 27, no. 4, pp. 964–977, Apr. 2016.

[68] M. E. Ahmed, J. B. Song, Z. Han, and D. Y. Suh, "Sensing-transmission edifice using Bayesian nonparametric traffic clustering in cognitive radio networks," *IEEE Trans. Mobile Comput.*, vol. 27, no. 4, pp. 964–977, Apr. 2016.

[69] C. She, C. Yang, and T. Q. S. Quek, "Joint uplink and downlink resource configuration for ultra-reliable and low-latency communications," *IEEE Trans. Commun., early access*, 2018.

[70] G. L. Choudhury, D. M. Lucantoni, and W. Whitt, "Squeezing the most out of ATM," *IEEE Trans. Commun.*, vol. 44, no. 2, pp. 203–217, Feb. 1996.

[71] J. Wu, Y. Bao, G. Miao, S. Zhou, and Z. Niu, "Base-station sleeping control and power matching for energy–delay tradeoffs with bursty traffic," *IEEE Trans. Veh. Technol.*, vol. 65, no. 5, pp. 3657–3675, May 2016.

[72] S. A. Ashraf, F. Lindqvist, R. Baldemair, and B. Lindoff, "Control channel design trade-offs for ultra-reliable and low-latency communication system," in *Proc. IEEE Globecom Workshops*, Dec. 2015.

[73] M. Mousaei and B. Smida, "Optimizing pilot overhead for ultra-reliable short-packet transmission," in *Proc. IEEE ICC*, May 2017.

[74] C. S. Chang and J. A. Thomas, "Effective bandwidth in high-speed digital networks," *IEEE J. Sel. Areas Commun.*, vol. 13, no. 6, pp. 1091–1100, Aug. 1995.

[75] S. Schiessl, J. Gross, and H. Al-Zubaidy, "Delay analysis for wireless fading channels with finite blocklength channel coding," in *Proc. ACM MSWiM*, Nov. 2015.

[76] Z. Hou, H. Chen, Y. Li, and B. Vucetic, "Incentive mechanism design for wireless energy harvesting-based internet of things," *IEEE Internet Things J.*, vol. 5, no. 4, pp. 2620–2632, 2018.

[77] D. Kubus, I. Weidauer, and F. M. Wahl, "1khz is not enough: How to achieve higher update rates with a bilateral teleoperation system based on commercial hardware," in *Proc. IEEE/RSJ International Conference on Intelligent Robots and Systems*, 2009, pp. 5107–5114.

[78] B. Soret, P. Mogensen, K. I. Pedersen, and M. C. Aguayo-Torres, "Fundamental tradeoffs among reliability, latency and throughput in cellular networks," in *IEEE Globecom Workshops*, 2014, pp. 1391–1396.

[79] C. She, C. Yang, and T. Q. S. Quek, "Joint uplink and downlink resource configuration for ultra-reliable and low-latency communications," *IEEE Transactions on Communications*, vol. 66, no. 5, pp. 2266–2280, 2018.

[80] M. Bennis, M. Debbah, and H. V. Poor, "Ultra-reliable and low-latency wireless communication: Tail, risk and scale," *arXiv preprint arXiv:1801.01270*, 2018.

[81] G. Berardinelli, N. H. Mahmood, R. Abreu, T. Jacobsen, K. Pedersen, I. Z. Kovács, and P. Mogensen, "Reliability analysis of uplink grant-free transmission over shared resources," *IEEE Access*, vol. 6, pp. 23 602–23 611, 2018.

[82] S. Feyzabadi, S. Straube, M. Folgheraiter *et al.*, "Human force discrimination during active arm motion for force feedback design," *IEEE Trans. Haptics*, vol. 6, no. 3, pp. 309–319, 2013.

[83] J. Marescaux, J. Leroy, F. Rubino *et al.*, "Transcontinental robot-assisted remote telesurgery: feasibility and potential applications," *Annals of surgery*, vol. 235, no. 4, p. 487, 2002.

[84] S. M. Kay, *Fundamentals of statistical signal processing, volume I: estimation theory*. Prentice Hall, 1993.

[85] G. Klančar and I. Škrjanc, "Tracking-error model-based predictive control for mobile robots in real time," *Robotics and autonomous systems*, vol. 55, no. 6, pp. 460–469, 2007.

[86] M. Shirvanimoghaddam, M. S. Mohamadi, R. Abbas *et al.*, "Short block-length codes for ultra-reliable low-latency communications," *IEEE Commun. Mag.*, 2018. [Online]. Available: https://arxiv.org/abs/1802.09166

[87] J. Mathews and K. Fink, *Numerical methods using MATLAB*. Pearson Prentice Hall, NJ, 2004.

[88] H. Kawabata, K. Ishibashi, S. Vuppala, and G. T. F. de Abreu, "Robust relay selection for large-scale energy-harvesting IoT networks," *IEEE Internet of Things Journal*, vol. 4, no. 2, pp. 384–392, April 2017.

[89] Z. Yang, W. Xu, Y. Pan, C. Pan, and M. Chen, "Energy efficient resource allocation in machine-to-machine communications with multiple access and energy harvesting for IoT," *IEEE Internet of Things Journal*, vol. PP, no. 99, pp. 1–1, 2017.

[90] P. Kamalinejad, C. Mahapatra, Z. Sheng, S. Mirabbasi, V. C. Leung, and Y. L. Guan, "Wireless energy harvesting for the Internet of Things," *IEEE Commun. Magazine*, vol. 53, no. 6, pp. 102–108, Jun. 2015.

[91] D. Niyato, D. I. Kim, P. Wang, and L. Song, "A novel caching mechanism for Internet of Things (IoT) sensing service with energy harvesting," in *Proc. ICC*, May. 2016, pp. 1–6.

[92] H. Chen, C. Zhai, Y. Li, and B. Vucetic, "Cooperative strategies for wireless-powered communications," *arXiv preprint arXiv:1610.03527*, 2016.

[93] K. Huang and V. K. Lau, "Enabling wireless power transfer in cellular networks: Architecture, modeling and deployment," *IEEE Trans. Wireless Commun.*, vol. 13, no. 2, pp. 902–912, 2014.

[94] K. Huang and X. Zhou, "Cutting the last wires for mobile communications by microwave power transfer," *IEEE Commun. Mag.*, vol. 53, no. 6, pp. 86–93, 2015.

[95] C. Zhong, X. Chen, Z. Zhang, and G. K. Karagiannidis, "Wireless-powered communications: Performance analysis and optimization," *IEEE Trans. Commun.*, vol. 63, no. 12, pp. 5178–5190, 2015.

[96] Y. Chen, D. B. da Costa, and H. Ding, "Interference analysis in wireless power transfer," *IEEE Communications Letters*, vol. 21, no. 10, pp. 2318–2321, Oct 2017.

[97] L. Chen, W. Wang, and C. Zhang, "Stochastic wireless powered communication networks with truncated cluster point process," *IEEE Trans. Veh. Technol.*, vol. PP, no. 99, pp. 1–1, 2017.

[98] J. H. Park, Y. S. Jeon, and S. Han, "Energy beamforming for wireless power transfer in MISO heterogeneous network with power beacon," *IEEE Communications Letters*, vol. 21, no. 5, pp. 1163–1166, May 2017.

[99] T. A. Khan, R. W. Heath, and P. Popovski, "Wirelessly powered communication networks with short packets," *IEEE Trans. Wireless Commun.*, vol. PP, no. 99, pp. 1–1, 2017.

[100] X. Jiang, C. Zhong, X. Chen, T. Q. Duong, T. A. Tsiftsis, and Z. Zhang, "Secrecy performance of wirelessly powered wiretap channels," *IEEE Trans. Commun.*, vol. 64, no. 9, pp. 3858–3871, 2016.

[101] H. Chen, Y. Li, Z. Han, and B. Vucetic, "A stackelberg game-based energy trading scheme for power beacon-assisted wireless-powered communication," in *Proc. ICASSP*, Apr. 2015, pp. 3177–3181.

[102] S. Sarma, K. Kandhway, and J. Kuri, "Robust energy harvesting based on a Stackelberg game," *IEEE Wireless Communications Letters*, vol. 5, no. 3, pp. 336–339, 2016.

[103] Y. Ma, H. Chen, Z. Lin, Y. Li, and B. Vucetic, "Distributed and optimal resource allocation for power beacon-assisted wireless-powered communications," *IEEE Trans. Commun.*, vol. 63, no. 10, pp. 3569–3583, Aug. 2015.

[104] R. Zhang, L. Song, Z. Han, and B. Jiao, "Physical layer security for two-way untrusted relaying with friendly jammers," *IEEE Trans. Veh. Technol.*, vol. 61, no. 8, pp. 3693–3704, 2012.

[105] H. Zhang, Y. Xiao, L. X. Cai, D. Niyato, L. Song, and Z. Han, "A multi-leader multi-follower Stackelberg game for resource management in LTE unlicensed," *IEEE Trans. Wireless Commun.*, vol. 16, no. 1, pp. 348–361, 2017.

[106] Y. Xu and S. Mao, "Stackelberg game for cognitive radio networks with MIMO and distributed interference alignment," *IEEE Trans. Veh. Technol.*, vol. 63, no. 2, pp. 879–892, 2014.

[107] S. Yin, E. Zhang, Z. Qu, L. Yin, and S. Li, "Optimal cooperation strategy in cognitive radio systems with energy harvesting," *IEEE Trans. Wireless Commun.*, vol. 13, no. 9, pp. 4693–4707, 2014.

[108] H. H. Chen, Y. Li, Y. Jiang, Y. Ma, and B. Vucetic, "Distributed power splitting for swipt in relay interference channels using game theory," *IEEE Trans. Wireless Commun.*, vol. 14, no. 1, pp. 410–420, 2015.

[109] I. Krikidis, G. Zheng, and B. Ottersten, "Harvest-use cooperative networks with half/full-duplex relaying," in *Proc. WCNC*, Apr. 2013, pp. 4256–4260.

[110] H. Ju and R. Zhang, "Throughput maximization in wireless powered communication networks," *IEEE Trans. Wireless Commun.*, vol. 13, no. 1, pp. 418–428, Dec. 2014.

[111] X. Lu, P. Wang, D. Niyato, D. I. Kim, and Z. Han, "Wireless networks with RF energy harvesting: A contemporary survey," *IEEE Commun. Surveys Tuts.*, vol. 17, no. 2, pp. 757–789, Nov. 2015.

[112] A.-H. Mohsenian-Rad, V. W. Wong, J. Jatskevich, R. Schober, and A. Leon-Garcia, "Autonomous demand-side management based on game-theoretic energy consumption scheduling for the future smart grid," *IEEE Trans. Smart Grid*, vol. 1, no. 3, pp. 320–331, Nov. 2010.

[113] S. Boyd and L. Vandenberghe, *Convex optimization*. Cambridge university press, 2004.